

Evaluation of a tsunami risk reduction system for Kamakura - Japan

Non Okumura



Evaluation of a tsunami risk reduction system for Kamakura - Japan

by

Non Okumura

to obtain the degree of Master of Science
at the Delft University of Technology,
to be defended publicly on Thursday July 28, 2016 at 11:00 AM.

Student number:	4407903
Project duration:	January 1, 2016 – July 28, 2016
Thesis committee:	Prof. dr. ir. S. N. Jonkman, TU Delft, supervisor Dr. M. Esteban, University of Tokyo Dr. ir. B. Hofland, TU Delft Ir. K. Lendering, TU Delft

An electronic version of this thesis is available at <http://repository.tudelft.nl/>.

ABSTRACT

In 2011, the Great Eastern Japan tsunami devastated a large part of the Tohoku area (Northeastern Japan), and since then, other coastal areas in Japan have realized the tragic consequence such event could pose for their cities. The challenge of reducing flood vulnerability of coastal areas due to tsunamis has been widely recognized and discussed amongst the government and the scientific community. Before the 2011 event, flood protection measures were designed according to the previous most extreme event, regardless of the type of hazard, i.e. typhoon, tsunami. In response to the impact of the 2011 tsunami a broad categorization that separates tsunamis into two protection levels has been made. However, a risk-based approach considering return periods of earthquakes and tsunamis as well as resulting damage could be more valuable. Therefore, it is expected to be a more valuable approach than the simple categorization of tsunami protection levels.

The risk-based approach to flood protection, similar to what is applied in the flood management strategy in the Netherlands, is becoming more popular internationally. It combines the knowledge on probability of the occurrence of flood events with their consequences, such as damage to buildings and loss of life, in order to reduce their product which is defined as total risk. Though Japan has a different setting, it has a comparable history of water-related hazards, therefore, the risk-based approach could be valuable. In this thesis, the effectiveness of a risk-reducing system is tested and evaluated for tsunami hazards in the case study of Kamakura. This area was chosen because it is the historical capital of Japan with abundant cultural heritage, with a dense population ($4,400 \text{ people}/\text{km}^2$), and it could be greatly affected due to the short tsunami warning time of 20 minutes which was observed in this thesis.

A flood risk assessment method was developed in order to determine how to evaluate a risk-reducing system against tsunamis for Kamakura. To have a risk assessment method, the following general steps (as numbered in the Figure 2): (1) Determine a probabilistic distribution of tsunami height and its return period, (2) Conduct flood scenarios, (3) Estimate damage, (4) Quantify risk, (5) Implement risk reduction measures, and (6) Evaluate risk. The steps are connected and coupled to each other.

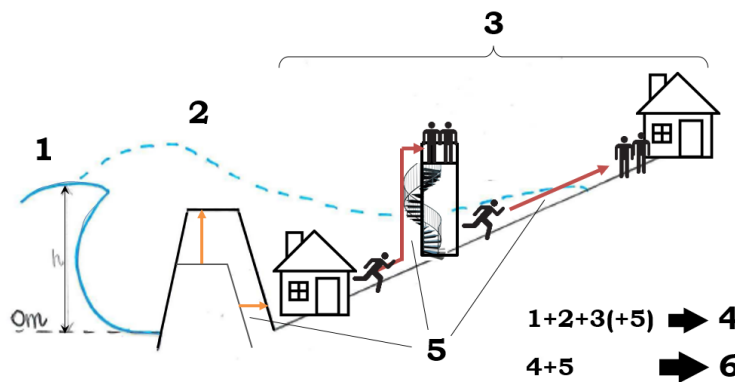


Figure 1: Schematization of risk assessment methodology with general steps

In step (1), data on the incoming wave height of tsunamis and its year of occurrence is needed for approximating the return period, and fitted with a probabilistic distribution. This is the most critical step as this chosen distribution, which was in this case the Generalized Extreme Value Type 3 distribution,

influences the results for the research. In step (2), SWASH was used to develop a 1D run-up model in order to estimate the possible damages resulting from a tsunami with real bathymetry and topography. Run-up distances and other flood parameters, such as depth and velocity, are dependent on the incoming wave height. In the flood scenarios, seven tsunami levels with incoming wave heights of 6, 8, 11, 12, 13.5, 14, and 14.5 m, corresponding to return periods ranging from 88 to 1809 years in the distribution, were simulated. The main determining factor for step (3), which was to estimate damage to buildings and the loss of life, is the maximum depth-velocity product.

As also seen in Figure 2, the results from steps (1), (2) and (3) are combined to quantify the baseline risk, which represents the risk under the current situation. The results of the baseline risk estimated the total damage to range from €12.1 to €37.6 billion depending on the tsunami considered (annual total risk of €257.5 million), which confirmed the vulnerability of Kamakura. And of these total damage costs, over 90% were associated costs with fatalities. From these results, it was clear that interventions which would reduce the casualties would be effective to reduce the total risk.

In step (5), interventions were chosen based on their feasibility and suitability for Kamakura, with the aim to reduce risk. The interventions included dike heightening to 4, 8, 12, and 16 m, and improved evacuation which consisted of implementing vertical evacuation buildings and distributing wireless receivers to improve evacuation behavior. The risk was then quantified for the scenarios with interventions to observe which intervention was the most effective for risk reduction. The results showed that dike heightening had limited risk reduction due to the large amount of wave overtopping, as tsunamis have a lot of energy. Vertical evacuation was only seen to be effective for large tsunamis with run-up distances going further than the location of the evacuation building. Wireless receivers were very effective for casualty reduction, reducing the amount of casualties by half or more for all tsunami scenarios.

Finally, the different risk reduction measures were evaluated, and compared with respect to the baseline condition. There are three ways of evaluating risk used in this thesis: cost-benefit analysis (CBA), individual risk (IR) and societal risk (SR). These evaluations are conducted based on the results and information derived from steps (4) and (5).

When only considering the results for IR and SR, the most favorable option was where the lowest risk level was observed, and when only considering the results of the CBA, the most favorable option was where the lowest total cost and maximized Benefit-Cost (B/C) ratio was observed. The final choice of the most favorable of the considered options was made based on the CBA, IR and SR, along with the expected stakeholder demands. It was assumed that the political decision makers most likely prefer solutions with low cost and high return (maximized B/C ratio), and the society prefers solutions which minimize the disruption of the coastal aesthetics. The preliminary solution for the risk assessment showed that the most favorable intervention of the considered options was to improve evacuation with both vertical evacuation buildings and distribution of wireless receivers, without any dike heightening.

The results of the flood risk assessment for Kamakura presented that a tsunami flood risk assessment is possible. It is true that there are constraints, such as the uncertainty which lies in the return period distribution, simplification of the run-up model, uniform distribution of people and houses, and other uncertainties decrease the accuracy of this thesis. Even then, a risk-based approach is believed to have more advantages than the simple categorization of tsunami protection levels and using the previous most extreme event. It provides a suitable framework for the design and evaluation of tsunami protection measures. Furthermore, the risk assessment results clearly substantiated the currently existing tsunami categorization method as a great approach for flood management, and provided a strategy to strengthen the currently existing method.

概要

2011年に日本で発生した東日本大震災により、東北地方の多くの地域が荒廃することとなり、それ以降、日本のその他の沿海地域においても大津波の可能性が恐れられることとなった。沿海地域における津波対策として、津波への脆弱性を克服することへの挑戦については、非常に重要であると認識されており、政府や科学者の間で広く議論されている。2011年の東日本大震災の発生までは、津波への防御対策は過去の最大級の災害を基準に設計されていた。それが大震災の衝撃により、津波からの防御を2段階のレベルへと分別することが新たに決められた。しかしながら、リスク視点のアプローチから、想定され得る地震や津波の発生間隔や被害が考慮されるべきである。それゆえ、単純な津波防御レベルの分類よりも、この考え方がより適切であるとする。

津波への防御に対するリスク視点のアプローチは、これはオランダにおける洪水対策と同様に、国際的に認識されつつあると言える。この手法を津波の発生確率の知見と組み合わせることで、日常生活への喪失や建物の損害といった津波の被害の甚大さを低減することを試みている。日本はオランダとは全く異なった社会環境ではあるが、水害に対する歴史は非常に似通っており、それゆえ、リスク視点のアプローチは価値があるとする。本論文においては、『リスク低減のしくみ』の効果を、鎌倉市の事例をケーススタディとし、検証及び評価を行なう。かつて日本の首都であった都市であり、文化的な遺産も豊富に存在していることから、この地域を事例として選定した。人口密度も高く（1平方キロメートル当たり4,400人）、津波の到達時間が短いことから大きな影響が出るであろうと想定した。

本研究を推進するに際して、『リスク低減のしくみ』をどのように評価するかを決定するため、津波リスク判定手法の開発を行なった。リスク判定手法を実施するには、いくつかの特徴的な段階を設定する必要がある。以下、その個々の内容を述べる。①津波が押し寄せる際の高さ及びその発生間隔の確率的分布を決定する。②津波浸水想定シナリオを設定する。③損害を見積もる。④リスクを定量化する。⑤『リスク低減のしくみ』を実行する。⑥リスクを評価する。これらはそれぞれ数値で説明され、またそれぞれ時系列に順番に結びついている。

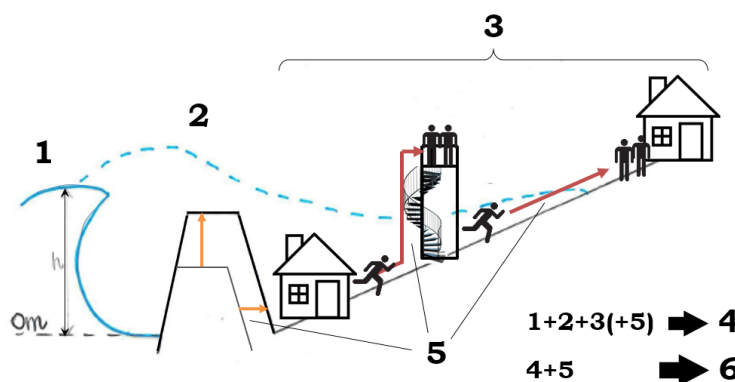


Figure 2: Schematization of the steps of the risk assessment method

段階①においては、津波の発生間隔の確率的分布を想定するために、津波の押し寄せる際の高さとその発生年度のデータが必要である。ここで想定した分布、今回の場合はGEV Type

3 分布であるが、これが本論文の全体に影響を与えることとなるため、最も困難な作業である。段階②においては、津波の想定される損害を見積もる必要性から、ID run-up（遡上）モデルを開発するため、SWASHを活用した。遡上高の距離、および浸水深や流速といった津波の変数は、津波到達高に依り決定される。津波のシナリオでは、津波到達高（7段階：6m/8m/11m/12m/13.5m/14m/14.5m）を選び、シミュレーションを行なった。選ばれた津波到達高に一致する発生間隔は確率分布から算出でき、88年から1809年の範囲であると分かった。段階③において、日常生活の喪失と建物の損害を見積もるための最も重要な要因は、浸水深と流速の最大の積の設定であった。

数値を前頁に記載しているが、段階①②③の結果は、基準リスクを定量化するために組み合わせられ、それが現状におけるリスクを表すことにもつながる。基準リスクの結果は、損害全体として1.41兆円から43.8兆円の範囲と見積もることができ（1年間の全体リスクは300億円）、鎌倉市の津波に対する脆弱性を実証する結果となった。また全体の損害費用においては、その90%以上が死者に関係していた。これらの結果から、死傷者を減らす対策が全体リスクの低減に効果的であることは明白であると考えている。

段階⑤においては、鎌倉市での実現性および適合性の観点から、対策を検討した。その内容は、堤防の高さを4m/8m/12m/16mにすること、そして垂直型避難施設の設置とワイヤレスレシーバーの配布といった避難手法を改善すること、といったことである。そして、リスク低減に最も効果的な対策を検証するために、シナリオに沿ってすべてのリスクを定量化した。その結果、まず防波壁は津波の膨大なエネルギーで大量の水がそれを乗り越え浸入してくることから効果が限定的であること、また垂直型避難施設については、大規模の津波が施設のロケーションを越えて更に内陸に押し寄せた場合に限り効果が認められた。ワイヤレスレシーバーについては、どのシナリオにおいても死傷者を半減或いはそれ以下にすることができる結果となり、多大な効果を確認することができた。

最後に、異なったリスク低減手法による評価を実施した。本研究においては、①費用便益分析、②個別リスク、③社会リスク、の3つの観点を採用し、段階④および段階⑤の結果及び情報と組み合わせ検証を行なった。

最も有効であると考えられる最終的な選択は、ステークホルダーの要望に沿い、費用便益分析と個別リスク、及び社会リスクを鑑みて決定されることとなる。個別リスクと社会リスクの結果のみに沿って考えられる場合は最もリスクが低い手法が選定され、他方で費用便益分析の結果が優先されるなら、最も好ましい選択肢は低コストで費用対効果が最大化できる手法となる。政策の意思決定者は、ローコストハイリターンで費用対効果を最大化させる手法をより好む傾向があり、共同体の人々は社会の崩壊を極小化できる手法が妥当であると考えている。準備が可能な解決策として最も有効な手法は、防波壁を高くすることではなく、垂直型避難施設の設置とワイヤレスレシーバーの配布の双方を避難改善策として推進することである。

鎌倉市を事例とした本研究の結果、津波リスク判定は可能であることを立証することができた。但し、津波発生間隔の分布や遡上モデルの単純化、人々や住居の配置設定等々、大前提となるシナリオ自体の精度にまだまだ改善の余地があることも事実である。それでもなお、今回採用したリスク視点のアプローチは、津波を単純な防御レベルに分類する現在の手法に比較し、はるかに有効的な打ち手であると考えている。なぜなら、津波防御の手法としてのグランドデザイン及び避難方法について、適切でかつ具体的な枠組みと成り得るからである。加えて、今回のリスク判定結果は、この手法が津波の分類方法として活用できることを実証しており、つまりはリスク判定の手法を用いることで、現行の分類手法の改善にも有用であることを示唆していると考えている。

PREFACE

This thesis is presented in partial fulfillment of the requirements for the degree of MSc. in Hydraulic Engineering, and has been complete at the Delft University of Technology. This report covers the evaluation of a tsunami risk reduction system for Kamakura, Sagami Bay, and aimed to demonstrate that a flood risk assessment for tsunamis is possible.

I would like to express my sincere gratitude to the members of my graduation committee, Bas Jonkman, Miguel Esteban, Bas Hofland and Kasper Lendering. Their kind guidance, feedback and assistance proved invaluable for my thesis. Furthermore, I would like to extend my thanks to my friends and colleagues who contributed to my thesis, while also motivating me through this tough time. I would also like to show my appreciation for my boyfriend, who always encouraged me through my ups and downs. Finally, I would like to thank my parents for giving me the opportunity to come to the Netherlands and have this valuable experience.

*Non Okumura
Delft, July 2016*

TABLE OF CONTENTS

Abstract	i
Preface	v
Table of Contents	1
1 Introduction	3
1.1 Research Motivation	3
1.2 Objective and Research questions.	4
1.3 Approach & Methodology	5
1.4 Structure of the Report	7
2 System Description of Kamakura, Sagami Bay	9
2.1 Background Information of Sagami Bay Area	9
2.1.1 History of tsunamis in Kamakura	11
2.1.2 Existing flood protection measures in Kamakura.	14
2.2 Introduction to tsunamis	15
2.2.1 Tsunami wave modelling.	16
2.2.2 Current tsunami research	16
2.3 Multi-Layer Safety system.	18
2.3.1 General Information	18
2.3.2 Cost-benefit Analysis	19
2.3.3 Individual & Societal Risk	20
2.3.4 Damage Assessment approaches	21
2.3.5 MLS System in Sendai, Tohoku.	22
2.4 Conclusion	24
3 Tsunami Categorization	25
3.1 Historical tsunami events & their characteristics	25
3.2 Method of Regression	26
3.3 Extrapolating tsunami return periods	27
3.3.1 Return Period Approximation	27
3.3.2 Distribution Fitting	28
3.3.3 Discussion	30
3.4 Conclusion	33
4 Tsunami run-up assessment	35
4.1 Selection of the wave theory	36
4.2 Analytical description of the deformation of the tsunami wave	38
4.3 Reference case study: Sendai	41
4.3.1 Boundary Conditions and Observational data	42
4.3.2 Validation based on Observational Data	43
4.3.3 Validation based on Analytical calculations	47
4.3.4 Conclusion.	50
4.4 Case Study of Kamakura	51

5	Risk Assessment Methodology	55
5.1	Risk Assessment Method	55
5.1.1	Risk estimation	57
5.1.2	Probability of flooding P_f	58
5.1.3	Damage Assessments	60
5.1.4	Real discount rate	64
5.2	Conclusion	65
6	Tsunami Risk Quantification for Kamakura	67
6.1	Baseline Risk Quantification	67
6.1.1	Existing protection measures	67
6.1.2	Evacuation Model	69
6.1.3	Risk Assessment	72
6.1.4	Results for baseline risk	74
6.2	Overview of possible interventions	77
6.3	Risk quantification with 1 intervention	77
6.3.1	Dike heightening.	77
6.3.2	Improvement of the evacuation system	80
6.4	Combination of interventions.	84
6.5	Discussions & Conclusions	86
7	Risk Evaluation	89
7.1	Risk Evaluation based on Cost Benefit Analysis	89
7.1.1	Conceptual Model	89
7.1.2	Investment.	90
7.1.3	Optimization of dike heightening	93
7.1.4	Optimization of combined interventions	94
7.1.5	Summary	96
7.2	Risk Evaluation based on Individual Risk	97
7.3	Risk Evaluation based on Societal Risk	98
7.4	Discussion	100
8	Conclusions and Recommendations	103
8.1	Conclusions.	103
8.2	Reflection on Methodology	105
8.3	Recommendations	106
	Bibliography	108
	Glossary	113
	List of Figures	115
	List of Tables	119
A	Method of Regression	121
A.1	Procedure for Method of Regression	121
A.2	Results	122
B	SWASH Computations	125
B.1	Governing Equations	125
B.2	Boundary Conditions	126
B.3	Time series of tsunami waves	126
B.3.1	Solitary wave.	126
B.3.2	N-wave	127

C Wave Formulation and Results 129

C.1 Observation Data 129

C.2 Tsunami wave breaking 130

C.3 Flood parameters from SWASH 130

C.4 Relationship between Dike height & Water level in front of dike. 133

D Discussion on risk quantification 135

D.1 Baseline risk Results 135

 D.1.1 Tsunami Hazard Map 137

D.2 Dike heightening Results 138

D.3 Improved evacuation Results 139

D.4 Combined intervention Results 141

D.5 Societal risk criteria in other countries 143

1

INTRODUCTION

1.1. RESEARCH MOTIVATION

In March 11th, 2011, the Great Eastern Japan earthquake and tsunami devastated the large part of the Tohoku area. Although Japan is a country which is relatively experienced with natural disasters such as earthquakes and tsunamis when compared to other countries, the amount of damage this disaster caused was drastic. Furthermore, even with the world class emergency management, especially in a tsunami prone area such as Tohoku, this disaster resulted in 15,867 casualties and 2,909 still missing as of 2012. From such a destructive event, other coastal areas in Japan fear the possibility of such a large tsunami attack as well.

The Netherlands has the best protected delta in the world, mostly due to that fact that without a good flood risk management policy, more than half of the country would be inundated. Furthermore, the flood risk management in the Netherlands has been at the forefront in flood risk and since the disaster in 1953, the protection standards were defined in terms of overflowing probabilities of flood defenses, and were derived by means of cost-benefit analysis [Jonkman and Schweckendiek, 2015]. Even though this approach has been improved to the use of exceedance probability [van Dantzig, 1956] and still continues to be improved in The Netherlands, a risk-based approach is still missing in the tsunami risk management in Japan, and could be explored in order to protect against future tsunamis. Although it is difficult to include the probabilistic assessment for protection against tsunamis, the cost-benefit analysis can at least be included in the design of tsunami protection measures. These strengths of the flood risk management existing in The Netherlands is preferred to be implemented into the tsunami risk management in Japan.

One approach for improving flood protection is the multi-layer safety system. This system is a "quasi-parallel" system [Jongejan et al., 2012], which aims to optimize the safety of the whole system with a combination of 3 layers. The three layers consist of a layer 1 - prevention, layer 2 - spatial solutions, and layer 3 - emergency management. This system is integrated in the National Water Plan of The Netherlands, and this kind of system could mitigate the damage caused by tsunamis when implemented in Japan. After the 2011 tsunami disaster in Tohoku, a risk management policy for tsunami levels were introduced, categorizing the levels of tsunamis into 2 levels depending on return period and tsunami wave height. Moreover, in some cities along the coast of the Tohoku area, the reconstruction implemented a MLS system with the expectation that this kind of system would allow the disaster risk zones to be substantially reduced. This MLS system designed for Tohoku, however, did not conduct the full probabilistic assessment as done in the Netherlands, and followed the categorizations included in the tsunami risk management policy.

1.2. OBJECTIVE AND RESEARCH QUESTIONS

The objective of this graduation thesis is to design, evaluate and optimize a multi-layered risk-reducing system according to defined and chosen tsunami levels. This thesis will conduct the whole loop of the flood risk management process, and the flow chart for this approach is illustrated in Figure 1.1.

The location to evaluate this multi-layered risk-reducing system will be Kamakura city, a coastal city located along the coast of Sagami bay in Kanagawa Prefecture. As will be explained in more detail later, Sagami Bay has its history of tsunamis, and could be affected greatly from tsunamis due to its short warning time. This system will be evaluated with the individual risk, societal risk and the cost-benefit analysis. It is important to note that Japan still has not included methods of evaluating risk such as cost-benefit analyses or probabilistic assessments in their flood management policies.

The research question for this thesis is:

How can a risk-reducing system be evaluated against future tsunamis for Kamakura?

The sub-questions derived from the above are listed below, they are the outline of the contents of this thesis and will act as a framework to evaluate the risk management of the system.

1. How to estimate tsunami risk of a system?
 - How to model return periods and probabilities of tsunamis?
 - How can tsunami risk be characterized?
2. How to model damage potential of tsunamis?
 - Model a threshold for inundation height for the mobility of people
 - Model a threshold inundation height for the complete destruction of a house or a low rise building
 - How to include the time parameter, to include the warning time and wave propagation speed, in order to optimize the multi-layer safety?
3. How to reduce flood risk?
4. What are the possible design alternative concepts?
 - How to compare and evaluate the current risk with the alternatives?
5. What other applications and relevance are there to other areas?

1.3. APPROACH & METHODOLOGY

To evaluate a risk reduction system for tsunami protection, the following approach seen in the flow chart illustrated in Figure 1.1 is taken.

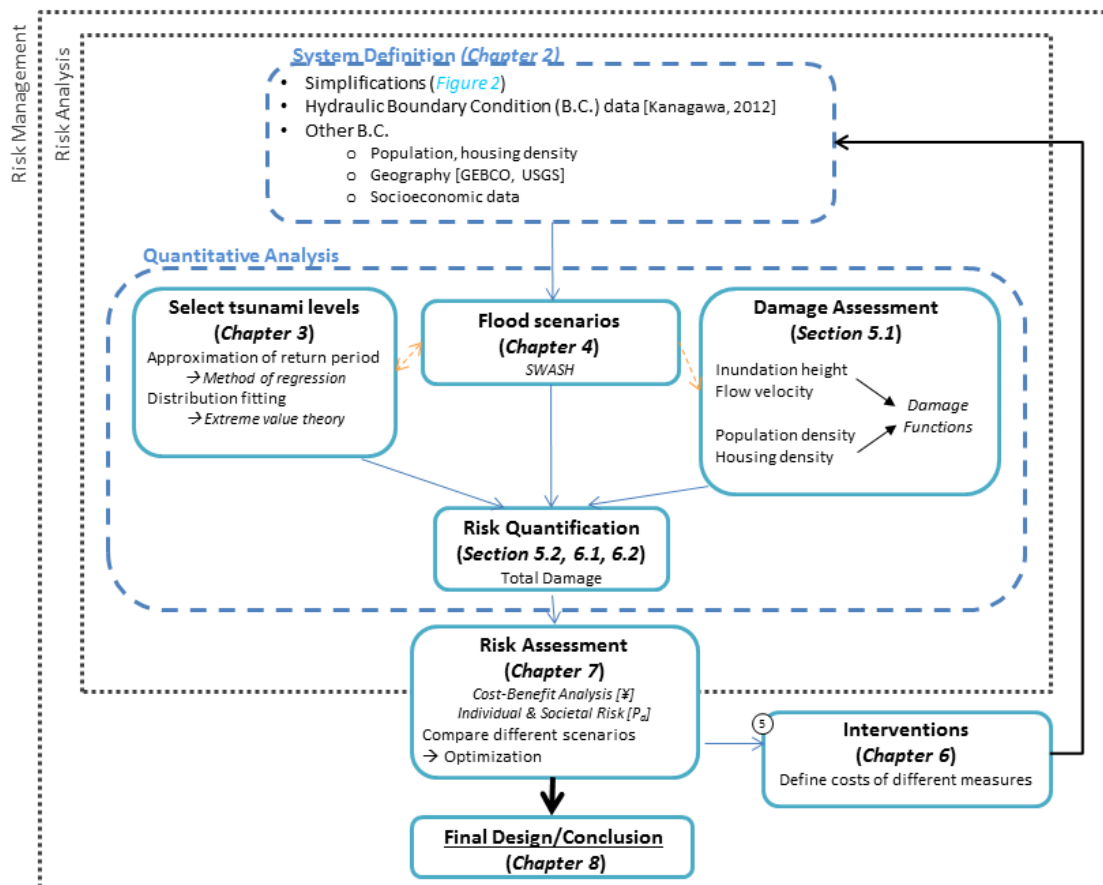


Figure 1.1: Flow chart for tsunami flood risk management

Firstly, the system will be simplified and all the data necessary to set the boundary conditions will be collected. These boundary conditions include tsunami wave height, topography, bathymetry and more.

In the quantitative analysis, the first step is to define the tsunami levels and return periods. This is a very difficult step because tsunami heights and its return periods are strongly dependent on earthquakes, while also being dependent on the bathymetry, location of the fault line, displacement of the fault, and many more factors. Hence the data for the maximum incoming undisturbed tsunami wave heights on the coast, available from simulations of historical tsunamis conducted by [Kanagawa Prefecture \[2012\]](#), will be collected in order to approximate the return periods of past tsunami events. The return periods will be approximated with the regression analysis, and these approximated values will then be fitted with a best-fit distribution from the extreme value theory. Different tsunami levels for Kamakura, including the Level 1 and Level 2 events, will be chosen along this distribution line.

With the tsunami levels defined, the next step is to conduct flood scenarios with these different tsunami levels. A 1-Dimensional (1D) run-up model will be used to obtain important parameters associated with run-up such as flow velocity, inundation height and propagation speed for a given cross-section. For this

step, the SWASH (Simulating WAVes till SHore) model will be used. Here, the effect of the defenses and other interventions can be observed. By knowing the inundation height and flow velocity in different locations, amount of damage on buildings and the loss of life can be estimated. This damage assessment can be carried out by creating a damage function based on the dv (depth-velocity) criteria.

The damage assessment is then followed by the risk quantification which assesses the amount of damage and life loss in monetary terms and in terms of the number of casualties. This is followed by the risk evaluation which analyses different situations (initial condition and interventions) by the cost-benefit analysis (CBA), individual and societal risk. Different interventions, will be considered to determine the amount of risk reduction. This risk management loop can be said to have reached a conclusion when the most optimal intervention based on all evaluation methods is chosen. The final result of the risk-reducing design for Kamakura will be compared with what is being done in Sendai city, Tohoku. Finally, applications and relevance to other areas will be discussed.

1.4. STRUCTURE OF THE REPORT

The system description of Kamakura and Sagami Bay, and the literature study of the research which is related to this thesis will be given in Chapter 2. The flood risk assessment methods used in The Netherlands cannot be directly applied in Japan due to the difference in the hazard, thus appropriate modifications will be made throughout this thesis to still be able to include the advantages of the flood risk management scheme used in the Netherlands.

In Chapter 3, a distribution of the incoming tsunami wave heights with its corresponding return periods will be derived. This process includes the approximation of the return periods from the historical data from the method of regression, and determining the relationship between return period and incoming tsunami wave height from extreme value distribution fitting. Finally, the level 1 and level 2 events, which is the tsunami categorization method used in Japan, will be discussed.

In Chapter 4, the selection of the wave type and boundary conditions to be used for the tsunami model for Kamakura is presented. The assumptions and inputs made for the model will also be introduced here. The physical process of the tsunami development, propagation and run-up will be described in detail, supporting the choice of the type of the wave used for the model. This model will be validated using the Sendai case study, in terms of both observation data and analytical calculation. Finally, multiple flood scenarios for Kamakura, using the boundary conditions which were derived for the model from the Sendai validation results, will be conducted under different tsunami levels.

In Chapter 5, the risk assessment methodology for tsunamis will be introduced. Here, the use of the results from chapters 3 and 4 will be explained. The flood scenarios must be analyzed with the damage functions to obtain damage results in terms of number of casualties or costs. The many assumptions and inputs which will be used for the risk assessment will be introduced here. Furthermore, a brief overview of the different risk evaluation methods (cost benefit analysis, individual risk and societal risk) will be given.

Following the introduction to the risk assessment, Chapter 6 quantifies the risk for the baseline situation and the situations with different interventions. The baseline risk illustrates the risk under the current situation, taking into consideration the existing protection measures. The risk for two different interventions, along with the combination of the interventions, will be quantified as well. In these steps, the main source of damage is determined, and the damage reduction for each intervention is also compared.

With the risks for the baseline and each intervention defined, the total costs, taking into account the direct investments, will be computed using the cost benefit analysis. The individual risk and societal risk will also be evaluated with the results from Chapter 6. The results of the different risk evaluation methods will then be discussed, and finally the most favorable of the considered options will be chosen. This is done in Chapter 7.

In Chapter 8, the conclusions for the thesis will be summarized, and the relevance of this risk management approach to other tsunami risk areas will be discussed. Finally, reflections on the methodology and recommendations for further research will be given.

2

SYSTEM DESCRIPTION OF KAMAKURA, SAGAMI BAY

In this chapter, the general information of the Kamakura area in Sagami Bay is described briefly, and the literature study for this thesis research is presented. Each section introduces the characteristics of Sagami bay and Kamakura, historical records of tsunamis and current research, and an introduction to the concept of the multi-layer safety system.

2.1. BACKGROUND INFORMATION OF SAGAMI BAY AREA

Sagami Bay is located in central Japan, containing both Kanagawa and Shizuoka Prefecture, and it lies approximately 40 km Southwest of Tokyo. The overview of Sagami Bay is illustrated in Figure 2.1.



Figure 2.1: Schematic overview of Sagami Bay

The major cities existing along the coastline of Sagami bay include Odawara, Fujisawa, Chigasaki, Hiratsuka, Ito and Kamakura. The population which would be affected and the unique characteristics of each city are shown in Table 2.1. Most of these cities are visited by many tourists and the existence of large grey structures on the coastline would greatly disrupt the beautiful aesthetics of the ocean, which

is one of its main touristic attractions.

Table 2.1: Information about major cities along the Sagami Bay coastline (Data from 01/09/2015 [[Kanagawa Prefecture, 2016](#)] and 31/12/2015 [[city, 2016](#)])

City	Population	Characteristics
Odawara	194,190 1,710 <i>ppl/km</i> ²	Major commercial center 'commuter town' Major transit point for hot spring resort area
Fujisawa	422,305 6,060 <i>ppl/km</i> ²	Most populated city in Shonan area
Chigasaki	238,629 6,680 <i>ppl/km</i> ²	Located east of Sagami river mouth Coastal area is made of shoals or sandbars 'commuter town'; major tourist spot during summer
Hiratsuka	256,347 3,789 <i>ppl/km</i> ²	Located west of Sagami river mouth Flat plain exists in between major rivers Important factories exist (eg. Nissan Shatai)
Kamakura	173,000 4,400 <i>ppl/km</i> ²	Beach and temples make popular tourist destination 21.93 million tourist in 2014
Ito	71,002 573 <i>ppl/km</i> ²	Tourism is main source of economy Rocky coastline with influence from surrounding volcanoes

Sagami Bay has different coastal characteristics depending on its area. The coast along the Miura Peninsula is a ria coast - a topographical characteristic which caused a very large tsunami wave to form in the Tohoku area in 2011. Furthermore, Sagami bay is located in an area where many tectonic plates meet. The North American Plate, the Pacific Plate and the Philippine Sea Plate meet approximately 300 km away. Not only do the plates meet nearby, there is a Sagami Trough located right outside of the bay area. There is also the Nankai Trough, larger than the Sagami Trough, which is also feared to cause a tsunami along the Honshu island, affecting densely populated cities such as Tokyo and Osaka as well as the cities in Sagami bay. This complex bathymetry of Sagami bay is illustrated in Figure 2.2.

Of the areas in Sagami bay, this thesis will focus on the city of Kamakura. Kamakura is located on the eastern side of Sagami bay, as can be seen in Figure 2.1. The plan view of the Kamakura city coastline is open and concave towards Sagami bay, and it is feared that the tsunami energy will concentrate there and large inundation will occur [[Kanagawa Prefecture, 2016](#)]. This can be justified as Kamakura has experienced quite some damage in the past due to tsunamis. It is also important to protect Kamakura because it is one of the most popular touristic locations for inhabitants of Tokyo, and especially in the summer, many people enjoy the beach and activities which are held very close to the coastline. To give an idea, in 2014 there were 21.96 million tourists recorded to have visited Kamakura [[Kamakura City, 2014](#)].

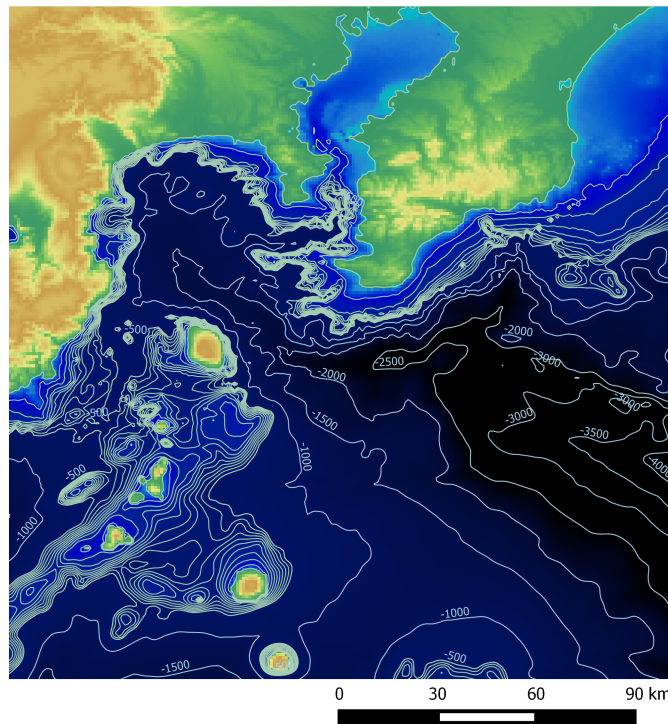


Figure 2.2: Bathymetry of Sagami Bay

2.1.1. HISTORY OF TSUNAMIS IN KAMAKURA

There have been several tsunamis recorded in the history of the Sagami Bay area, which of course also had influence on Kamakura. The characteristics of these tsunamis are briefly summarized in Table 2.2.

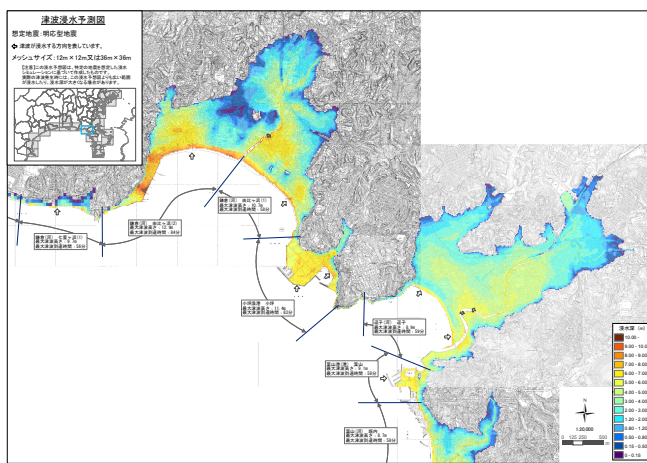
Table 2.2: History of earthquakes which resulted in tsunamis in Sagami bay [Kumagaya, 2011]

	Year	Name of Event	Magnitude	Type of Earthquake	Damages & Casualties
1	1498	Meiou	8.4	normal fault	- \approx 200 casualties - causes largest damage - Kamakura Buddha destroyed
2	1605	Keicho	8.5	normal fault	- \approx 153 casualties - 4-5 m tsunami at Misaki
3	1633	Sagami Bay	7.0	-	-
4	1703	Genroku	7.9 - 8.2	reverse fault	- \approx 600 casualties in Kamakura
5	1782	Sagami Bay	7.0	-	-
6	1854	Ansei Tokai	8.4	-	- 7 m tsunami at Shimoda - 20+ casualties in Kamakura
7	1923	Kanto	7.9	-	- Subsidence recorded in Chigasaki - 12 m tsunami at Atami

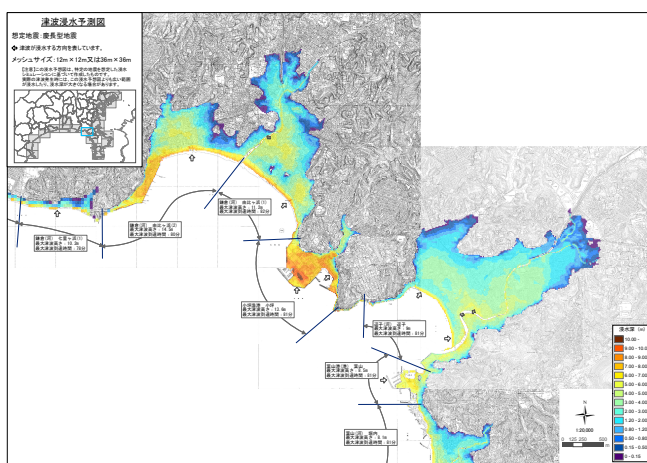
Of these historical tsunamis, the most destructive ones were the Meiou tsunami, Keicho tsunami and

Genroku tsunami. Furthermore, these tsunamis occurred a very long time ago, so there is a lack of data, especially on exact values of inundation height, run up height, evacuation time, casualties and more. However, after the 2011 Tohoku tsunami, the Kanagawa Prefecture Government created tsunami hazard maps with numerical simulations, recreating the past tsunami events. This was done in order to observe the amount of possible damage caused by tsunamis affecting the coastal cities of Kanagawa. The tsunamis were simulated with the current bathymetry and topography. The hazard map for the Meiou, Keicho and Genroku event, chosen specifically for Kamakura area, can be seen in Figure 2.3. When viewing the expected inundation for the Genroku Earthquake, it is interesting to keep in mind that it has the same plate movement, a downward movement called subduction, as the disastrous tsunami of 2011 in Tohoku.

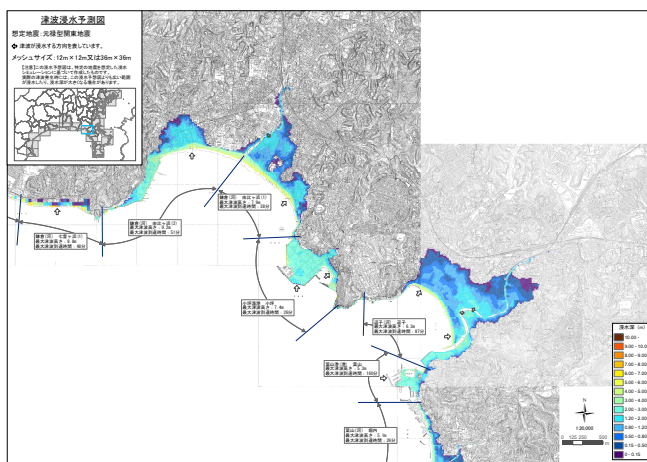
It is important to note that these tsunamis have different characteristics. On one hand, Meiou has a relatively high expected maximum inundation height of 14.5 m but a longer expected warning time of 58 minutes, allowing more time for the people to evacuate. On the other hand, Genroku has a lower maximum expected inundation height of 9.5 m, but a much shorter warning time of 28 minutes. Which scenario is the more dangerous one is difficult to assess without research.



(a) Meiyou Earthquake



(b) Keicho Earthquake



(c) Genroku Earthquake

Figure 2.3: Tsunami hazard maps for earthquake simulations under current bathymetric and topographic conditions [Kanagawa Prefecture, 2012]

2.1.2. EXISTING FLOOD PROTECTION MEASURES IN KAMAKURA

The most recent tsunami in Kamakura was in 1923 which is almost 100 years ago, hence the current generation in Kamakura have not experienced a tsunami in their city before. Even with this disadvantage, the awareness of tsunamis and the evacuation process is well implanted in the peoples' behavior, as evacuation measures for different disasters are taught starting in primary school. Furthermore, after 2011 the Kanagawa Prefectural Government has been working hard to improve the readiness to possible future tsunamis.

The plan view of the coastline of Kamakura is shown in Figure 2.4a. In some parts the protection is a combination of a sea wall with an elevated road, while in other parts, especially where there are beaches, the road is situated on a dike located behind the beach. The sea walls and dikes are on average approximately 3 m high, as can be seen in Figure 2.4b. In front of the beach, there are no breakwaters or flood defense structures. This reason is the high touristic value of the beach, so large concrete or earthen structures would not be acceptable. There are also four small river mouths with gates located along the coast, one of which can be seen on the bottom of Figure 2.4b.



(a) Existing protection structures [Google Earth, 2016]



(b) Sea wall behind Shichirigahama Beach [Fujisawa Civil Engineering Office, 2015]

There are currently no plans for drastic changes in the spatial use of disaster prone areas, however, the Kanagawa Prefectural Government has made a brochure of a tsunami hazard map with the locations of evacuation centers. This allows both the citizens of Kamakura city and the tourists to know their closest evacuation center and which areas are less prone to flooding in case of a tsunami [Kamakura City, 2012].

2.2. INTRODUCTION TO TSUNAMIS

A tsunami is a wave, or series of waves in a wave train, generated by the sudden, vertical displacement of a column of water [Bryant et al., 2008]. The term *tsunami* is Japanese where *tsu* means harbor, and *nami* means wave. Tsunamis are directly related to the movement of plate tectonics. These plates have converging, diverging and sliding movements which generate an enormous amount of energy. A tsunami which is generated from a slip in the plate is illustrated in Figure 2.5. To explain the process in the figure in more detail: (a) the two plates interact, (b) strain between the plates build up and slowly the distortion of the upper plate occurs, (c) the energy built up between the plates is released and the plate deflects, and (d) the tsunamis caused by the plate deflection spread in both directions perpendicular to the fault [Arcas and Segur, 2012].

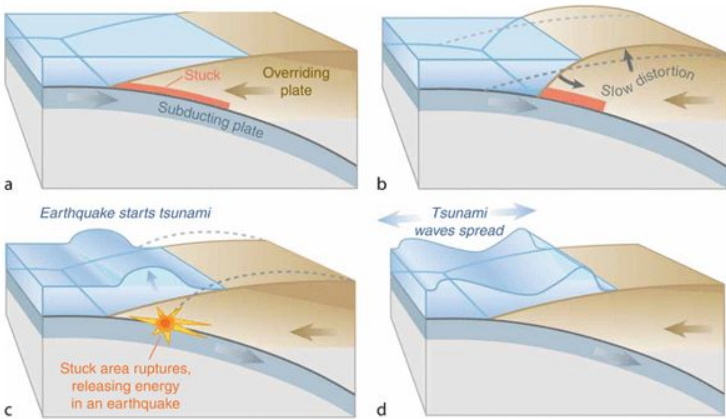


Figure 2.5: Tsunami Mechanism [Arcas and Segur, 2012]

One of the factors which determine the size of the tsunami is the magnitude of the earthquake. There are general guidelines in accordance with the procedures of the Pacific Tsunami Warning Center illustrated in Table 2.3, which should give an idea of the relationship between earthquake magnitude and tsunami size. From the table, it is clear that although the areas near Japan are prone to experience many earthquakes, only a few of them cause tsunamis. Other factors which affect the generation of a tsunami is the type of earthquake - thrust as opposed to strike-slip - and the water depth which is displaced at the moment of the event. The length and the width of the fault plane is also a factor.

Table 2.3: Guideline of tsunami scale relative to earthquake magnitude *Procedures of the Pacific Tsunami Warning Center* [USGS, 2016]

Size of Earthquake (Magnitude)	Resulting Tsunami Characteristic
$M < 6.5$	Unlikely to trigger a tsunami
$6.5 < M < 7.5$	Non-destructive tsunami, but secondary effects (landslides, etc.) can cause damages
$7.6 < M < 7.8$	May produce destructive tsunami near epicenter
$M > 7.9$	Destructive local tsunamis near epicenter & broader region, aftershock can also cause problems

2.2.1. TSUNAMI WAVE MODELLING

Tsunamis are long waves with very large wave periods which range from 10 to 20 minutes. Since the wavelength of a tsunami is also long, the ratio to water depth is very small. For this reason, even in deep water, tsunamis can be considered a shallow water wave, and the propagation speed can be expressed in the simple form of $c \approx \sqrt{gd}$ [Battjes and Labeur, 2014]. Similar to all other waves, tsunamis change as they propagate due to reflection, shoaling, diffraction and refraction [Jager et al., 2013]. In the case of this thesis, changes to the wave caused by these phenomena will be not be studied in detail and the main focus will be on tsunami run up, and its resulting inundation height and flow velocity.

Tsunamis can be modeled as a solitary waves, by means of long wave approximation, N-wave theory and more. There are many discussions of which approximation is the most accurate, and for the case of solitary waves, some argue that the tsunamis never fully develop as a solitary wave before arriving on land [Madsen et al., 2008]. Moreover, the amount of run-up resulting from a tsunami is still difficult to calculate analytically, but an important "run-up law" for solitary waves [Synolakis, 1987] and N-waves [Tadepalli and Synolakis, 1994] gives a first estimate of the run-up. The equation for the solitary wave run-up is:

$$\frac{R}{d} = 2.831 \sqrt{\cot \beta} \cdot \left(\frac{H}{d} \right)^{5/4}$$

Here, R is the vertical run-up height [m], d is the water depth of where the tsunami started [m], β is the linear slope of the shore, and H is the height of the tsunami wave [m]. This equation is derived from the shallow water equations and has been tested in laboratory flumes for validation. The equation for the N-wave just differs by the constant on the right side of the equation to be 3.86 instead of 2.831. This "run-up law" is still used to validate newly developed numerical models for tsunami run-up.

For the case of this thesis, the SWASH (Simulating WAVes till SHore) software, a hydrodynamic model for simulating non-hydrostatic, free-surface rotational flows [The SWASH team], is used to model tsunamis. Also, the complex bathymetry and topography can be included in the model, allowing a more realistic result for run-up than with a linear slope.

2.2.2. CURRENT TSUNAMI RESEARCH

The tsunami risk management in Japan was traditionally based on historical data or expected earthquakes, not on worst-case scenarios. The flood defenses were also designed based on the previously occurred extreme event. Therefore, this does not take into account the return period, or the tendency of one event occurring more often than another. This was seen in flood protection structures existing in the Tohoku in 2011 where storm resilient structures existed but should have been tsunami resilient. Although the Japanese flood risk management has improved after 2011, there is still no risk-based approach or cost-benefit analysis incorporated. Here, a risk-based approach refers to the approach for flood defences which are used in the Netherlands. This approach considers the probability of failure due to water levels, based on the data extrapolated from historical events, and designs according to a chosen failure probability. This can be altered for tsunamis, where the water level can be replaced by wave heights, and also simplify this approach by only considering overtopping and or overflowing, which is the main cause of failure for tsunamis. Moreover, the quantified risk can then be evaluated by a cost-benefit analysis based on the benefits and the costs which would result from the project, as well as acceptable risk levels. This will be further discussed in Section 2.3.

The flood risk management was improved due to the issue of frequent tsunamis and its severity, and two different tsunamis levels have been identified [Shibayama et al., 2013]. These levels are chosen based on political decisions, with some insight from coastal engineers from governmental institutes [Miguel Esteban, personal communication, June 6 2016]. Level 1 events have a return period of several decades to 100+ years while Level 2 events would be more rare, taking place at intervals between every few hundred

to a few thousand years apart. Furthermore, the idea that hard measures can always protect against the loss of life has been discarded, and instead, the objective of coastal structures would thus be to attempt to protect human lives and property only against Level 1 events. Additionally, evacuation buildings and tsunami shelters will be designed taking into consideration Level 2 events in order to prevent overtopping during the most extreme events. This Level 2 event also implies no structural failure will occur on the primary defenses, such as breakwaters and dikes, although overtopping and overflowing can be observed, and this hydraulic behavior would affect the risk for people behind the defenses. These levels are a very broad categorization, and are chosen mainly with respect to political reasoning.

One of the reasons tsunamis have only been categorized into 2 levels and not designated return periods is because of the low frequency of occurrence. To accurately extrapolate or interpolate return periods, there must be a sufficient amount of data, however, as you can see in Table 2.1, Sagami bay has only experienced 7 tsunamis. This is a similar problem which is experienced when approximating the levels of hurricanes. For tsunamis, however, it is a bit more complex as the knowledge on seismic studies is also necessary.

Consequently, tsunamis were not only categorized into levels of events based on return period, but also different levels based on risk to human life [Yamano et al., 2015]. This level of risk to human life is calculated with the following equation.

$$r = 5.68 \log H - 0.03t - 1.05$$

Here, r is the potential risk to human life, H is the maximum tsunami height [m], and t is the time for the maximum tsunami wave height to arrive to each location [min]. This potential risk to human life r only takes into consideration H and t . This equation is obtained empirically from the casualty data of the Tohoku 2011 tsunami, and aims to give an idea of the scale and destructiveness of tsunamis based on the maximum tsunami height and maximum wave height arrival time. The different categories are illustrated in Table 2.4.

The main factors which influence the casualties are inundation height and tsunami arrival time. The conclusion of this analysis was that the most important consideration is to have enough time for residents to evacuate before the defenses are overcome. This calculated risk provides three categories of tsunamis, followed by the damages and casualties for each level. These categorizations can give a rough indication of which areas are at greater risk for casualties, and where the improvements of tsunami protections should be prioritized.

Table 2.4: Tsunami categorization in Japan for different levels of risk to human life r [Yamano et al., 2015]

Category	Risk of Human Damage (r)	Rate of Death in Inundated Areas (% of People Who Died)	Notes
0.00	$r < 1$	Almost none	Minor damage to fishery and tourism infrastructure (boats, beaches, hotels, etc.) Depending on the situation, some limited human casualties
1.00	$1 \leq r \leq 2$	0.01 - 1.99	Start of human casualties
2.00	$2 \leq r \leq 3$	2.00 +	Medium to catastrophic damage to human settlements and population

2.3. MULTI-LAYER SAFETY SYSTEM

In the following sections, the general information regarding the multi-layer safety is given, along with the risk evaluation schemes and damage assessments. Finally, the multi-layer safety system which was implemented in Sendai will be given as an example of tsunami flood protection in Japan.

2.3.1. GENERAL INFORMATION

Multi-layer safety (MLS) is a flood risk management concept that introduces the integration of probability-reducing and loss-mitigating measures in a flood protection system. This term is mainly used in the flood risk management in the Netherlands, and is also included in their National Water Plan. The multi-layer safety classifies measures into 3 safety layers (Figure 2.6):

- Layer 1 - Prevention
- Layer 2 - Spatial Solutions
- Layer 3 - Disaster & Emergency Management

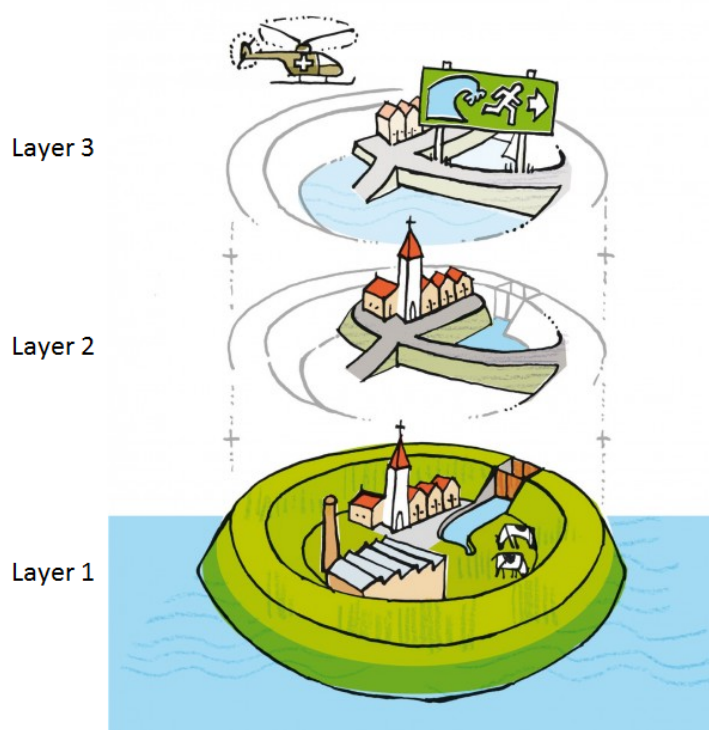
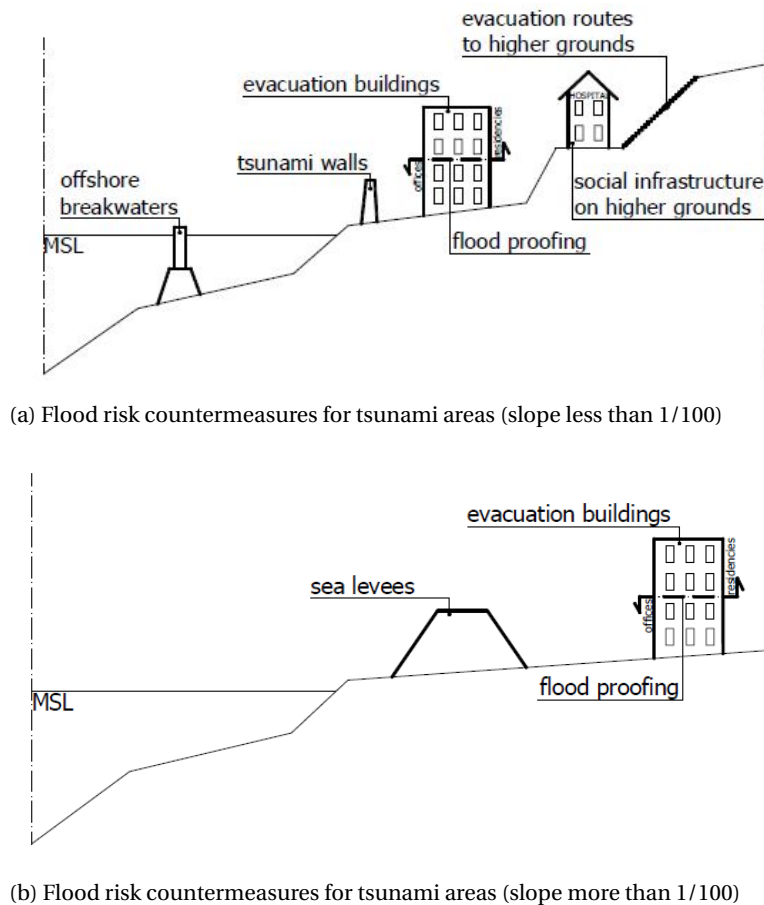


Figure 2.6: Schematic overview of a Multi Layer Safety (MLS) system

This system is neither series nor parallel - it is a 'quasi-parallel' system [Jongejan et al., 2012]. This means that if one layer fails it could have the whole system fail but it could also not have the whole system fail, so there is no perfect representation for the system. To give an overview of each of the layers in the MLS system, Layer 1 prevents river or sea water from inundating areas which are usually dry. This is done by building a flood defense structure or by preventing the cause of inundation. Layer 2 decreases the loss by spatial planning and adaptation of buildings when a flood occurs. Finally, Layer 3 focuses on the organizational preparation for floods such as disaster plans, hazard maps, early-warning

systems, evacuation, temporary physical measures such as sand bags, and medical help when needed [Tsimopoulou et al., 2012]. This layer considers measures for before, during and after a flood occurs. A multi-layer safety system for a tsunami for Japan with a leading edge coastline will be schematized as illustrated in Figure 2.7. In the following sections, possible measures for each layer is introduced in more detail.



(a) Flood risk countermeasures for tsunami areas (slope less than 1/100)

(b) Flood risk countermeasures for tsunami areas (slope more than 1/100)

Figure 2.7: Flood risk countermeasures for tsunami areas [Tsimopoulou, 2015]

Furthermore, this MLS system must be assessed through a cost-benefit analysis and meet requirements for acceptable risk levels to optimize the combinations of the measures. This is what is done in the flood management in the Netherlands, but it must be adjusted in order to be able to be implemented into Kamakura.

2.3.2. COST-BENEFIT ANALYSIS

Cost-benefit analysis (CBA) is a decision-making tool used to evaluate all types of projects. The practical development of the CBA came as a result of an act which required the U.S. Corps of Engineers to carry out projects for the improvement of waterway system when the total benefits which would result from the project exceeds its cost. In the Netherlands, the cost-benefit analysis is used to economically optimize a project, taking into consideration the flooding risk and the cost of a preventive measure such as dike raising. This allows the design of the dike to be within the acceptable thresholds and costs from a political point of view [Jonkman and Schweckendiek, 2015].

The CBA uses a social optimisation criterion, the maximization of the net economic benefits over the total affected individuals, which can be calculated in the form of a net present value as follows:

2

$$NPV = \sum_{t=0}^{\tau} (B_t - C_t) \cdot d_t$$

Where, NPV = net present value [μ (=monetary unit)], τ = planning period [years], B_t = benefits in year t [μ], C_t = costs in year t [μ], and d_t = discount factor. The costs represent the amount of damage and loss of life in monetary terms, while the benefits can be expressed in the amount of risk reduction which resulted from a given investment. The discount factor can be calculated as,

$$d_t = \frac{1}{(1+r)^t}$$

Where, r = annual discount rate. The CBA aims to include all consequences that can be given economic value, but there are some disagreements to which consequences are quantifiable. For example, indirect economic evaluation make it possible for intangible goods such as human life to be assigned a monetary value which may affect people's moral judgment. Despite these arguments, these will be included in the cost benefit analysis when looking at casualties, as it may reflect the importance of protecting a densely populated coastal city like Kamakura.

2.3.3. INDIVIDUAL & SOCIETAL RISK

The level of risk to life is commonly evaluated from two perspectives in the Netherlands: that of the individual and that of the society [Vrijling et al., 2014]. Individual risk is concerned with the distribution of the probability of danger over the population, while societal risk is concerned with the large scale effects throughout the economic and social life. Individual risk, which prevents that certain people are exposed to disproportionately large risks, is computed in the following way [Jonkman and Schweckendiek, 2015].

$$IR(x, y) = \sum_i P_{f,i} \cdot P_{d|f}(x, y) \quad (2.1)$$

Where, IR is the probability that a person gets killed due to a flood at a certain location, $P_{f,i}$ is the probability of the flood scenario, and $P_{d|f}$ is the probability of being killed given that flood scenario. Individual risk has an acceptable risk limit value, which the computed value cannot exceed, but it differs depending on the hazard.

Societal risk, which optimizes the total level of risk, is often represented by the FN-criterion. This FN-criterion is assessed by a limit line for different safety levels which can be represented mathematically as,

$$1 - F_{N_{dij}}(n) < \frac{C}{n^2} \quad (for \ all \ n \geq 10) \quad (2.2)$$

In which, $1 - F_{N_{dij}}(n)$ is the exceedance frequency of the number of fatalities in a year as a results of a tsunami in a given location, n is the realisation of N_{dij} and the steepness of the limit line, C location of limit line, and N_{dij} is the number of people dead in a given location as a result of a tsunami. Here, the desired level of safety is balanced against the cost where a more stringent criteria would be required [Vrijling et al., 2014].

2.3.4. DAMAGE ASSESSMENT APPROACHES

To conduct the risk evaluations, whether it is by the CBA, individual or societal risk, there must be damage assessments for the tsunami events. The damage assessments can look at many factors, but for this thesis it will look at the two main factors: damage to residential buildings and the loss of life.

One approach for assessing damage to buildings is looking at the threshold of inundation depths. The allowable inundation height of course depends on the construction style of the building [Shuto, 1993].

This approach was further updated by combining the load of inundation depth and the flow velocity to estimate the damage from a flood. This depth-velocity (dv) product is considered as a critical variable for damage of residential buildings [Pistrika and Jonkman, 2010]. The physical background of the dv product is related to the definition of flow momentum, and is illustrated in the equations below.

$$\text{Momentum} = \text{mass} \times \text{velocity} = \text{density} \times \text{volume} \times \text{velocity} \Rightarrow$$

$$\text{Momentum} = \text{density} \times \text{flooded horizontal area} \times (\text{depth} \times \text{velocity})$$

During a flood, the maximum values of depth and maximum values of velocity do not need to have occurred simultaneously, therefore, $d_{\max} v_{\max} > (dv)_{\max}$. The criteria for structural damage to buildings relative to the dv values and velocity are illustrated in Table 2.5.

Table 2.5: Criteria for structural damage to buildings based on analysis of New Orleans [Pistrika and Jonkman, 2010]

Velocity [m/s]		dv value [m ² /s]	Damage Levels
$v < 2$	OR	$dv < 3$	"inundation damage"
$v > 2$	AND	$3 < dv < 7$	"partial damage"
$v > 2$	AND	$dv > 7$	"total destruction"

For the damage assessments for the loss of life, the capability of evacuating becomes very important. The ease of evacuation is further improved when the location of evacuation centers are clear and evacuation routes are short before a tsunami occurs. This also strongly depends on a time parameter which relates to the arrival time of the tsunami, and its propagation speed. Inclusion of a threshold of mobility in the damage assessment would directly influence the capability of evacuating.

Research on human instability in flood flows have been done, and is categorized into two physical mechanisms: moment instability (toppling) and friction instability (sliding). A criterion for these human instabilities in floods were derived from empirical analyses in the past work, but here it is distinguished by three hydrodynamic mechanisms - moment, friction and floating [Jonkman and Penning-Rowse, 2008]. To simplify this mechanism, similar to the case for residential buildings, the depth-velocity dv criteria will be used. This is more clearly illustrated in Table 2.6.

Table 2.6: Criteria for Loss of Life [Jonkman and Penning-Rowse, 2008]

dv value [m ² /s]	Stability
$dv < 0.5$	"stable"
$0.5 \leq dv < 2$	"practical instability"
$dv \geq 2$	"instable"

Based on Table 2.6, for the damage assessment of the loss of life, it is assumed that if the dv value ranges in the "instable" values, the mortality is 100%. Practical instability refers to the state at which people will experience difficulties in walking through the water [Jonkman and Penning-Rowse, 2008], thus, not being able to evacuate efficiently. For the case of a CBA, this would mean to put a value on human

life and while this may be a subject of controversy, it could prove important to do it since Kamakura is so densely populated. In the Netherlands, the typical value for the cost of human life used for water related hazards is €6.7 million [Deltares, 2011]. This is much higher than the cost of human life of €2.1 million in Japan, which is derived from the amount of compensation in the occasion of a death.

2

2.3.5. MLS SYSTEM IN SENDAI, TOHOKU

Sendai city is one of the largest cities located in the southern half of the Tohoku coastline. It is characterised by low-lying coastal plains with mild-sloped sandy beaches located in front of them, resulting in a longer warning time compared to the ria coastline in the Northern part of Tohoku, where the rias have fjord-like coastal inlets and the shallow coasts slow the tsunamis down as it starts with very large speed in deep water.

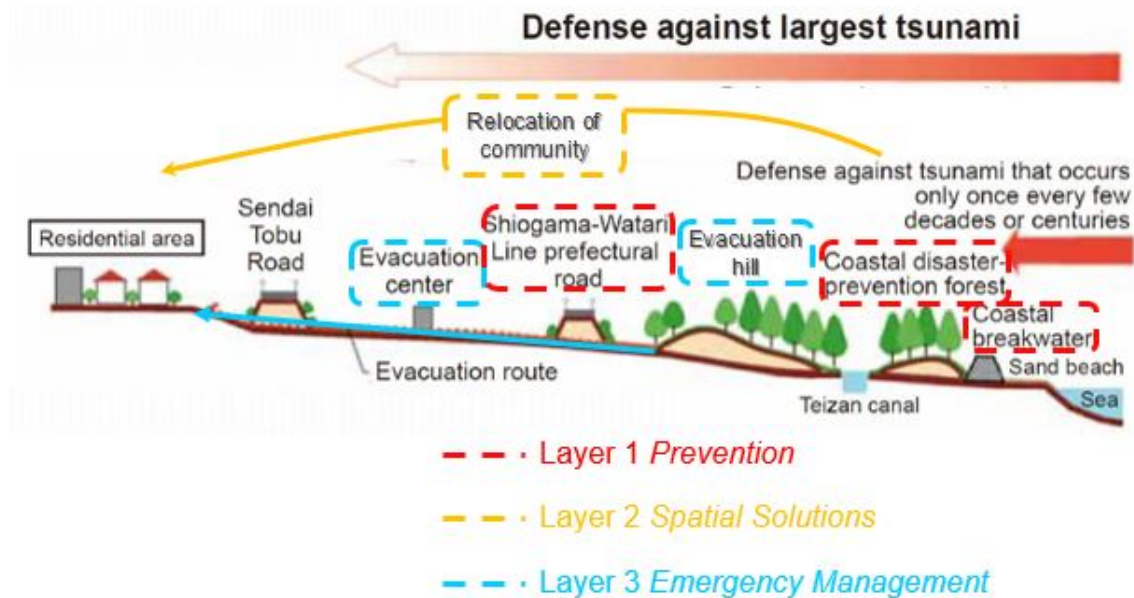


Figure 2.8: Cross-sectional view of an MLS system in Sendai, Tohoku [Sendai City Post disaster reconstruction division, 2011]

The flood protection in Sendai city before the disaster in March 11, 2011 consisted mainly of seawalls and coastal dikes based on the most extreme event in the past which was at most 3 - 6 m. However, the tsunami in 2011 had a maximum inundation height of 19.5 m, and the tsunami propagated as a bore for approximately 4 - 5 km inland. Furthermore, it was only after the event that it was discovered that the main cause of failure of dikes from tsunamis was due to the scour at the toe of the dike once the dike was overflowed. Due to these reasons, Sendai city was severely affected by this tsunami. Sendai had dikes built behind the beaches to protect against storm surges and high waves, but none that was specifically meant to protect against tsunamis. To have better protection for future tsunamis, a MLS system is currently being implemented and constructed with hope that an integrated approach will mitigate the damage caused by tsunamis. Some of the measures applied in Sendai city are illustrated in Figure 2.9 along with the cross-sectional view of all of the measures in Figure 2.8, and is also explained in detail below.

Layer 1 measures in Sendai include the coastal embankment (coastal breakwater) also seen in Figure 2.8, the coastal disaster-prevention forest, and the Shiogama-Watari line prefectural road. All of these



Figure 2.9: Construction of MLS system in Tohoku: Embankments along the coast and ground heightening in the disaster risk zones [BBC, 2016]

measures were designed as a defense against a Level 1 event. The coastal and river embankments were raised by approximately 2 m, and the prefectural road which was not elevated before, is now elevated by 6 m. Having both the coastal embankment and the elevated prefectural road allows the disaster risk zone to be substantially reduced. In some areas of Tohoku, the primary defense has been built to be approximately 15 m as shown in Figure 2.9 (left and center).

As most of the coastal areas of Sendai was severely damaged by the tsunami in 2011, most of the city was no longer intact. This allowed layer 2 measures to be built flexibly, without the need to consider the resettlement of houses and interfering with infrastructure when implementing new spatial solutions. Therefore, layer 2 measures mainly focused on the building houses away from the disaster risk areas and restoring damaged residential land by heightening them. The vast area which went under ground heightening can be seen in Figure 2.9 (right).

Layer 3 measures are what Japan is most reliable on as people are educated from a young age about evacuation procedures, thus many measures are made as an addition to what already exists. Roads specifically built for evacuation are constructed from the coast to inland, more high ground evacuation centers are made in the disaster risk areas, and many more. It is worth noting that in Japan where disaster awareness is high, layer 3 measures, which could increase the efficiency of evacuation, have an important role in reducing casualties.

These preventive measures were designed according to this categorization of a Level 1 event which was created after the 2011 tsunami, however, a cost benefit analysis was not conducted. Thus, the costs for reconstruction is not economically optimized. The reconstruction costs for Sendai are not openly available. An example of the reconstruction costs is given for Otsuchi town, where the town is said to receive 100 billion yen (800 million euros) from the national government [Esteban et al., 2015]. Although the scale of the areas are different, this gives an idea of the amount of money which is spent by the national government for the areas affected by the tsunami.

2.4. CONCLUSION

After the disastrous tsunami in 2011 which struck the Tohoku area located in the North of Japan, tsunamis were categorized into 2 levels: Level 1 event and Level 2 event [Shibayama et al., 2013]. Level 1 events have a return period of several decades to 100+ years, and hard measures are built according to this level in order to protect human life and property. Level 2 events are more rare, and have a return period of few hundred to a few thousand years. This level allows overtopping and overflowing of the primary defenses, but implies no structural failure will occur to those defenses. These categories were developed as it is very difficult to assign return periods for tsunamis, but is hoped to be a start to including a probabilistic assessment in tsunami risk assessment. The inclusion of a probabilistic assessment means to define tsunami wave frequencies and determine the possible damages as a result of tsunamis, in order to estimate annual risk. However, the flood risk assessment within Japan still does not include cost-benefit analyses and setting acceptable risk levels, which is a integral part of the risk assessment.

The area of interest covers Kamakura, a city which has a open and concave coast and is located in Sagami Bay. Kamakura has a population of 173,000 people, and have recorded 21.93 million tourists in 2014. Not only are there a large number of people to protect, Kamakura is also the historical capital of Japan, having a large amount of historically valuable infrastructure, for example 174 shrines and temples, within the city. Kamakura has experienced seven tsunamis in its history, but unfortunately, most of the tsunamis do not have reliable data available as it occurred too far in the past. However, the Kanagawa Prefectural Government conducted numerical simulations in order to determine the possible inundation of Kamakura.

Tsunamis are sensitive to the bathymetry, changing the resulting inundation height and run-up for different cities along the coast from the same earthquake. The bathymetry for Kamakura is similar to the that of North Tohoku where large tsunami waves were recorded in the 2011 event. Moreover, the concave coast is believed to concentrate the tsunami energy, resulting in higher inundation heights.

The multi-layer safety (MLS) system is an integrated approach to flood risk management which is used in the Netherlands. This flood risk management concept is a 'quasi-parallel' system which integrates the probability-reducing and loss-mitigating measures in a flood protection system. The MLS system will be adjusted in order for it to be implemented for tsunamis in Japan. The tsunami risk-reducing system will be optimized by doing a cost-benefit analysis based on different criteria available for damages on houses and casualties. The criteria for the damage on buildings is the $d\nu$ relationship, which illustrates the amount of damage caused on buildings based on the inundation depth and velocity. The other criteria for human instability relating to casualties in floods, illustrates the two different types of instabilities and the mobility limit also using the d and ν -values.

3

TSUNAMI CATEGORIZATION

In this chapter, the method of determining the distribution of incoming tsunami wave heights, which will later be used for the risk assessment, is illustrated. Firstly, the historical tsunamis and their characteristics are looked at in more detail to get a better overview. Secondly, the method of approximating the return period based on historical tsunamis is explained. Finally, the best-fit extreme value distribution will be fitted to the approximated plots derived from the second step. The details of approximating the return period with the method of regression and distribution fitting, along with other statistical analyses, can be found in Appendix A.

3.1. HISTORICAL TSUNAMI EVENTS & THEIR CHARACTERISTICS

In the previous chapter, the overview of the historical tsunami events in Sagami Bay were given. This information will be expanded with the differences in the earthquakes and their predicted earthquake return periods. By doing this, the seven different tsunamis can be categorized into three types as illustrated in Table 3.1.

Table 3.1: Troughs/Faults and Approximated Return Periods for historical earthquakes which resulted in tsunamis [Kumagaya, 2011] [Kanagawa Prefecture, 2012]

<i>Name of earthquake</i>	<i>Year</i>	<i>Magnitude</i>	<i>Earthquake Fault/Trough</i>	<i>Approximate Return Period (years)</i>
Genroku	1703	7.9 - 8.2	Sagami Trough	2300
Kanto	1923	7.9	Sagami Trough	200 - 400
Sagami Bay	1633, 1782	7.0	West Sagami Fault	70
Meiou	1498	8.4	Nankai Trough	-
Ansei-Tokai	1854	8.4	Nankai Trough	119
Keicho	1605	8.5	Bousou Fault/Nankai trough	-

The Meiou and Keicho earthquakes have occurred too long in the past, and do not provide a distinct return period. Although the return periods for these earthquakes are given, these values are not reliable enough to be used for categorizing tsunami event based on return periods, also because these are return periods for earthquakes and do not necessarily directly correspond to those of the tsunamis. Instead of looking at the return periods for earthquakes to define tsunami return periods, using the data on the incoming tsunami wave height on the coast given by the Kanagawa Prefecture [2012] and approximating return periods based on that is assumed to have less uncertainty as the link between earthquakes return periods and tsunami return periods has not been clearly defined yet. By looking at the relationship

between incoming tsunami wave heights on the coast and their return periods, the influence of factors which are unique to each area, such as the effect of bathymetry, can be included. Although all of these earthquakes in Table 3.1 have differing faults and earthquake return periods, the incoming tsunami wave height are all within a range from each other. Hence, this variable will be used to approximate the return period of tsunamis.

Currently in Kamakura, there is no value set for a Level 1 and Level 2 tsunami event. However, the Kamakura Municipality have created hazard maps and evacuation plans from the expected maximum tsunami height based on historical tsunami events. This representative 'worst-case scenario' provided by the government is simulated from the Meiou earthquake and tsunami.

3

3.2. METHOD OF REGRESSION

To overcome the high uncertainty with the earthquake return periods given in Table 3.1, the method of regression for extreme values will be used to correlate the incoming tsunami wave height and return period.

The method of regression is the most basic and commonly used statistical analysis, and is used to describe data and explain the relationship between one dependent variable and one or more independent variables. This method is a good approximation for determining return periods, however, the distribution model must be selected properly. The advantage of this method is its simplicity of fitting a single line after deriving its return period to a selected distribution model, and the accuracy increases with more data available. The disadvantage of this method is that the analysis is highly dependent on the selected distribution, and that this analysis can underestimate the fit especially when there is a lack of data. Moreover, the regression model becomes very inaccurate when forecasting data far from the range. The extrapolation is limited to double the number of years data was recorded $2n$ [van Gelder, 2015]. However, others state more abstract definitions, limiting the extrapolation not far from the number of years recorded n [Dallal, 2012]. As an example, with the extrapolation limit given by van Gelder [2015], if 500 years of data is measured, the extrapolation is limited to 1000 years. It is worth noting though that currently in the Netherlands, there is 100 years of data but is extrapolated to 10000 years of return period, hence, the extrapolation limit could also be said to be $100n$.

In the case for tsunami events, the Gumbel regression analysis is used to approximate the return period. Tsunamis can be categorized as extreme value events, and does not have to have continuous data to make an approximation [Savenije, 2007]. Thus, given the number of years of recorded data, the tsunami wave heights of the events are ranked. The Gumbel method of regression computes the probability of exceedance using this formula:

$$p = \frac{m}{n+1} \quad (3.1)$$

Where p is the probability of exceedance, n is the total number of years in the record, and m is the rank number of the event. The return period T can then be computed as,

$$T = \frac{1}{p} \quad (3.2)$$

This Gumbel method of regression is often used to analyze wave records for short waves, and other uses include hydrological data. Since the focus is on tsunamis, the fact that it is used for data on short waves could be seen as promising. This method will be conducted for tsunamis in Kamakura, and will be explained in Section 3.3.1.

3.3. EXTRAPOLATING TSUNAMI RETURN PERIODS

The return period is approximated with the method of regression, and these approximated return periods will be plotted and fitted with the best fit extreme value distribution curve. The chosen best fit curve will be used to determine the relationship between return periods and incoming tsunami wave heights on the coast for Kamakura throughout this thesis.

3.3.1. RETURN PERIOD APPROXIMATION

The coastline of Kamakura is separated into four sections as illustrated in Figure 3.1. This allowed for more data plots and included the variations of incoming wave heights along the coastline. The maximum incoming tsunami wave height on the coast for each section is given in the tsunami hazard map [Kanagawa Prefecture, 2012], and these maximum incoming tsunami wave heights will be analyzed with the method of regression. The maximum incoming tsunami wave heights for each section along the coast of Kamakura corresponds to each historical tsunami event are illustrated in Table 3.2.



Figure 3.1: Coast of Kamakura separated into sections [Google Earth, 2016]

Table 3.2: Expected Maximum Incoming Tsunami Wave height [m] at each section on the coast [Kanagawa Prefecture, 2012]

Name of earthquake	Year of occurrence	Time since occurrence	A	B	C	D
Genroku	1703	307	9.1	9.9	8.3	7.9
Kanto	1923	93	8.8	9.2	7.9	7.4
Sagami Bay	1633	383	6.2	8.0	7.1	5.7
Sagami Bay	1782	234	5.5	7.3	6.0	5.4
Meiou	1498	518	9.7	12.9	10.7	11.4
Ansei-Tokai	1854	162	2.9	3.8	3.9	3.5
Keicho	1605	411	10.2	14.5	11.2	13.6

The expected maximum incoming tsunami wave height taken from the governmental inundation maps refers to the maximum undisturbed, incoming tsunami wave height measured on the coastline relative to the High Water Level (HWL). This is more clearly shown in Figure 3.2. This is assumed to be the 'worst-case scenario' in these simulations conducted by the Kanagawa Prefectural Government as it includes the high tide. The change due to tide is approximately 1 m, thus, looking at the tsunami relative to mean sea level is also appropriate [Kanagawa Prefecture, 2016].

Here, the variable used for the regression analysis is clarified and defined as illustrated in Figure 3.2. The tsunami wave heights which are used for the regression analysis are the maximum undisturbed, incoming tsunami wave heights which have no influence from existing protection measures along the coast; it is measured on the coast before the location of any protection measures. This maximum undisturbed, incoming tsunami wave height will be referred to as incoming (tsunami) wave height from now on. The

water levels, which include the influence of the dikes and other protection measures, will be referred to as inundation height. Thus, everything past the coastline is assumed to have water levels with the influence of flood protection measures, being called inundation heights. The offshore wave height is just to clarify that the wave does go through shoaling and breaking before it reaches its representative value of the incoming tsunami wave height.

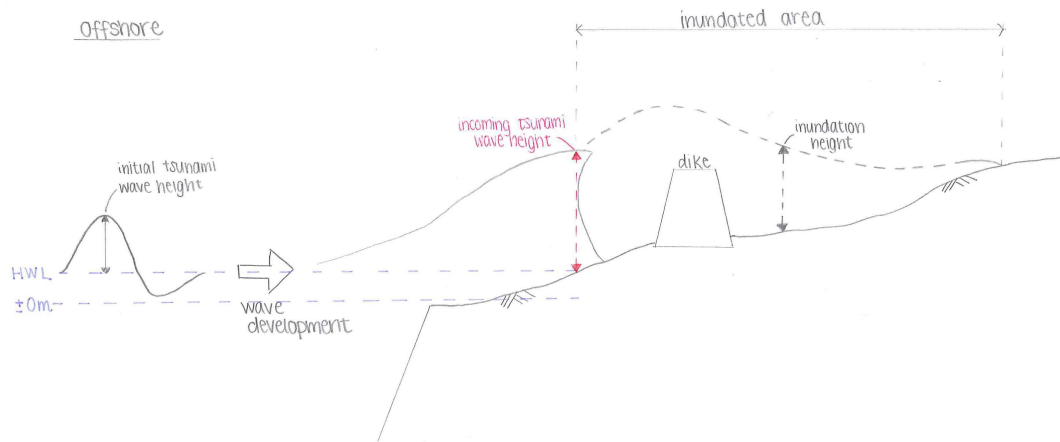


Figure 3.2: Measurement locations of initial tsunami wave heights, maximum incoming tsunami wave height, and inundation heights [Kanagawa Prefecture, 2012]

These incoming tsunami wave heights at each section are analyzed with the method of regression to approximate the return periods. The maximum incoming tsunami heights for each section are given a rank in the order from largest to smallest. Once the different historical tsunamis are ranked, equation 3.1 is used to find the probability of exceedance; n is 518 years for this case as can be seen in Table 3.2. Once the probability of exceedance, or in other words the probability of occurrence is determined, the return periods of each event can easily be determined with equation 3.2. The results of these steps are given in more detail in Appendix A.

3.3.2. DISTRIBUTION FITTING

From the method of regression, the incoming wave heights now have corresponding return periods. In order to determine the complete distribution of incoming wave height and return period, the approximated points must be fitted with a line. Since tsunamis are extreme values, a line will be fitted based on the data behavior using the extreme value theory.

For extreme values of sea water level, the most commonly used distribution are the three types of Generalized Extreme Value (GEV) distributions [Caires, 2014]. It is important to note that for normal water levels, Caires [2014] is much in favor of the Generalized Pareto distribution, but in this case, tsunamis are not taken to be normal water levels. These GEV distributions are extreme value distributions, and the three types allow the flexibility of having concave, linear and convex distribution curves. These distributions are often used for extreme sea water levels, and was chosen over other distributions for its flexibility and better fitting for extreme water levels. All the Generalized Extreme Value (GEV) distribution is fitted to determine which distribution type yields the best-fit.

Firstly to give an idea of each of the types of the GEV distributions, the type I is the Gumbel distribution used for distributions with a short tail, type II is the Frechet distribution used for distributions with a fat

tail, and type III is the Reverse Weibull distribution. The general equation for the cumulative distribution function of the GEV distribution is:

$$F_X(x) = e^{-\left(1+\xi\left(\frac{x-\mu}{\sigma}\right)\right)^{1/\xi}} \quad (3.3)$$

Here, ξ is the shape parameter, and equals zero for the type I, negative for type III and positive for type II. μ is the location parameter, and σ is the scale parameter. Given the probability of exceedance from the cumulative distribution function, the associated return periods T were computed.

$$T = \frac{\text{number of years}}{(1 - F_X(x)) \times \text{number of samples}}$$

Now the different types of GEV distributions are illustrated in Figure 3.3.

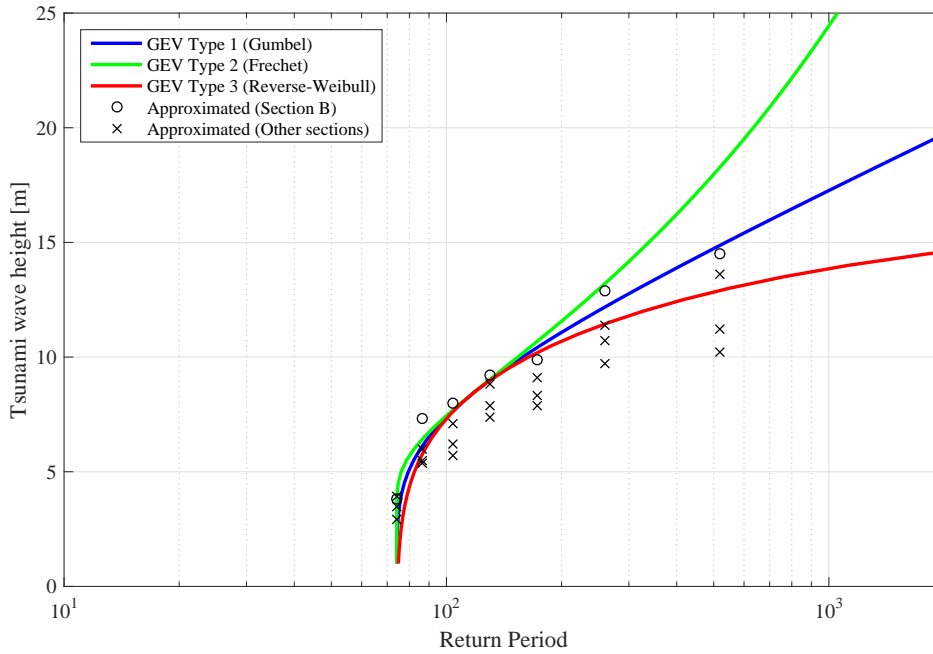


Figure 3.3: Return period with its corresponding incoming wave height derived from the method of regression, and fitted with different GEV distributions for section B

In Figure 3.3, the plots which are labeled 'Approximated' refer to the results of the return periods which were approximated by the method of regression from the simulated historical tsunami data in Section 3.3.1.

3.3.3. DISCUSSION

Fitting the Generalized Extreme Value (GEV) distributions, three different types of distributions were fitted to the approximated return periods and tsunami wave heights for section B - Type I (Gumbel), Type II (Frechet), and Type III (Reverse-Weibull). These distributions were fit for each section from A to D of the coastline, and for all of the plots combined - hence, a total of 15 different lines were fit, and the best fit result is illustrated in the chapter. The different distributions of each coastline section and the goodness of fit tests can be found in Appendix A. In Figure 3.3 the distributions for section B is shown, as the curve fitted the approximated return periods and corresponding incoming wave heights well based on goodness of fit test. Moreover, the type of distribution which was the best fit for section B allowed the extrapolation of data for many years, while some of the other sections only allowed the extrapolation of a few hundred years due to the distribution limitations.

The distribution illustrated in Figure 3.3 does not overestimate the frequency of the lower tsunami wave heights, and neither does it underestimate the wave heights which range in the more frequent return periods of 100-200 years. Looking at each of the distribution types individually, all the distributions slightly underestimate one of the wave heights for a one in 87 year tsunami, and for the less frequent tsunamis, the Reverse-Weibull underestimate three large tsunamis, Gumbel underestimates one, and Frechet lies above all the plots. As for the shape of the curves, the Reverse Weibull distribution creates a convex curve which has a bound, while the Frechet distribution is the opposite, creating a concave curve which increases exponentially. As for the Gumbel curve, it lies between the two curves, not having a bound but increasing somewhat linearly.

GOODNESS OF FIT TESTS

To have a more objective judgment on which curve is the best fit, two tests have been executed for the distributions. The first test conducted is the least square principle, and the second test is the Kolmogorov/Smirnov (KS) test. The same is done in Appendix A for the other coastline section distribution curves.

The least square principle results in outcomes which return the sum of the difference between the data and the fitted distribution squared [van Gelder, 2015]. The data set must be transformed by the method of regression, as done in this thesis, to compare the goodness of fit using this test. This data set is illustrated in the equation as an α matrix. Equation 3.4 is used for the least square principle test. A higher value illustrates the larger deviation of the distribution with respect to the given data set.

$$\text{least square outcome} = \min \sum_{i=1}^n \{y_i - (1 - F(x|\alpha))\}^2 \quad (3.4)$$

Here, $F(x|\alpha)$ illustrates the probability of exceedance for the given values, and y_i are the probability values derived from the method of regression.

The KS-test results in a hypothesis test result and a p-value [Natrella et al.]. The hypothesis test result either give a value 1 or 0, where 1 indicates the rejection of the null hypothesis at the 0.05 significance level, while 0 indicates a failure to reject the null hypothesis at the 0.05 significance level. The p-value is a value which illustrates the probability of observing a test statistic as an extreme, or more than extreme, than the observed value under the null hypothesis. In other words, small values of p casts doubt on the validity of the null hypothesis. So a p-value below 0.05 illustrates a rejection in the null hypothesis, and a p-value above 0.05 does not reject the null hypothesis, therefore, there is a higher than 5% chance that the fit is distributed according to the null hypothesis.

As illustrated in Table 3.3, the goodness of fit of the different GEV distributions for section B are all not rejected by the hypothesis test. This means that all these distributions have a 5% larger probability of

Table 3.3: Goodness of fit for different GEV distributions for coastline Section B

Distribution	Hypothesis test result (KS-test)	p-value (KS-test)	Least Square test outcome
Section B GEV Type 1	0	0.9159	2.5191
Section B GEV Type 2	0	0.7552	2.6524
Section B GEV Type 3	0	0.9506	2.3681

being observed under the null hypothesis. Furthermore, by looking at the p-values, the larger the p-value, the better the fit, so the Section B GEV Type 3 distribution is computed to be the best. This is further supported with the results of the least square principle test, as the GEV Type 3 distribution gives the smallest outcome. This is good as the smaller the outcome values, the closer the distribution is to the plots. The GEV Type 1 distribution also illustrates results which are close to that of GEV Type 3, but the least square test outcome is slightly larger, and the p-value is slightly smaller. Therefore, it can be said that these two test results will give the choice of the GEV Type 3 distribution.

Looking in more detail at the GEV Type 3 (Reverse-Weibull) distribution for a longer return period [Figure 3.4] shows that this distribution line seems to reach a bound.

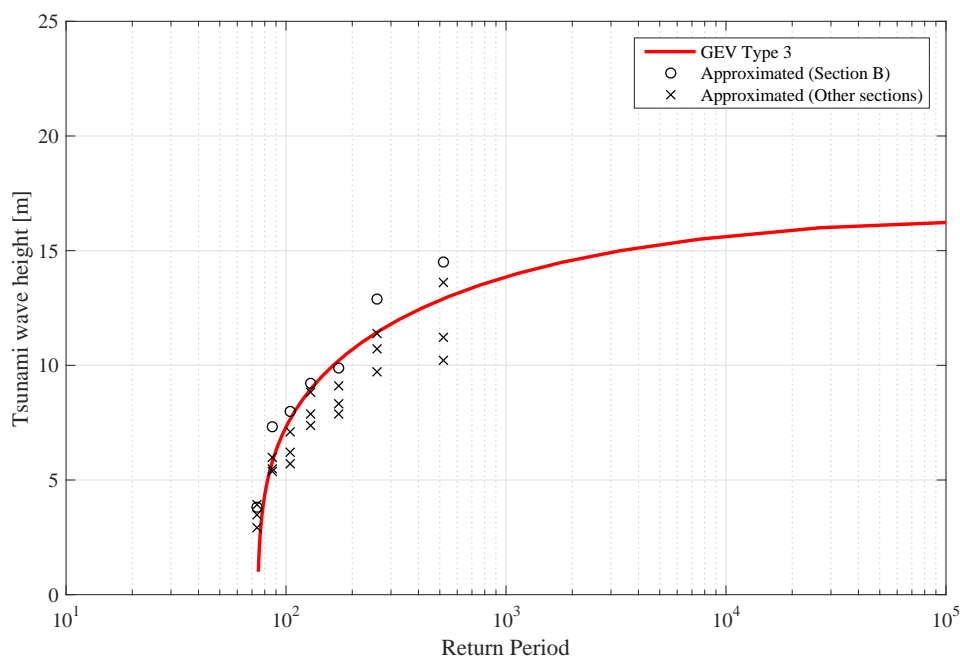


Figure 3.4: Return period with its corresponding incoming wave height derived from the method of regression, and fitted GEV Type III distribution for section B

This limit may exist due to the bathymetry, or the distance of tsunami development, as the troughs and fault lines are located relatively close to the coast compared to other locations in Japan. Furthermore, it is logical to think that there is a bound to the height of a tsunami wave as it is a shallow water wave, and there is a limit to the steepness before the wave breaks. For a certain steepness the wave is expected to start breaking before the coast. This is not the case for a deep water wave where the GEV Type 2 Frechet distribution is used to determine the wave heights [van Gelder, 2015]. Moreover, it is worth noting that

although it is not clearly stated that there is a bound to earthquake intensity relative to return period, the intensity of the earthquake is not only dependent on the deflection of the fault but also on the length of the deflected fault. This length of the fault creates an upper bound, as the length of the plates are limited to a certain length on earth [Southern California Earthquake Center, 2007]. Therefore, if there is such a limit of earthquake intensity with respect to the size of the fault, it could be argued that there is a bound to the incoming wave heights, although tsunamis are also dependent on other parameters.

For these reasons, this assumption that there is a bound to the height of an incoming tsunami wave will be made, and thus further supporting the choice of the GEV Type 3 (Reverse-Weibull) distribution to be used to describe the return period with its corresponding wave height. This statistical bound which this distribution line reaches from Figure 3.4 is approximately 17 m.

The large scatter for the larger return periods, which is the disadvantage of this GEV Type 3 distribution, may exist due to the low frequency of certain earthquakes. This link between earthquakes and tsunamis, however, was not looked at in detail in this thesis. Nevertheless, this underestimation of incoming wave heights for less frequent tsunamis can be overcome with confidence intervals. The method of using confidence intervals are used in the Netherlands in cases such as for the extrapolation of river discharges to avoid the underestimation of high river discharges. Adding confidence intervals allows the inclusion of outliers in the probabilistic distribution, and avoids the underestimation of possible extreme events with less frequency [Silva et al., 2004]. This inclusion of confidence intervals can be conducted by the bootstrapping method, illustrating the increase of uncertainty as the uncertainty of the event also increases. Therefore, if a conservative design is preferred, a 90 % or 95 % confidence can be used for the design tsunami level with additional measures such as freeboards on top of a seawall or dike. In this way, it can be assumed that the maximum tsunami wave heights for rare events will also not be underestimated.

DEFINING LEVEL 1 AND LEVEL 2 EVENTS

A Level 1 and Level 2 event is defined by the local and national government based on the political demands. From Chapter 2, it is known that a Level 1 event is defined as a tsunami event which occurs every several decades to 100+ years, and protections built for this level must completely protect human lives and property. Tsunamis at this level are assumed to generate relatively low inundation depths, typically less than 7-10 m. A Level 2 event is a more rare event with a return period of a few hundred to few thousand years. Vital infrastructure, such as hospitals and evacuation centers, should be built or moved to where the water does not reach these locations even when the primary defenses are overtopped. This level would generate much larger inundation depths of over 10 m, and encompass up to 20-30 m for worst-case scenarios such as those measured during the event in Tohoku in 2011. Due to the fact that the Level 1 and Level 2 events are very broad categorizations of tsunamis and highly differ depending on location based on bathymetry and topography. Tsunami levels for Kamakura will be chosen simply through the definitions of the return periods for each level.

As mentioned in Section 3.1, there is currently no value set for a Level 1 and Level 2 tsunami event for Kamakura. Therefore, these levels will be chosen based on the distribution line computed in this chapter. The Level 1 event for Kamakura will be chosen to have a return period of 100 years, and the corresponding incoming wave height is 8 m taken from the distribution line. Similarly, the Level 2 event for Kamakura will be chosen to have a return period of 1000 years, and the corresponding incoming wave height is 14 m. The return periods lie within the range of the categorization, however these levels are defined in terms of inundation height instead of incoming wave height. This can be overcome by the inferences that the incoming wave heights and inundation heights are in the similar range. Moreover, the inaccuracy of the fitted distribution increases if the extrapolation is conducted for more than double the amount of recorded years. The amount of years of data is assumed to be equal to the amount of years since the oldest tsunami, which occurred 518 years ago. Thus, setting the Level 2 event at 1000 years allowed the extrapolation to stay within a reliable range.

3.4. CONCLUSION

For Kamakura, there are only seven historical tsunami events available for determining the return period and wave height distribution, of which some events lack data as it occurred hundreds of years ago. Even with this lack of data, the method of regression was used to approximate the return periods of tsunami events. This method can cause inaccuracies for extrapolating data, however, the accuracy is stated to still hold within a range double its recorded amount of years. Knowing the limits of this method, the seven historical events were extrapolated for different sections along the coastline in Kamakura using the simulations from the Kanagawa Prefectural Government.

These approximated plots, derived based on the regression method, were fitted with the Generalized Extreme Value (GEV) distribution line. Due to the facts that the distribution line had a good statistical fit with the approximated return periods, and that it is approaching a physical bound, the GEV Type 3 distribution line for section B was chosen to best represent the coastline of Kamakura. The distribution line was reaching a physical bound of approximately 17 m. If a conservative value of the maximum tsunami wave height is needed, the 90% or 95% confidence interval can be taken. It could also be argued that the GEV Type 1 distribution can be chosen, as it is unsure whether a bound for wave height exists or not, and the goodness of fit test results for this distribution were also satisfactory. For this thesis, however, the return period considered is short, from 1000 to 2000 years, and the analysis illustrated that GEV Type 3 is sufficient.

In spite of the many assumptions and simplifications which had to be made to obtain a distribution illustrating the relationship between the incoming wave height and its return period, this distribution was also able to take into account area specific factors, such as the influence of bathymetry. Moreover, the statistical analysis of the distribution line, with respect to the approximated plots was made in a appropriate range to be used for the risk assessments in the following chapters. Of course there are inaccuracies and uncertainties in this distribution relationship, however, it is a necessary cost when conducting probabilistic assessments, which also is present in the assessments done in the Netherlands.

Table 3.4: Level 1 and Level 2 event return periods and incoming wave heights for Kamakura

	Return Period [years]	Incoming wave height [m]
Level 1 Event	100	8
Level 2 Event	1000	14

Here, the Level 1 and Level 2 events are distinctly shown to clarify the tsunami levels when considered under the Japanese tsunami categorization scheme. In the coming chapters, multiple tsunami events along the GEV distribution line will be used, instead of just two tsunami events, to conduct the risk quantification followed by the economical, individual and societal risk evaluation and analysis. The categorization of Level 1 and Level 2 events will just be referred to as one of the different tsunami levels simulated in the remaining chapters, as the categorization is broad. Still, the assumption that the dike would not collapse for return periods of over 1000 years which was included in the categorization scheme is kept.

4

TSUNAMI RUN-UP ASSESSMENT

This chapter is created in collaboration with Bas Horsten.

This chapter covers the derivation of the modeling of tsunami run-up for Kamakura for multiple tsunamis. The goal is to gain deeper insight in the tsunami wave behavior and to derive the boundary conditions for a tsunami. This run-up model will be used to conduct flood scenarios, which later will be analyzed to determine the amount of damage resulting from tsunamis for the risk assessment.

There are multiple ways to model a tsunami, such as solitary waves, by means of long wave approximation, N-wave theory and more. The solitary wave and N-wave theory have a 'run-up law', which gives a preliminary idea of the amount of run-up caused by a solitary wave [[Synolakis, 1987](#)]. This formula has its limits as the slope of the 1 dimensional cross-section is a simple linear slope, while in reality, the bathymetry and topography would have its unique characteristics. Moreover, in the later parts of this thesis, interventions will be included in the model. This is very difficult to analyze with this simple equation, as it does not include protection measures and just a run-up on a simple linear coast.

For these reasons, the use of the SWASH (Simulating WAVes till SHore) software was considered. SWASH is a hydrodynamic model for simulating non-hydrostatic, free-surface, rotational flows and transport phenomena in one, two or three dimensions [[The SWASH team](#)]. It is also capable of describing the wave transformation in the surf-zone including non-linear interactions, wave-current interactions, wave breaking and run-up.

Information on SWASH computations can be found in [Appendix B](#), and more information on the results can be found in [Appendix C](#).

4.1. SELECTION OF THE WAVE THEORY

Tsunami waves can be approximated by several different theories, each with different characteristics. Therefore it is important to consider which theory is best applicable to be implemented for the SWASH model.

The simplest way of representing a wave is by sine or cosine functions [Figure 4.1a]. Its features can be characterized mathematically by linear, trigonometric functions known as the Airy wave theory. This theory can represent local tsunami propagation in water depth greater than 50 meter [Camfield, 1980]. However when waves propagate towards the shore, they become more and more asymmetric. This is due to the shoaling process, which is characterized by an increase in wave height and by the gradual peaking of the wave crest and flattening of the trough. The separation between wave crest becomes so large that the trough disappears and only one peak remains, resembling a solitary wave [Figure 4.1b] [Bosboom and Stive, 2015].

Many observations of a tsunami approaching the shore state that first the water is drawn before the wave crest arrives. this is caused by non-linear effects that produce a trough in front of the wave. This can be modeled with a so-called N-wave [Figure 4.1c] [Tadepalli and Synolakis, 1994].

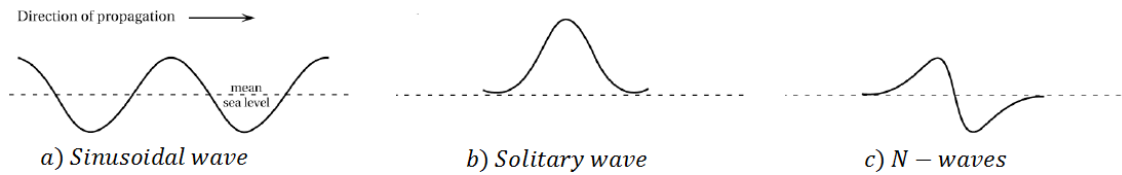


Figure 4.1: The different types of wave theories [Tadepalli and Synolakis, 1994]

This selected wave is intended to illustrate the characteristics of the first wave, or in other words the wave at first impact. This is pointed out as it is very difficult to portray the entire tsunami wave accurately, for example, the 2011 tsunami had bores in the beginning of the wave, however, the main wave was following behind. Hence, this selected wave is generated for a first approximation.

SOLITARY WAVE THEORY

Since the early 1970's, it has been frequently assumed that solitary waves can be used to model some of the important features of tsunamis approaching the beach and shoreline. The solitary wave can be seen as an amount of water riding completely above the mean sea level. Solitary waves have the advantage, although nonlinear, that they can be described with just two parameters, namely the initial wave height [H_0] and the initial water depth [h_0], and they propagate with constant form in constant depth [Holthuijsen, 2007]. Another advantage is that there are many studies executed to discuss the hydrodynamics of solitary waves shoaling and breaking on a slope.

The main problem with this wave theory, is that the link to geophysical scales is not well established. Therefore the use of solitary waves to model tsunamis and conclusions in relation to tsunamis modelled as a soliton should be made with great care [Madsen et al., 2008].

To generate a times series of a solitary wave, the following formula will be used:

$$\eta = a \cdot \text{sech} \left(\sqrt{0.75 \cdot \frac{a}{h^3}} x \right)^2 \quad (4.1)$$

Where η is the surface water level, a is the amplitude of the wave, h is the initial water depth, and x is the distance from the initial location. The shape of the solitary wave does not change with constant depth.

The propagation speed c of a solitary wave is given by:

$$c = \sqrt{gh} \left(1 + \frac{\alpha}{2}\right) \quad (4.2)$$

Where, $\alpha = \frac{a}{h}$. Here, a is the amplitude of the wave, h is the water depth and η is the surface water level. By altering the a and h , solitons with different characteristics can be modeled.

N-WAVE THEORY

Depending on the geophysical characteristics of the earthquake, there are two types of N-wave. The leading-depression or the leading-elevation. In the paper of [Tadepalli and Synolakis \[1994\]](#) a class of N-shaped waves were found that displayed very interesting and counterintuitive behavior of the tsunami wave. Thus, the main advantage of the N-wave is that the physical characteristics of the wave fits better with the geophysical scales. Furthermore it is suggested that the solitary wave may not be adequate for predicting an upper limit for the run-up of near-shore generated tsunamis. However, the N-wave has no mathematical connection. The wave is obtained by manipulating a soliton until it quantitatively changes to give the required shape with a leading or following trough. Also, the amount of studies available is limited compared with the solitary waves.

The N-wave can be obtained by multiplying the equation of the soliton [Equation 4.1] with an equation of a linear line. The N-wave can have a leading elevation or a leading depression depending on the positive or negative slope of the linear line. The equation to generate a N-wave is derived from the report of [Tadepalli and Synolakis \[1994\]](#):

$$\eta(x, 0) = (\epsilon \cdot H)(x - X_2) \cdot \text{sech}(\gamma_s(x - X_1))^2 \quad (4.3)$$

Where,

$$\gamma_s = \sqrt{0.75 \cot H} \quad (4.4)$$

And the factor $\epsilon \cdot H$ is a scaled N-wave amplitude.

CONCLUSION

Both models have their positive and negative features, therefore, it has been decided to model both type of waves for the reference case of Sendai to observe which type of wave correlates better with the observational data and analytical calculations. After analyzing the results of both waves, a best fit is chosen for the case study of Kamakura.

Modeling the entire depression of the sea floor might be the best approach which currently exists to model tsunamis, but this is outside of the scope of this thesis.

4.2. ANALYTICAL DESCRIPTION OF THE DEFORMATION OF THE TSUNAMI WAVE

The SWASH model can be validated by studying the wave deformation for both the solitary wave as well as the N-wave. The deformation is characterized by four stages, namely:

- Shoaling of tsunami waves,
- Breaking of tsunami waves,
- Dissipation of tsunami waves,
- Run-up of tsunami waves.

4

SHOALING OF THE TSUNAMI WAVE

Shoaling is the effect of increasing wave height due to decreasing water depth. A decreasing water depth, yields a decreasing wave speed. So when a tsunami wave travels into progressively shallower water, the wave energy will be concentrated, causing the wave to steepen and rise to many meters in height [Bosboom and Stive, 2015]. The relation between the wave height $[H]$ and the water depth $[d]$ is known as the Green's law [Camfield, 1980], where subscript 1 stands for location 1 and subscript 2 for location 2.

$$\frac{H_1}{H_0} = \left(\frac{d_0}{d_1} \right)^{0.25} \quad (4.5)$$

BREAKING OF THE TSUNAMI WAVE

The wave shoals until the wave becomes too steep and starts to break. The wave steepness depends on the wave height $[H]$ and the wave length $[L]$. In the report of Grilli et al. [1997] the breaking characteristics for solitary waves on a slope are discussed. Non-dimensional parameters are derived to predict whether waves will break or not, and which type of breaking will occur.

In the report, the slope parameter $[S_0]$ is used, which depends on the slope $[s]$ and the initial wave height $[H_0]$.

$$S_0 = 1.521 \cdot \frac{s}{\sqrt{H_0}} \quad (4.6)$$

The breaker type can be estimated in terms of values of the parameter S_0 as [Grilli et al., 1997]:

- Surging breaker: $0.30 < S_0 < 0.37$
- Plunging breaker: $0.025 < S_0 < 0.30$
- Spilling breaker: $S_0 < 0.025$

From the computations of this report, the following relationship between the breaking index and breaking depth $[h_b]$ is derived:

$$\frac{H_b}{h_b} = 0.841 \exp 6.421 S_0 \quad (4.7)$$

DISSIPATION OF THE BREAKING TSUNAMI WAVE

Normal wind waves lose most of their energy in the surf-zone during breaking [Equation 4.8]. Tsunami waves, however, retain a significant amount of energy leading to high run-up heights and inundation depths. So the next step is to determine the height $[H_{sh}]$ and wave celerity $[c_{sh}]$ of the incoming wave at the shoreline.

$$H(x) = \gamma h(x) = \text{const.} \quad (4.8)$$

In the report of Battjes [1986], an energy dissipation model for breaking solitary waves is derived for gentle slopes ($s < 1 : 30$), which corresponds with a spilling breaker. The dissipation rate of the spilling breaker is estimated from a bore with the same height of the spilling foam region. Observations of breaking waves in constant or increasing depth suggest that the height of the foam region decreases more rapidly than the total wave height [Battjes, 1986].

A dissipation formula is derived from the energy balance and can be written as a function of the breaker conditions. The formula [Equation 4.9] resembles the dissipation formula for normal wind waves [Equation 4.8], where the breaking index γ is replaced by the dissipation factor K' which depends on the bottom and spilling conditions.

$$\tilde{H}^{-\frac{9}{2}} = (1 - \frac{1}{3}K')\tilde{h}^{\frac{9}{2}} + \frac{1}{3}K'\tilde{h}^{-\frac{9}{2}} \quad (4.9)$$

Where,

$$\tilde{H} = H/H_b \quad \tilde{h} = h/h_b$$

The Battjes model is checked by comparing data on solitary waves breaking on a 1:100, illustrated by the solid line in Figure 4.2, from Street and Camfield [1966]. Choosing $K' = 32.4$ gives a curve which in most of the decay region agrees remarkably well with the data. It must be noted that this Battjes model does not predict the fitted hyperbola of "observed" surviving wave height at the shoreline from Street and Camfield [1966].

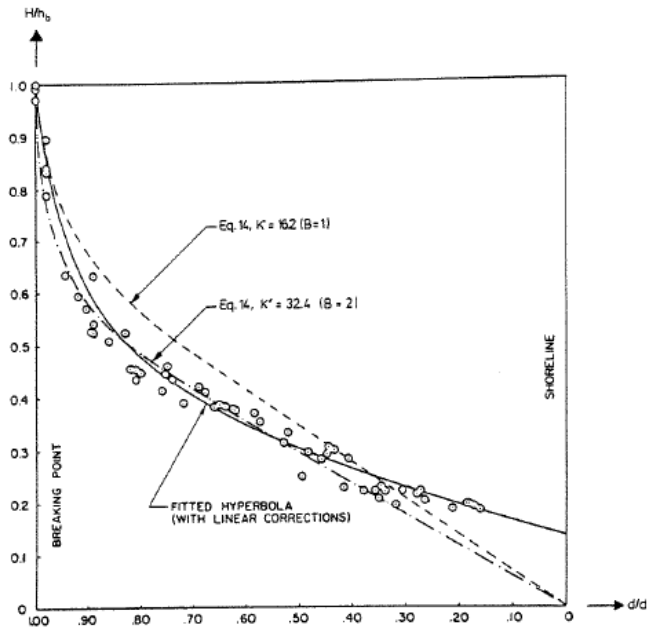


Figure 4.2: Decay of solitary waves near the shoreline [Battjes, 1986]

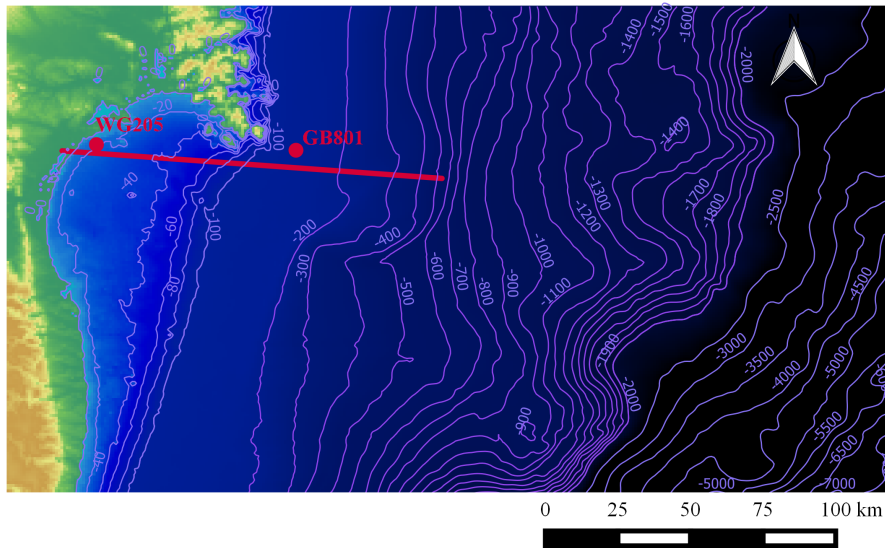
The main advantage of the Battjes model is that the dissipation model depends only on the breaking wave height [H_b] and the breaking depth [h_b] with a dissipation factor [K'] which is equal to 32.4. However, this model does not predict the incoming wave height at the shoreline [H_{sh}]. Thus, the Battjes formula is only used to check if the modeled SWASH wave dissipates energy in the breaking zone.

RUN UP OF THE TSUNAMI WAVE

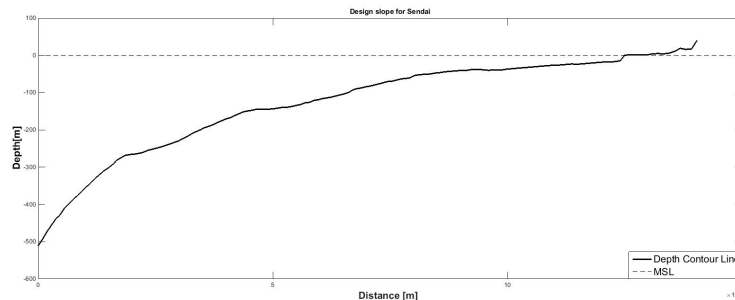
The run-up of a modeled tsunami wave on a linear slope can be quasi-analytically derived for both a solitary wave [Synolakis, 1987] and an N-wave [Tadepalli and Synolakis, 1994] tsunami model. Several studies have been conducted to describe the relation between the offshore wave conditions and the amount of run-up on shore. However, these relations are for non-breaking waves. Therefore the modeled run-up will be validated by the measurements of the report of Mori et al. [2011].

4.3. REFERENCE CASE STUDY: SENDAI

The wave development and impact of the Tohoku tsunami of 2011 for the city of Sendai is chosen as a reference case study. Sendai is chosen as a case study because a lot of data and measurements are available. Sendai is also a similar case to Kamakura [Figure 4.3b] as the characteristics of the bathymetry is similar (mild slope). Both cases have a bay type of coast and the average slope nearshore is approximately 1/100. The bathymetry data is obtained from [General Bathymetric Chart of the Ocean](#) [2016], and the topography data is obtained from [USGS](#) [2016].



(a) Plan view of chosen 1D cross-section of bathymetry, along with the PARI buoy stations GB801 and WG205



(b) Representative cross-sectional bathymetry and topography of Sendai

Figure 4.3: Cross-sectional information for Sendai case study

The first step to calibrate the model is to analyze and choose the right data from observational data and other sources, in order to derive the wave boundary conditions [Sec. 4.3.1]. The different waves are modeled, and are first validated with the observation data [Sec.4.3.2], and compared and contrasted with the suggested analytical models [Sec. 4.3.3]. Finally, based on the two methods of validation, a conclusion can be made for which wave type and boundary conditions are appropriate to be used to model the case study of Kamakura [Sec. 4.3.4].

4.3.1. BOUNDARY CONDITIONS AND OBSERVATIONAL DATA

The initial tsunami wave height is derived from the inversion analysis of the buoy and satellite data collected from different institutes [Saito et al., 2011] [Kawai et al., 2013].

In Figure 4.4, there is a large water level rise approximately 250 km away from the coast of Sendai, and a slight water level drop 100 km away from the coast of Sendai. This whole rise and drop of the water level for the cross-section can be modeled in a time-series as one large wave. To model this initial tsunami as accurate as possible, a wave of approximately 120 km in length and a period of approximately 30 minutes is generated. At the starting node of the boundary, the period of the modeled tsunami is close to that of the data, however, it is difficult to create a time series of a wave with a trough and crest far away from each other. Therefore, the slight drop of the water level is neglected, and instead the time series of the buoy GB801 located 60 kilometers off the coast of Sendai was used, to come up with the final length and period of the tsunami wave.

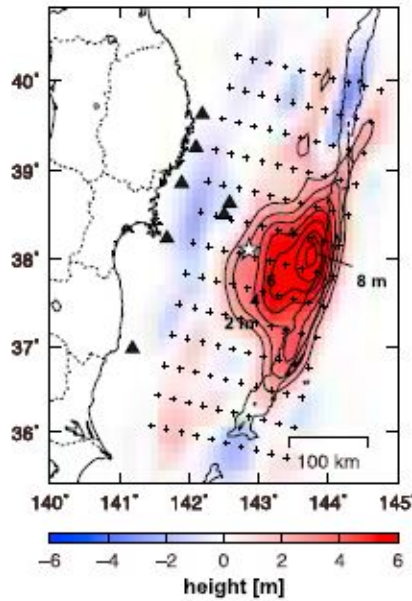


Figure 4.4: Initial tsunami wave height distribution [Saito et al., 2011]

There are also buoys deployed by the Port and Airport Research Institute (PARI), which were able to collect the time series of the 2011 tsunami [Kawai et al., 2013]. The location of buoys GB801 and WG205, also illustrated in Figure 4.3a, are obtained in coordinates from PARI. The given coordinates for GB801 are 38°13' 57", 141°41' 01", and for WG205 are 38°15' 00", 141°03' 58", and are illustrated to scale. There is also data available for other buoy stations along the coastline of Tohoku, but for this thesis, only these two buoy stations are looked at.

As can be seen in Figure 4.3a, the chosen cross-section to model the tsunami in SWASH is not directly going through the buoy stations, however it is clear that if the relative depth chosen to compare the wave development with the buoys are within the same depth contours, the comparison can be said to be adequate. Furthermore, this transect in Figure 4.3a is chosen in such way that the islands and shallow parts of the North are not incorporated. This is because the main wave travels faster in the deeper parts of the ocean with refraction having some effect, hence the wave at the coast is expected to be governed by this.

The 2011 Tohoku Earthquake Tsunami Joint Survey Group have also comprehensively recorded the in-

undation height and its impact along the coastal region affected. Observations were made on the maximum inundation height for different locations along the Tohoku coastline. Here, the definitions which were specified in Chapter 3 are kept, and the inundation height refers to the tsunami height with influence from flood protection measures such as dikes and seawalls. The undisturbed wave height, or in other words the incoming wave height, could not be measured. Based on the inundation heights recorded, the incoming tsunami wave height on the coast is inferred to be in the range from 5 to 15 meter in the Sendai plain depending on location [Yamao et al., 2015].

Finally, the measured run-up distance and inundation heights are observed. Figure C.1 illustrates the envelop of the run-up distance with its relative inundation heights in multiple locations which were surveyed by Mori et al. [2011]. The relative inundation heights in multiple locations illustrated as plots can be found in Figure C.1.

4.3.2. VALIDATION BASED ON OBSERVATIONAL DATA

In the previous sections, the offshore wave conditions and other boundary conditions are derived, some of which are from observational data. With this information, SWASH models both the solitary wave and N-wave.

To model a tsunami well in SWASH, specific boundary conditions must be chosen. Based on the previous work on solitary wave and tsunami modeling, similar boundary conditions were chosen [The SWASH team]. The boundary condition on the left, or what is referred to as the west side in SWASH, includes the wave time series which was created from equation 4.1 and 4.3, with a weak reflection as it is one large wave which acts as a shallow water wave and has minimal disturbances that follow. On the right side, or the east side in SWASH, the Sommerfeld or radiation boundary condition is chosen.

The computation grid length is 140 km with 20,000 cells, resulting in a resolution of cells with 7 m. For different scenarios which were run for Sendai, the number of cells were sometimes changed to 10,000 in order to increase the speed of the computations. This reduction in the resolution of the cell to 14 m had negligible effect on the tsunami wave modeled. The SWASH simulations for this thesis are only modeled with 1 vertical layer. Including multiple layers will improve the accuracy of the wave development and the flow velocity.

Run-up distance computed in the SWASH model is influenced from the slope roughness set by a Manning's coefficient of 0.019, which illustrates a roughness of a smooth earthy surface. This roughness coefficient is lower than what is recommended in Bricker et al. [2015] for tsunami modeling, where the coefficient ranges from 0.08 to 0.17 for urban high density areas. However, for the simulations, a uniform Manning's coefficient was implemented instead of it being site specific. The first impact of the tsunami wave would be on the sandy coast, thus a Manning's coefficient for sand is chosen as a representative value. For the case of this thesis, the effect of this will not be looked at in detail, and will be considered as one of the steps to be included to improve the accuracy of the results in this chapter.

The observed time series for the tsunami wave heights are illustrated in Figure 4.5. This will be compared later with the SWASH results.

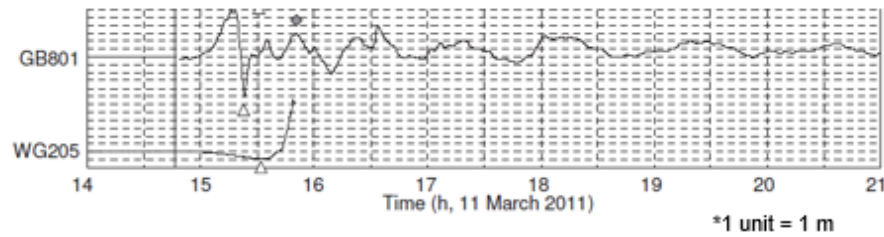


Figure 4.5: The observed time series for the tsunami wave heights for the 2011 event at buoys GB801 and WG205 [Kawai et al. \[2013\]](#)

4

The Tohoku tsunami of 2011 had a dramatic amount of run-up inland. It is already mentioned that the maximum wave height observed at the Sendai coast lays in the range between 5 and 15 meter [\[Yamao et al., 2015\]](#). The maximum measured run-up and inundation heights is shown in Figure 4.6, and the maximum run-up distance lays between the 6 and 7 kilometers inland.

From the SWASH model results, the modeled run-up can be derived for the N-wave [blue] and the solitary wave [Red]. Both models lie in the range of the measured inundation depths. The maximum run-up of the N-wave corresponds with the measured run-up. The solitary wave however, overestimates the run-up.

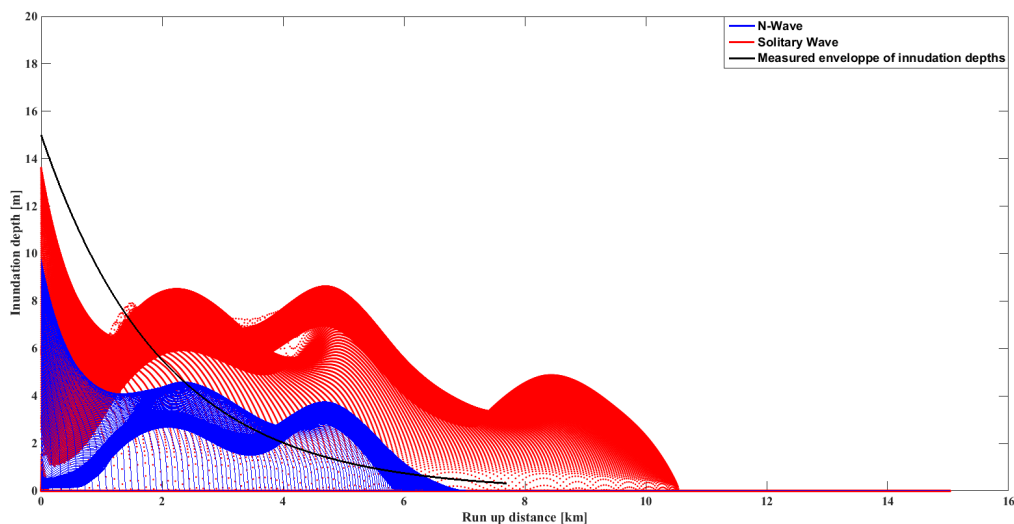


Figure 4.6: Run-up and inundation depths of the solitary and N wave SWASH results with the observed run-up distribution line

A detailed description of the model and the time series of the solitary wave and N-wave can be found in [Appendix B](#).

SOLITARY WAVE

First the solitary wave is modeled. The different stages of the wave deformation are shown in Figure 4.7. The right most graph in this figure has a different scale, and is zoomed at the coast for a more detailed view of the wave about to run-up on land.

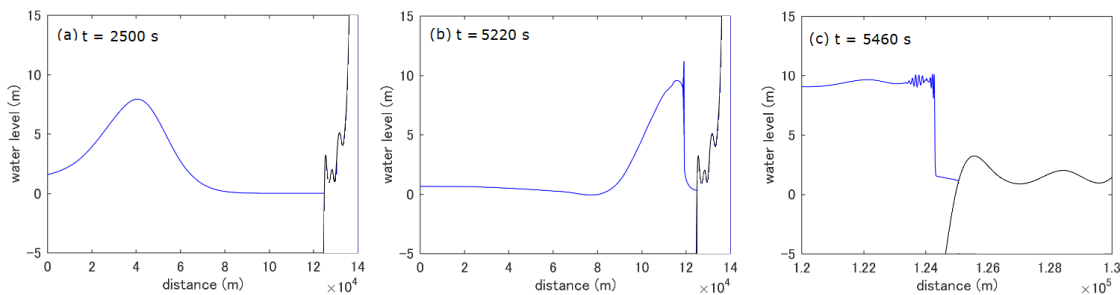


Figure 4.7: Results of the SWASH model for the solitary wave illustrating (a) Shoaling, (b) Dissipation/breaking, and (c) Incoming wave near coast (different scale)

The modeled solitary wave does not measure any trough, and the wave height is also much larger than what is recorded. This can be seen in Figure 4.10.

N-WAVE

Thereafter, a crest-leading N-wave is applied to the reference case of Sendai. Figure 4.8 shows the different stages of the wave deformation. The right most graph in Figure 4.8 has a different scale, and is zoomed at the coast for a more detailed view of the wave running up.

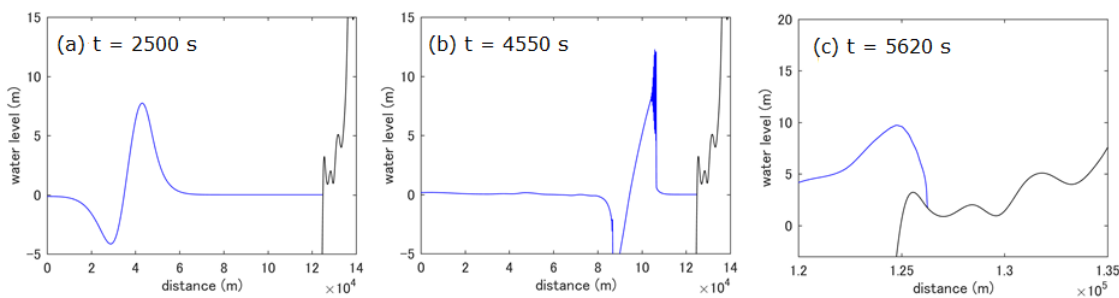


Figure 4.8: Results of the SWASH model for the N-wave

The maximum tsunami wave height also coincides with the measured range between 5 and 15 meters. The N-wave does not fully correspond with the measured wave height of buoy WG205 [Figure 4.5] but the results are better than the solitary wave.

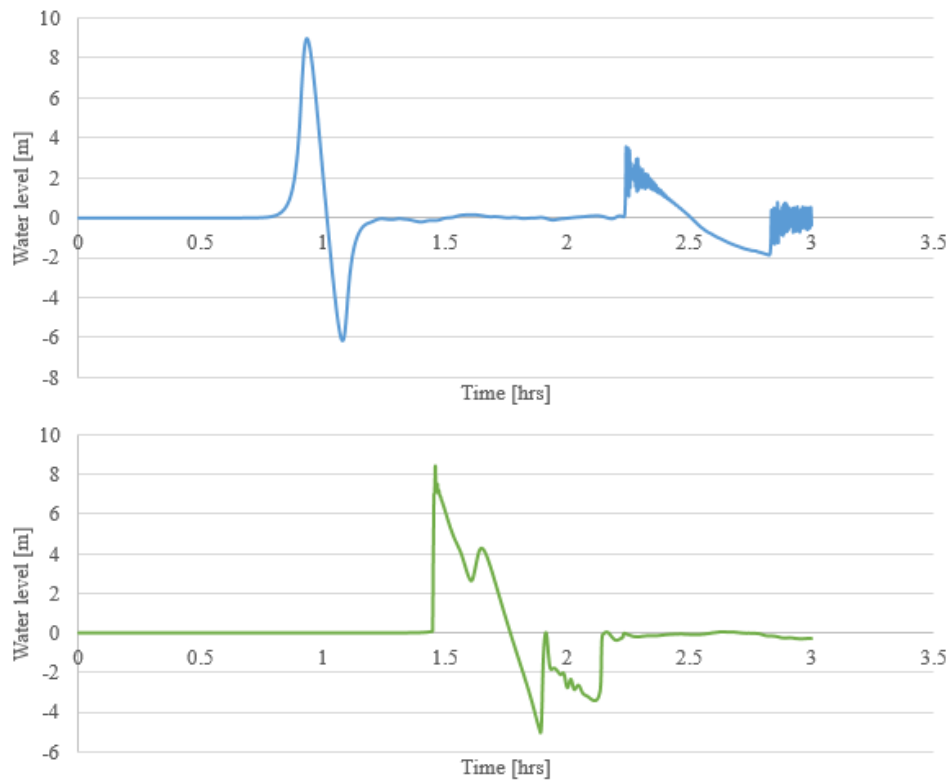


Figure 4.9: The time series of similar depth contours (in the transect) as the buoy stations of GB801 (top) and WG205 (bottom) retrieved from the SWASH results

The simulated wave slightly overestimates the measured wave height of buoy GB801 [Figure 4.9] and is equal to 6.7 meters. The wave does not coincide with the measured wave height of buoy WG205 [Figure 4.9] because the observed wave height is approximately 9 meters, but the wave falls within the range of the maximum incoming tsunami height given in Yamao et al. [2015]. The main difference with the model and the observed data, is that the data shows a slight water retreat before the bore is measured [Figure 4.5]. The steepness of the front and the total duration are also noticeably different. The modeled N-wave somewhat satisfies the rest of the measured wave data. Again, the wave shoals, breaks and eventually runs-up.

4.3.3. VALIDATION BASED ON ANALYTICAL CALCULATIONS

To consider which model is most applicable for the case study of Kamakura, it is also validated with analytical calculations. This will be done by studying the different wave transformations and comparing the results with the proposed analytical models introduced in Section 4.2.

SHOALING

The incoming wave will increase in amplitude when it is approaching the shore due to the decreasing water depth. In Section 4.2, it is stated that this effect can be approximated by Green's Law [Equation 4.5] [Black Line]. This is compared with the results of the modeled solitary wave [Blue Line] and N-wave [Red line]. These results are printed in Figure 4.10. Note that the shoaling effect for both modeled waves stop when the wave starts breaking. This effect will be further elaborated in the following section.

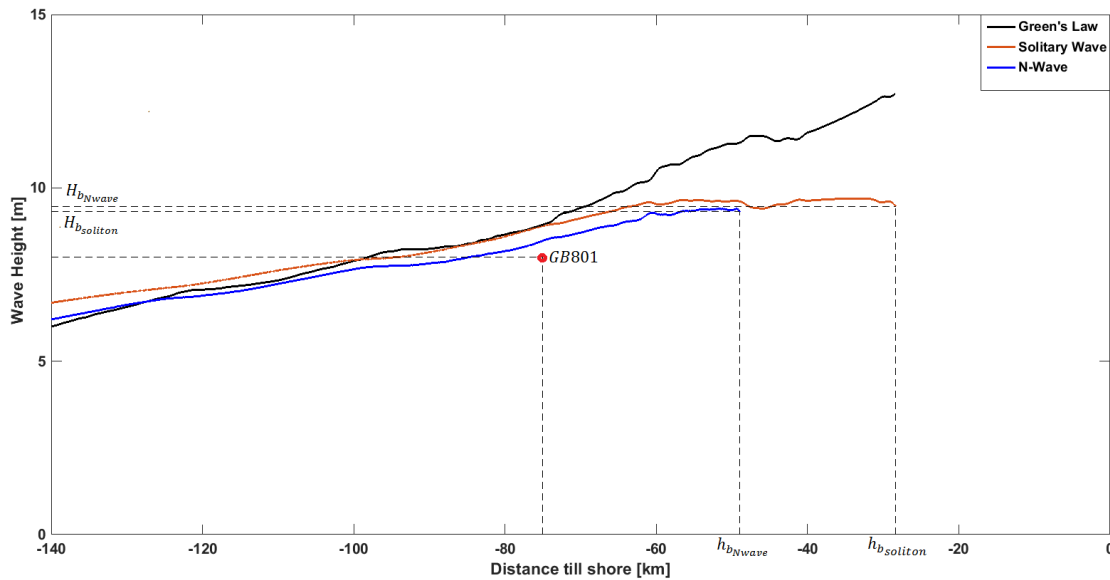


Figure 4.10: Maximum wave height during the simulation for the non-broken wave, compared with Green's Law and the measured wave height at buoy station GB801

From Figure 4.10, it can be concluded that both modeled waves shoals to a wave height of approximately 9.5 m. It also shows that the amount of shoaling for both the N-wave as well as the soliton is less than that of the analytical model. However, at the buoy location of GB801, the modeled maximum wave height for the N-wave is equal to 8.5 m and for the solitary wave equal to 8.9 m, which corresponds to the measured wave height of 8 m.

BREAKING

The breaking of the tsunami wave can be characterized by the breaking wave height [H_b] with the corresponding water depth [h_b], and the type of breaker. The latter phenomenon can be estimated by the theory of [Grilli et al. \[1997\]](#) by calculating the slope parameter [S_0], Equation 4.6. For both SWASH results, this value is less than 0.025, thus corresponding to the analytical results, which imply that the breaking wave is expected to be a spilling breaker. The spilling breaker will eventually transform to an incoming bore. Both SWASH results fulfill this requirement [Figure 4.7 and Figure 4.8]. This result can be validated with the available video and photo material of the Tohoku tsunami of 2011 [Figure 4.11].

There is no data about the breaking wave height or breaking location. What is available is the video and

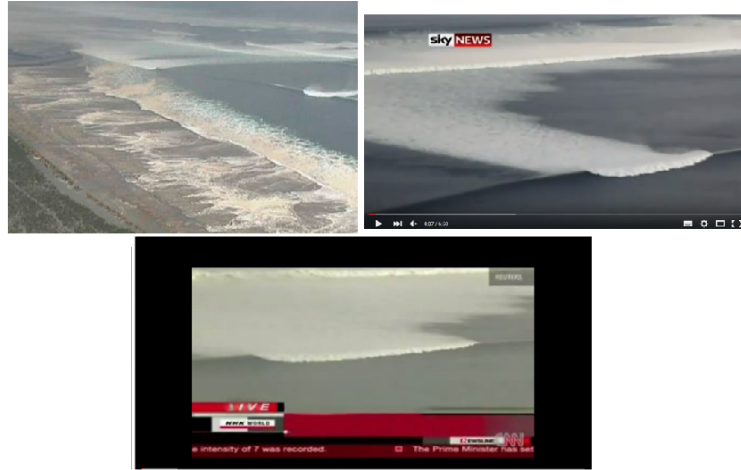


Figure 4.11: Video and photo material of the Tohoku tsunami at Sendai [[Youtube, 2016](#)]

photo material. More information about tsunami breaking, bore development profile, and details about 'soliton fission' which are observed in SWASH and in reality, are given in Figure C.2 in Appendix C.

WAVE DISSIPATION

A tsunami wave retains a significant amount of energy when it reaches the coastline. In fact, when the 'tsunami soliton fission' occurs, and the first wave splits from the incoming wave, an increase of the wave height can be seen [Figure 4.12] for both the N-wave as the solitary wave. This phenomenon is also measured in the report of Matsuyama et al. [2007]. After the wave height amplifies, the wave dissipates energy, the split waves will finally disappear, and the incoming wave will transform to an incoming bore. In Section 4.2 the dissipation model of Battjes [1986] is proposed [Figure 4.2]. Next step is to check and estimate the dissipation of both SWASH results.

In Figure 4.12, the maximum wave height of the incoming wave is plotted for both the N-wave [Red Line] as the solitary wave [Blue Line]. It can be concluded that the solitary wave hardly dissipate any energy but the N-wave however, does dissipate some energy.

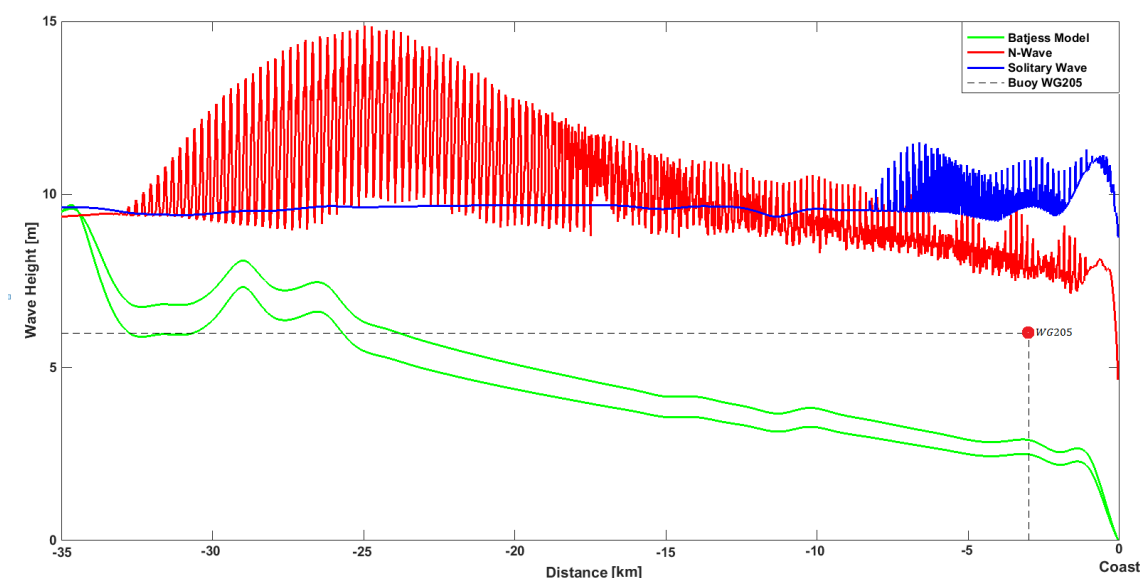


Figure 4.12: Comparison of the SWASH results with the analytical model of Battjes [1986] and the measured wave data

The energy dissipation for a breaking solitary wave for gentle slopes is studied by Battjes [1986]. A dissipation formula is proposed [Equation 4.9] in function of the breaking condition [H_b and h_b]. The dissipation formula is implemented [Green Line] for the N-wave breaking conditions. It is already mentioned that the Battjes formula is only used to check if the modelled SWASH wave dissipates energy in the breaking zone. The average dissipation of the N-wave has approximately the same slope as the dissipation model of Battjes. Therefore it can be concluded that the N-wave dissipates energy between the point of breaking and the coast.

4.3.4. CONCLUSION

From both SWASH results it can be concluded that the applied N-wave model approaches the data of the Tohoku tsunami in 2011 [Table 4.1] and the analytical models the best. It is assumed to give a good first estimate to describe the Tohoku tsunami in 2011.

The N-wave, however, still has some drawbacks which must be mentioned. First of all, the mathematical background of the N-wave is a simple model to capture the essential characteristics. The solitary wave has explicit input parameters, while the N-wave is manipulated until the initial conditions are met. Also, the point of breaking for an N-wave cannot be clarified with the proposed analytical models. The changes in steepness and amplitude of an N-wave could significantly change the results which are seen on the shore. Nevertheless, the N-wave shoals and breaks into multiple solitons, eventually transforming into an incoming bore.

Another missing phenomena in the N-wave simulation used for this thesis, is a retreat of the water along the coast, which is often observed for tsunami events. One reason this could be happening is due to the fact that the design tsunami path [Figure 4.3ba] is not chosen correctly. For Sendai, a slight retreat was observed by the buoys and the videos, so the simulation can be said to be missing this phenomena, but this retreat could also be influenced by different coastal boundary conditions. Hence, the missing phenomena is not looked at in detail.

For the present aim of this thesis, the N-wave is taken as it captures the essential features as observed in 2011. Therefore, the N-wave will be used to model the tsunami for the case study of Kamakura.

	Data [m]	N-wave [m]	Solitary Wave [m]
Initial wave height	6	6.2	6.5
Wave height just off-shore	6.5	7	9
Maximum inundation depth	5-15	10	15
Run-up	6500	7000	10500

Table 4.1: Comparison of the SWASH model results with the measured data

Several improvements could be made to improve the model. First of all, a 2- or 3-Dimensional model for real sea-bed changes for different tsunamis can be simulated. New tsunami models could be used, such as [Smith et al. \[2016\]](#) to include the direct geophysical impact to the water, allowing the initial tsunami wave to have its unique wave form. Secondly, different sensitivity analyses can be conducted to check the influence of different parameters. For example, the influence of the Manning's coefficient on the run-up could be checked, and also insight on the relationship between the steepness and amplitude of an N-wave could be obtained to improve the results.

4.4. CASE STUDY OF KAMAKURA

Now the SWASH model validated for the Sendai case is applied to the Kamakura case study. The first step is to define the path of the design tsunami wave [Figure 4.13]. This path intends to model the tsunamis which result from earthquakes caused by the Sagami trough or the Nankai trough. These troughs are connected, therefore, we assume that the simulations cover the possible damages resulting from tsunamis caused by both troughs. Moreover, this cross-section was chosen in order to have a smooth slope, avoiding large bars and troughs which exist on the complex bathymetry in Sagami Bay. Refraction is not taken into account when choosing the cross-section, but this can be included in further research to see if this creates a large difference in the results. The worst-case scenario occurs when the tsunami wave directly reaches Kamakura. Otherwise, there is no dynamic impact of the wave, only a rising water level.

The computational grid in SWASH for Kamakura is 55 km, with 5000 cells, resulting in a 1D resolution of 11 m per cell. The remaining boundary conditions in SWASH are kept the same as in the case study for Sendai.

4

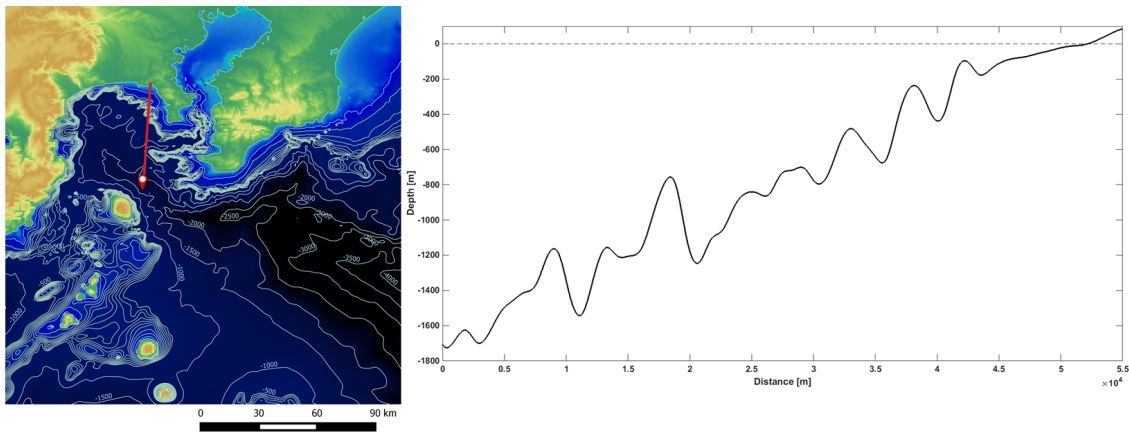


Figure 4.13: Bathymetry and chosen design slope for Kamakura case study

Similar to the case of Sendai, it is assumed that the tsunami resulting from an earthquake is an N wave with a leading crest. The period of the N wave is kept constant, and this is logical as the fault size is limited.

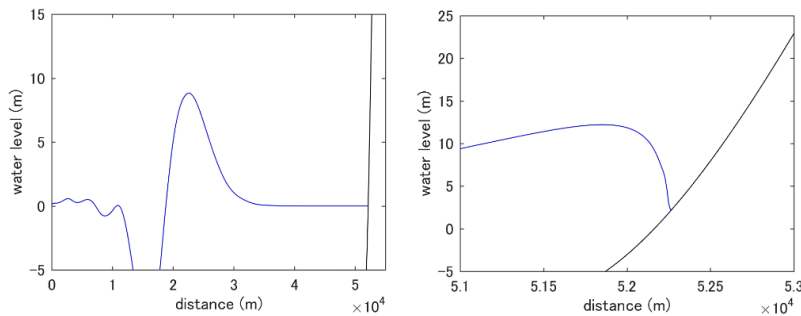


Figure 4.14: Results from the SWASH model for the Kamakura case study

In Chapter 3 it is stated that a primary defense must protect the city from a tsunami wave defined with a return period of one in a hundred years, in other words a level 1 event tsunami. This corresponds with a wave height of 8 meters. In the SWASH model, the initial wave conditions are varied until the incoming wave height input nearly coincides with this expected incoming wave height on the coast. An example of one of the tsunami levels are illustrated in Figure 4.14. Here, the level 1 tsunami is shown, and has an incoming wave height of 8 m, holding a characteristic like a bore. For the case of Kamakura, multiple tsunami scenarios are conducted in order to determine the damage caused under different scenarios - thus, seven different tsunami levels which range along the distribution curve which was derived in Chapter 3 are modeled.

In the following chapters, these seven different tsunami levels will be evaluated with a baseline risk for the current situation and then be intervened with risk reduction measures. The different tsunami scenarios modeled and its corresponding return periods are illustrated in Figure 4.15. As seen in Figure 4.16, seven different tsunami levels were modeled in SWASH to result with different flood scenarios and outcomes.

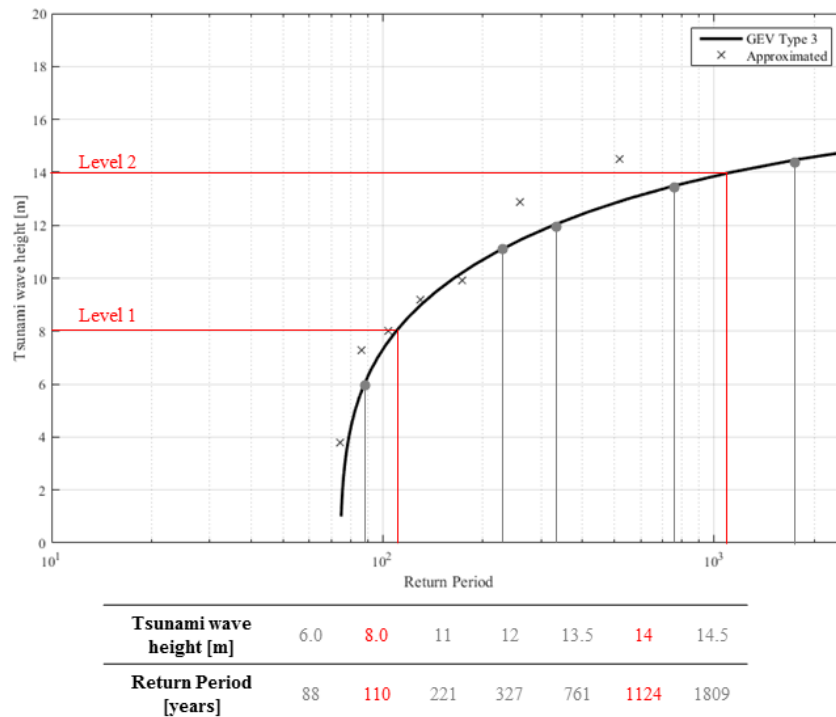


Figure 4.15: Different tsunami levels obtained from SWASH simulations along the return period distribution line

This run-up distance is derived for the current situation, with a 3 m dike, and is measured relative to the inner toe of the dike. For example, the purple line which illustrates the largest tsunami of 14.5 m, only gives 20.5 minutes till the tsunami arrives on the coast, and propagates approximately 1400 m inland, resulting in a large run-up distance. Here, the arrival time refers to the time from the wave appearance, since for the SWASH simulation the wave is not developed instantaneously, till the tsunami arrives and overtops the primary defense, in this case the road dike. The SWASH simulation is taken so that it starts exactly at the fault area (it can also be seen that the transect is taken to start from a fault in Figure 4.13). The slope of these lines illustrate the speed of the propagating wave inland, and the less steep the line,

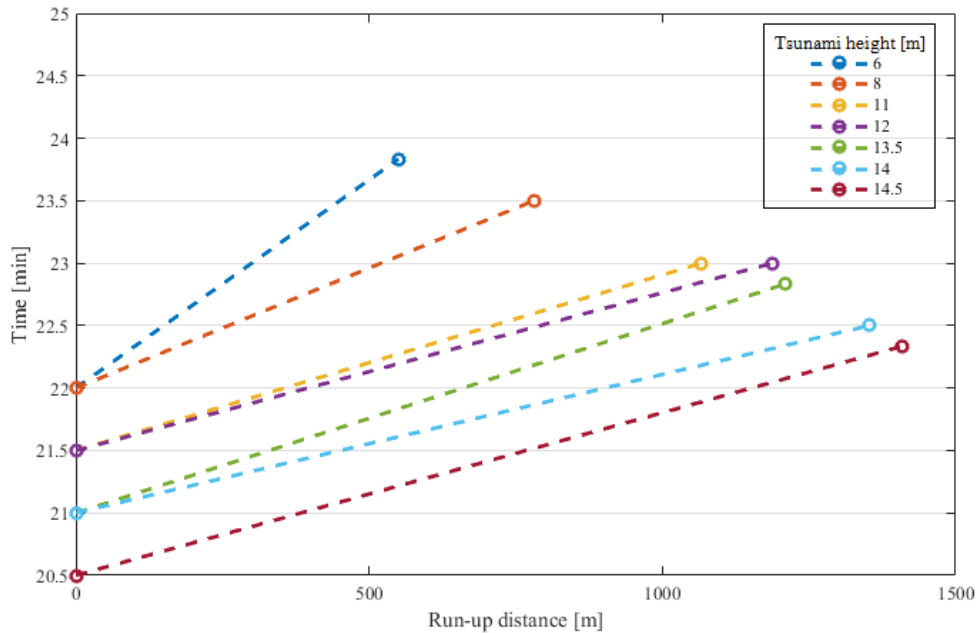


Figure 4.16: Arrival time, wave propagation speed and run-up distance for all tsunami levels

the faster the propagation speed on land.

The amount of damage caused by these different tsunami levels will be determined based on the depth times velocity (dv) criteria. The inundation depth and flow velocity values will be obtained from the SWASH results, as the model outputs give results for water level and flow velocity in each cell for each time step. It is worth to note that the flow velocity is assumed to be the same throughout the depth as only one layer in the vertical direction is run for this thesis in SWASH.

To determine the most influential dv -values to assess the damage for the entire tsunami run-up in the 1 dimensional cross-section, the maximum value of the depth \times velocity value in each cell will be derived. By taking the maximum dv -value, the maximum possible damage in the given time period of the tsunami run-up can be considered. Here, it is important to note that it is not the maximum depth multiplied by the maximum velocity value, but the maximum value of the product of the depth and velocity - these are two different values as the maximum depth and maximum velocity may not occur at the same place and time. An example of the inundation depth, flow velocity, and depth-velocity product at the time of maximum run-up is illustrated in Figure 4.17, for a flood scenario of an 8 m tsunami with the existing dike.

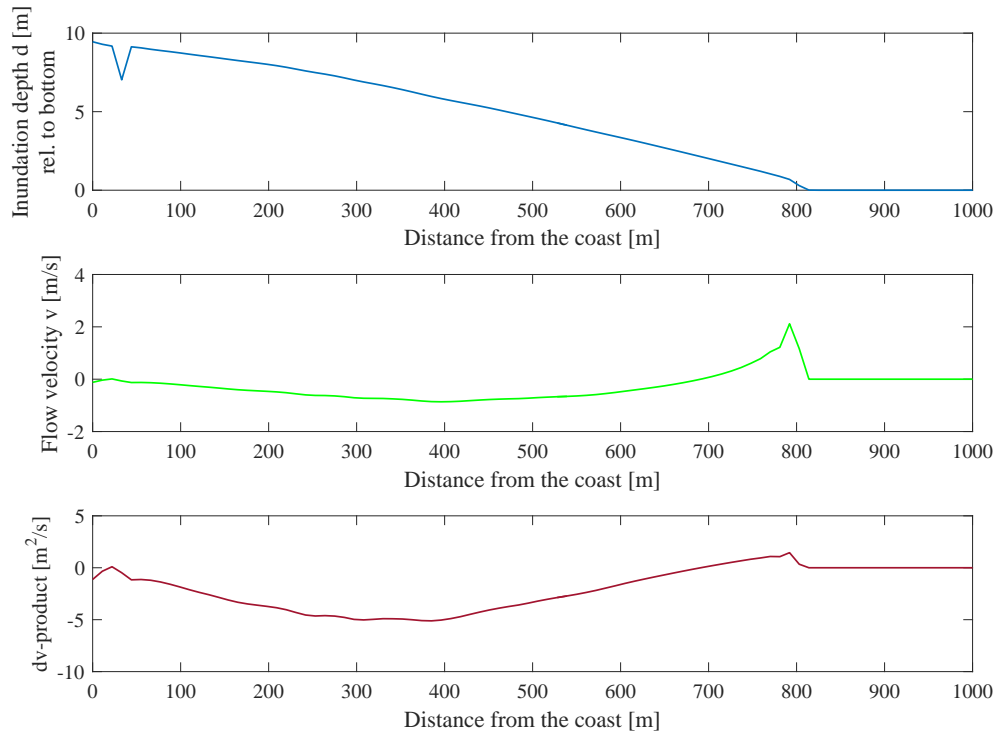


Figure 4.17: The inundation depth, flow velocity and dv -product along the 1D cross-section at the time of maximum run-up for a 8 m tsunami flood scenario with the existing dike

Figure 4.17 illustrates the inundation depth d , flow velocity v and their product dv -value at the time of maximum run-up for an 8 m tsunami under the baseline condition. In the graph showing the inundation depth, there is a dip at approximately 30 m from the coast. This is the inundation depth on top of the dike, and is seen as a dip as the inundation depth is taken relative to the bottom. Thus, for this case, if 3 m is added to that point of the dip, the curve can be made smooth.

Next, in the graph showing the flow velocity, it can be seen that most of the flow is negative. This means that the flow is already in the seaward direction at the point of time of maximum run-up, thus the water is already retreating. It is worth noting that the flow observed here is supercritical flow. Finally, the dv -product is determined by multiplying the inundation depth and flow velocity values. Due to the fact that the flow velocity can be negative, the dv -product is also can also be negative. For the damage function, the maximum absolute value of the dv -product is taken, as it does not matter whether which direction the flow is in to affect the number of casualties or the damage to buildings.

The amount of damage in terms of fatalities, damage to buildings and in monetary terms will be given in more detail in Chapter 5.

5

RISK ASSESSMENT METHODOLOGY

This chapter describes the risk quantification and evaluation methods which will be used in this thesis. Firstly, risk and its ways of evaluation are introduced. Next, the underlying assumptions and inputs for each step of the risk analysis will be presented.

5.1. RISK ASSESSMENT METHOD

The steps taken to conduct a risk analysis for tsunamis in this thesis are illustrated in Figure 5.1 and Figure 5.2 are taken in this thesis. The numbers in the two figures are correlated to each other, and it is important to recognize that the risk analysis is simplified for a 1D schematized cross-section as illustrated in Figure 5.1.

Risk is defined as $\text{probability} \times \text{consequence}$, and is the amount of annual expected damage resulting from an undesired event. Risk can be quantified in multiple ways, and in this thesis it will be done in terms of monetary values and acceptable risk levels. There are many different parameters which could be used to measure this risk such as loss of life, damage to buildings, environmental impacts and more. For the case of this thesis, two main variables are considered to measure the amount of risk: loss of life and damage to buildings. These two variables are evaluated together to determine the total risk.

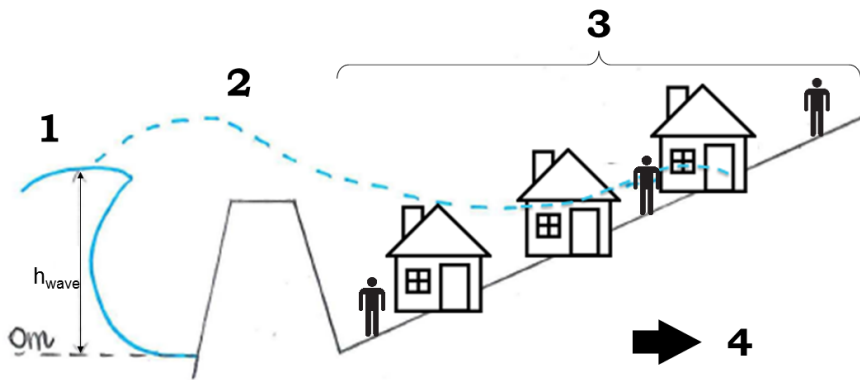


Figure 5.1: 1D Schematization to illustrate steps in the risk analysis

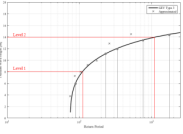
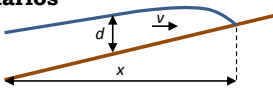
	Source	Output	Selection/ Assumptions
1 Tsunami wave frequencies 	<ul style="list-style-type: none"> Historical simulations (Ch. 3) 	<ul style="list-style-type: none"> Frequency dist., GEV Type 3 Probability of exceedance (Ch. 3) 	<ul style="list-style-type: none"> H: incoming wave height 7 different return periods to obtain wide range of curve T = 88, 110, 221, 327, 761, 1124, 1809 years (Ch. 4) $P_{exc} = P_f$
2 Flood Scenarios 	<ul style="list-style-type: none"> SWASH simulations (Ch. 4) 	<ul style="list-style-type: none"> Inundation depth d Flow velocity v Run-up distance x (Example in Tab. 6.4, Fig. 6.6, 6.7) 	<ul style="list-style-type: none"> Simplified to 1D Limitations: <ul style="list-style-type: none"> uniform distribution of houses & people wave development is highly dependent on chosen transect etc. (Ch. 4,5,8)
3 Determination of Damage	<ul style="list-style-type: none"> SWASH results $(d, v, x) \rightarrow$ (Ch. 4) $(dv)_{max}$ used in damage functions 	<ul style="list-style-type: none"> Loss of Life Damage to buildings Damage in € for all 7 tsunami levels 	<ul style="list-style-type: none"> Only direct costs
4 Risk Estimate	<ol style="list-style-type: none"> Tsunami wave frequencies Flood scenarios Damage Discount rate r (for NPV) 	<ul style="list-style-type: none"> NPV Risk Individual Risk Societal Risk 	$R = \sum \frac{P_f \cdot (L+D)}{r}$ <p>(Example in Fig. 6.5)</p> <ul style="list-style-type: none"> $P_{d f}$ = mortality fraction as a function of dv $N_A = 1$ (1 polder)

Figure 5.2: Flow chart of risk analysis for tsunamis

Before the risk assessment methodology is presented, the three different methods of estimating and evaluating risk are introduced in Section 5.1.1. This is followed by sections which aim to augment each of the steps illustrated in Figure 5.1 and 5.2 by further elaborating on each of the inputs and assumptions. Section 5.1.2 discusses the assumptions to determine the probability of flooding to be used for the risk analysis, Section 5.1.3 introduces the variables necessary to determine the damage, along with the assumptions and inputs for the damage functions for loss of life and damage to buildings. Finally, Section 5.1.4 provides the adjusted value of the real discount rate along with the steps leading up to this choice, which is conducted in order to maximize the net present value for this thesis. This is all summarized in Section 5.2.

5.1.1. RISK ESTIMATION

As mentioned in Chapter 2, risk can be estimated in terms monetary terms of net present value, or in acceptable risk levels of individual risk and societal risk. A short overview of these different ways of estimating risk will be given.

NPV Risk

Risk can be represented as the Net Present Value (NPV) to take into account the lifetime of the structure, and to do this the discount rate must be included in the basic equation as well. This present value of risk can be written as Equation 5.1.

$$R = \sum_{n=1}^N \frac{P_f \cdot D \cdot (1+i)^n}{(1+r)^n} \quad (5.1)$$

Here, N is the lifespan of the system, i is the inflation rate, r is the discount rate, P_f is the probability of failure, and D is the damage in monetary terms. For small values of inflation rate i and discount rate r , the present value may also be written as:

$$R = \sum_{n=1}^N \frac{P_f \cdot D}{(1+r-i)^n} = \sum_{n=1}^N \frac{P_f \cdot D}{(1+r')^n} \quad (5.2)$$

Here, r' is the actual interest rate which takes into account the inflation and it is of impact on the economy ($r' = r + i$). When assuming the life span of the system to be infinite (letting $N \rightarrow \infty$), the equation converges to [Vrijling et al., 2014]:

$$R(h_i) = \sum_i \frac{P_f(h_i) \cdot (L(h_i) + B(h_i))}{r'} \quad (5.3)$$

Here, $R(h_i)$ is the NPV risk, $P_f(h_i)$ is the probability of flooding, $L(h_i)$ is the costs resulting from the Loss of Life, $B(h_i)$ is the costs of damage to residential buildings, h_i is the incoming wave heights on the coast, and r' is the real discount rate. Equation 5.3 is the formula which will be used to compute NPV risk for this thesis. Hence, the damage costs is now represented as $L + B = D$ specifying the damage costs which will be considered for this thesis unlike the previous equations.

INDIVIDUAL RISK

Another way to represent risk is in terms of individual risk. Individual risk is defined as the probability of death of an average, unprotected person that is constantly present at a certain location, and is also known as local risk [Jonkman and Schreckendiek, 2015]. Individual risk can be computed with this general equation:

$$IR(x) = \sum P_f \cdot P_{d|f}(x) \quad \text{where} \quad P_{d|f}(x) = (F_D(x) \cdot (1 - F_E(x))) \quad (5.4)$$

Here, IR is the individual risk, P_f is the probability of flooding, $P_{d|f}$ is the probability of death given a flood event, x is the location of the individual, F_D is the mortality fraction, and F_E is the evacuation fraction. For the calculations in this thesis, there are multiple evacuation fractions as the evacuation behavior is distributed differently with behaviors such as immediate or delayed evacuation, thus, the probability of death given a flood event is assumed to be dependent to the mortality fraction derived from the dv_{max} product. Since the IR is dependent on dv , the IR is taken to be spatially dependent on the two fatality zones of the dv which will be explained in Section 5.1.3 (Figure 5.6).

The limit value of individual risk for areas in the Netherlands protected by flood defenses is proposed to be 10^{-5} per year [Jonkman and Schreckendiek, 2015]. It is important to note that this acceptable individual risk in the Netherlands is set for natural hazards which exist in the country such as storm surges and river floods, not for disasters such as tsunamis. Thus, the individual risk which will be computed may not lie within the acceptable limit for flood protection in the Netherlands. However, this acceptable level is not defined for tsunamis in Japan.

SOCIETAL RISK

Risk can also be represented in terms of societal risk with the relationship between failure probability of events and the number of fatalities, also known as the FN criterion. To evaluate the societal risk, first the FN curve must be calculated, and then the limit line is defined. The FN curve is calculated from the probability of exceedance determined in Chapter 3, and the amount of casualties estimated from the flood scenarios. The Netherlands have very high safety standards for societal risk, or group risks as they are also called, and they are determined on a national level for various activities [Vrijling et al., 2014]. A system can be considered safe if the FN curve lies within the limit line. This limit line is given by the following general formula:

$$1 - F_N(N) < \frac{C}{x^n} \quad \text{where } C = \left(\frac{\beta \times 100}{k \cdot \sqrt{N_A}} \right)^2 \quad (5.5)$$

Where $F_N(N)$ is the probability distribution function of the number of fatalities per year, N is the number of fatalities per year, n is the steepness of the limit line and C is the constant that determines the position of this limit line. The variables which determine C are a policy factor β , risk aversion index k , and the number of polders N_A . Lower values of β correspond with higher requirements of safety. It is important to keep in mind that these variables which determine C are specific for the Netherlands where high safety standards are required.

This limit line can be altered by changing the coefficients, such as β and k , of the current limit line used in the Netherlands. The policy factor $\beta = 1$ is commonly used in the Netherlands to assess flood risk, the steepness of the limit line is $n = 2$, and the risk aversion index $k = 3$ is the national societal risk criterion proposed by the TAW (Technical Advice Committee for Water) [Vrijling et al., 2014]. Similar to the case with individual risk, Japan does not define an acceptable level of societal risk.

5.1.2. PROBABILITY OF FLOODING P_f

As mentioned before, risk is defined as probability \times consequence. The probability which will be used here is the probability of flooding for an event, and is derived from the first step in Figure 5.2. In Chapter 3, tsunami frequencies, in other words the probability of exceedance of incoming tsunami wave heights, were given a distribution curve. This distribution curve starts at a return period of approximately 75 years, and this curve approaches an incoming wave height bound of 17 m for the less frequent tsunamis. Along this distribution curve, seven different tsunami levels are chosen to represent a wide range of tsunami levels depicted on this curve.

The probability of exceedance of incoming tsunami wave heights $P_{exc,wave}$ is assumed to be equal to the probability of exceedance of the foreshore or dike $P_{exc,dike}$. This idea is often used when the considered flooding variable is water level. This assumption is still acceptable for wave heights, although it is important to keep in mind that waves have energy, so there will be some reflection on the dike which will result in more overtopping than it would with a flood variable of water level.

$$P_{exc,wave} = P_{exc,dike} = P_f$$

Next, the probability of flooding P_f is assumed to be equal to the probability of exceedance of the foreshore or dike, thus, only the overtopping and overflowing failure mechanisms of flooding were considered. Here, it is assumed that even if the dike is overtopped or overflowed, the dike will not be eroded.

Looking at Figure 5.3, the assumption of the probability of flooding being equal to the probability of exceedance of a flooding variable is more easily explained. In the Netherlands, this assumption was used in the past because once the water level exceeds the dike height, there will be flooding and thus the failure of the sea defense; this directly links the probability of exceedance of the dike and probability of flooding.

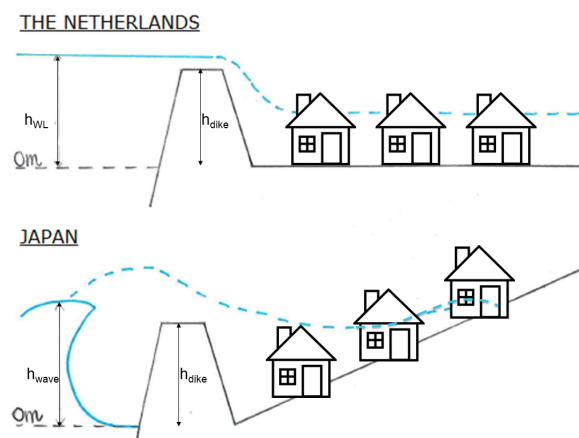


Figure 5.3: Schematization of dikes and land behind dikes in the Netherlands and Japan

5

In Japan, it is slightly different as now instead of water level, the variable used is incoming wave height. Considering the incoming wave height with the probability of exceedance of the dike leads to more overtopping than this would with considering the water level, as waves have energy. Even with more overtopping, which would also lead to more damage, the assumption that probability of exceedance of the dike is equal to the probability of flooding is presumed to hold for the case of Japan where incoming wave height is the variable used to derive the probability of exceedance. The dike is also assumed to not fail for a large incoming tsunami wave heights that exceeds the dike. If there was to be structural failure in the dikes, the damage will probably result to be larger than the computed results in the following sections where it has been assumed that coastal dikes do not fail.

In the simplified risk analysis which was previously used in the Netherlands, it was assumed that once a polder or a dike ring was flooded, all of the assets would be damaged [Jonkman and Schweckendiek, 2015]. Thus, the damage is constant, as illustrated in Figure 5.3. This however, is not the case in Japan, as the topographical characteristic behind a coastal dike is not flat but increasing in height in the landward direction. Therefore, the amount of damage highly depends on the amount of run-up resulting from the flood scenario, which results in the damage to not remain constant. The run-up distance and other flood parameters are dependent on the tsunami height. As illustrated in Figure 5.4, a larger tsunami results in a greater run-up distance than a smaller tsunami would.

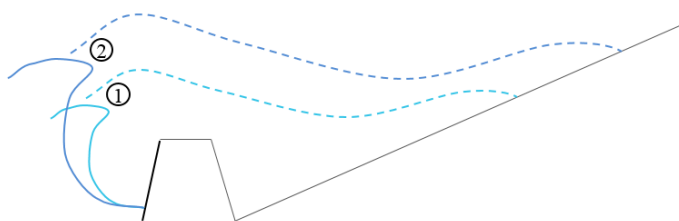


Figure 5.4: Sketch of the relationship between run-up distance and incoming wave height

5.1.3. DAMAGE ASSESSMENTS

To conduct the damage assessments, inundation heights d , flow velocities v and run-up distances x are obtained from the SWASH results for the different flood scenarios which are simulated. The flood scenarios are conducted in 1D, and the details of the SWASH inputs can be found in Chapter 4.

The two variables for damage which will be considered for the risk assessment is the loss of life and damage to residential buildings. For the damage functions used for the risk assessment, the product of the two parameters, inundation height and flow velocity, can be related to the amount of damage which would result for buildings and for the loss of life. The different damage functions of the inundation depth and flow velocity, in other words dv -values, will be given in Section 5.1.3 and 5.1.3. Since the d and v values in each time step for each cell is determined, there are many possible values of the dv product. For the computation of damage, the maximum dv product (dv_{max}) will be used; in other words, the maximum product of depth and velocity, which occur at the same time and space. This prevents the underestimation of damage, as the dv_{max} for a given cell will be the representative damage determining parameter throughout the tsunami run-up.

5

The dv -values representing practical instability in the damage assessment can be considered in the evacuation calculations. This practical instability of people occur when and where the dv -value ranges from 0.5 to $2m^2/s$, and cause fatalities when it is larger than $2m^2/s$. In this range of practical instability, it is assumed that people have a difficult time evacuating but the mortality fraction is reduced to 50%. The disaster risk area, which was previously determined simply by how far the water ran up the coast, is now correlated to the location of fatal dv -values, thus neglecting the areas where the water exists but do not cause fatalities.

Before the damage functions are introduced, Figure 5.5 is given to clarify the spatial distribution of economic values and densities of the population and houses along the cross-sectional slope. No indirect costs, such as business loss or opportunity costs, which could possibly result from a tsunami event is considered in the damage costs in the thesis. The 1D schematization which is illustrated in Figure 5.1,



Figure 5.5: Schematization of spatial distribution economic values and densities along the cross-sectional slope

is a representative cross-section which is given by the line labeled 'cross-section' running through Kamakura in Figure 5.5. The SWASH simulations are conducted in 1D, thus, the spatial distribution is interpolated from the 1D computation results, assuming a uniform distribution of people and buildings.

LOSS OF LIFE

The estimated number of the loss of life can be computed in the following equation [Jonkman and Schweckendiek, 2015]:

$$N = P_{d|f} \cdot N_{PAR} = F_d \cdot (1 - F_E) \cdot N_{PAR} \quad (5.6)$$

Here, N is the estimated number of the loss of life, N_{PAR} is the number of people at risk, and $P_{d|f} = F_d \cdot (1 - F_E)$ is the mortality/evacuation fraction which is also used to evaluate individual risk. The relationship between mortality, inundation depth, and flow velocity is known from past research [Jonkman and Penning-Rowse, 2008]. Hence, the mortality fraction will be illustrated as a function of flow velocity and inundation depth, in other words the dv -criteria :

$$F(dv_{max}) = \begin{cases} 1, & \text{if } dv_{max} \geq 2 \text{ m}^2/\text{s} \\ 0.5, & \text{if } 0.5 \leq dv_{max} < 2 \text{ m}^2/\text{s} \\ 0, & \text{if } dv_{max} < 0.5 \text{ m}^2/\text{s} \end{cases} \quad (5.7)$$

As it is a mortality function, 1 illustrates that above a dv_{max} -value of $2 \text{ m}^2/\text{s}$, the mortality is 100%. To have $F(dv_{max})$ as a mortality fraction, the whole computation grid of SWASH will be considered.

The relationship between dv_{max} and mortality is illustrated in Figure 5.6 for the current (baseline) situation. The figure is zoomed into the small outlined square in the smaller right figure, as the determining dv values cannot be seen clearly in the large scale. This is a very important figure as it is the determining factor of the amount of fatalities resulting from a tsunami, and will also be later used to quantify individual risk.

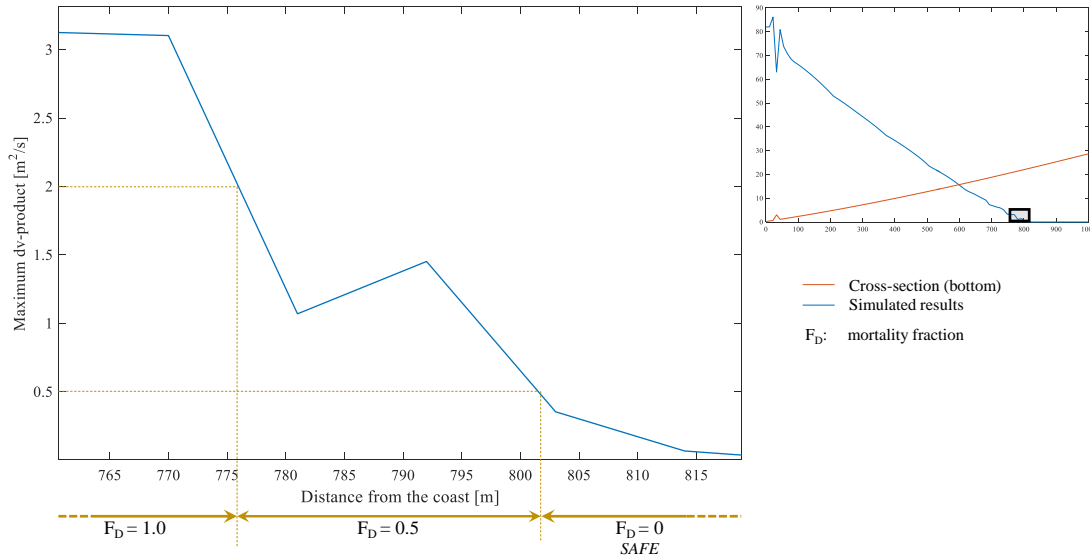


Figure 5.6: Relationship between dv_{max} and mortality

First, to discuss the overall dv_{max} curve, it is smoothly decreasing in the landward direction, however, there is a large dip seen on top of the dike. This is due to the fact that the inundation depth d is taken relative to the bottom, so on top of the dike, d is 3 m smaller. Thus, the curve would be smooth if the absolute water level would be used for inundation depth curve. Next looking at the figure with the mortality fractions, all the people who have not evacuated and are in the region where $dv > 2$, which is from the coast till approximately 775 m inland, will not survive - this region has 100% mortality. After this region, there is the 50% mortality region, then if $dv < 0.5$, it can be considered safe ground. This figure

will be referred to many times in the following chapters.

The sum of the cells which result to have mortality of 100% will be divided by the total amount of cells considered. The final damage function to estimate the damage resulting from loss of life is then:

$$L(h) = C_{human} \cdot \left(\sum_{i=1}^M cells(F(dv_{max}) = 1) \right) \cdot N_{PAR,i} \cdot F_E + C_{human} \cdot \left(\sum_{i=1}^M cells(F(dv_{max}) = 0.5) \right) \cdot N_{PAR,i} \cdot 0.5 \cdot F_{E,no} \quad (5.8)$$

Where, $L(h)$ is the estimated damage costs resulting from the loss of life, M is the total amount of cells in the simulation, $N_{PAR,i}$ is the number of people at risk in each cell, F_E is the evacuation fraction (of which $F_{E,no}$ is the fraction of those people which do not evacuate), and C_{human} is the cost of a human life. In Japan, there is a value for the cost of human life, which is derived from the amount of compensation in the occasion of a death. This value of human life is ¥260 million (2.1 M€) [Cabinet Office Government of Japan, 2007].

5

The variable F_E is dependent on the evacuation distribution, and this will be explained further in Section 6.1.1. The population at risk $N_{PAR,i}$ is estimated from the size of the SWASH computational grid and the population density assuming uniform distribution of population. This is computed using the following equation:

$$N_{PAR,i} = N_{dense} \cdot n \cdot L \quad (5.9)$$

Here, the population density of Kamakura is 4400 ppl/km² ($N_{dense} = 0.0044 \text{ ppl/m}^2$), the size of each grid cell n is 11 m, and the coastal length L is 8 km. With this, the SWASH model considers approximately 57% of the total population of Kamakura, as the computation grid does not cover the entire city. Of course, this is a very simplified model, assuming uniform distribution of people, and implying the area at risk to be like a rectangle.

DAMAGE TO RESIDENTIAL BUILDINGS

The damage to residential buildings can be estimated from the approximate cost of repairs which has the general equation:

$$\text{cost of repairs} = \text{market value of building} \times \text{percentage damage value}$$

The amount of damage on a residential building is determined in terms of dv -values, but unfortunately, the dv -value does not have an exact relationship with the damage percentage of a residential building. It is important that the dv -value is the only variable considered for damage, as the Clausen damage criterion, which included velocity as well as dv , showed a poor relationship between observed damage and predicted damage. Therefore, for this thesis, assumptions based on the approach which is adjusted from the Clausen criterion, by only looking at the dv -value, will be used [Pistrika and Jonkman, 2010].

$$F(dv_{max}) = \begin{cases} 0.00, & \text{if } v = 0 \cup d = 0 \\ 0.50, & \text{if } 0 < dv_{max} < 3m^2/s \\ 0.75, & \text{if } 3 \leq dv_{max} < 7m^2/s \\ 1.00, & \text{if } dv_{max} \geq 7m^2/s \end{cases} \quad (5.10)$$

Here, 0.00 refers to 'no damage', 0.50 refers to 'inundation damage', 0.75 refers to 'partial damage' and 1.00 refers to 'total destruction'. There is a large jump in the damage function from 'no damage' to 'inundation damage', however, this allows the inclusion of non-structural damage costs in the 'inundation damage'. This includes costs of goods inside the house, when the inundation damage is not causing much structural damage to the building.

This damage criterion proposed by Pistrika and Jonkman [2010] was developed for wooden houses for the flooding case in New Orleans. This criterion is used for this thesis because unlike the other cities in Japan, 67% of the residential buildings in Kamakura are wooden [Kanagawa Prefecture, 2016], most probably due to the conservation of historical buildings for tourism. By considering the criteria for wooden buildings, it is conservative for the remaining 33% of the houses, however, the advantage is that it includes the most vulnerable type of building.

The damage function for the amount of damage on residential buildings is the following:

$$B(h) = \sum_{i=1}^M (C_{house} \times F(dv_{max})) \times H \quad (5.11)$$

Here, $B(h)$ is the estimated damage costs from the damage to residential buildings, M is the total number of computation grid cells in SWASH. H is the number of houses per cell length, which is assumed to be uniformly distributed along the whole 1D cross-section. The value of H is taken as cell length as all the costs are interpolated to have an estimate for the entire area of Kamakura. Knowing the number of households in Kamakura is 17101 as of 2015 [Kanagawa Prefecture, 2016], the number of houses per cell length is 66 houses per cell length. The C_{house} refers to the market value of a residential building and the average value for a house in Japan will be used. An average house in Japan is defined as a living space of less than 80 meters squared in area, and as of 2016, the average market value is ¥35 million (0.28 M€) [Real Estate Shonan, 2016].

5.1.4. REAL DISCOUNT RATE

The real discount rate plays a very important role when evaluating risk in terms of Net Present Value (NPV) risk. The real discount rate in Japan is currently 0.3% [Bank of Japan, 2008], and the inflation rate i is so small it is negligible. When adjusting the computed total risk to NPV, the real discount rate plays an important role. In the Netherlands, discount rates which range between approximately 2 - 5 % has mostly been used (Prof. S.N. Jonkman, Personal Communication, 25/5/2016). This is because if the discount rate is very small such as in the case of Japan, the calculated NPV becomes too large.

To overcome these problems, there is a general rule for engineering managers to use risk adjusted discount rates to calculate the NPV for projects in order to maximize the value [de Neufville, 1990]. Therefore, a sensitivity analysis is conducted to determine a value for the discount rate r which is within a range which does not cause the values to be too large.

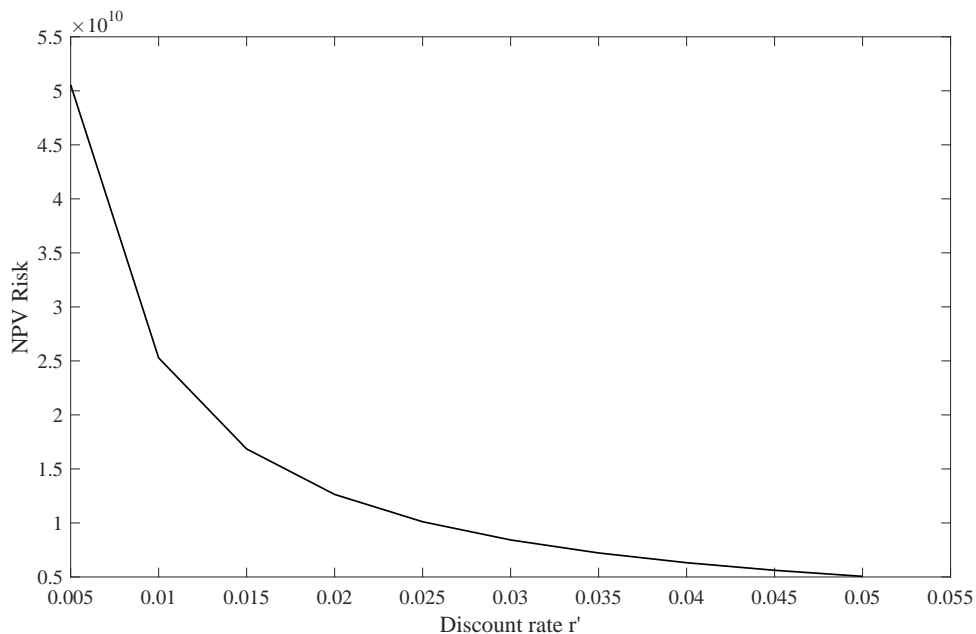


Figure 5.7: Sensitivity analysis for discount rate r

From the outcomes of the sensitivity analysis, the discount rate r to be used as a representative value for this thesis is chosen to be 2.5%.

By using this value for the discount rate, the baseline NPV risk value is reduced by a factor of approximately 5 from the original discount rate value of Japan (0.3%). Even if the discount rate is further increased, the reduction in NPV risk is minimal, ranging within the same magnitude as the other larger values. In addition, this value on one hand keeps adjustments from the original value to a minimum, and on the other hand closer to the more familiar discount rate of 5% that is used for risk analyses in projects in the Netherlands. Moreover, increasing the discount rate further causes the risk curve to become more linear, which is not preferred.

An example of adjusted discount rates can be given with the projects conducted by the recent, second Delta Committee. Currently, the interest rate in the Netherlands is 0.13%, however, to compute the NPV for projects, the discount rate of 5.5% is being used [Deltares, 2011].

5.2. CONCLUSION

Many assumptions, inputs and simplifications are made to conduct a risk assessment for tsunamis. These are summarized below.

- "Semi 1-Dimensional Schematization"
- There is a uniform distribution of population and houses in each cell in the considered cross-section
- Probability of flooding is assumed to be equal to probability of exceedance of the dike height (explained in Section 5.1.2)
- Assumption of no structural failure to the road dike (layer 1)
- Both the damage to residential buildings and the loss of life is considered in the total risk in monetary terms
- The maximum dv -value for each cell (dv_{max}) is the indicator for the amount of damage to residential buildings and loss of life in each cell
- Discount rate r is adjusted to be 2.5 %
- The exchange rate of €1 = ¥125 will be used throughout this thesis

The damage function is also summarized in Figure 5.8.

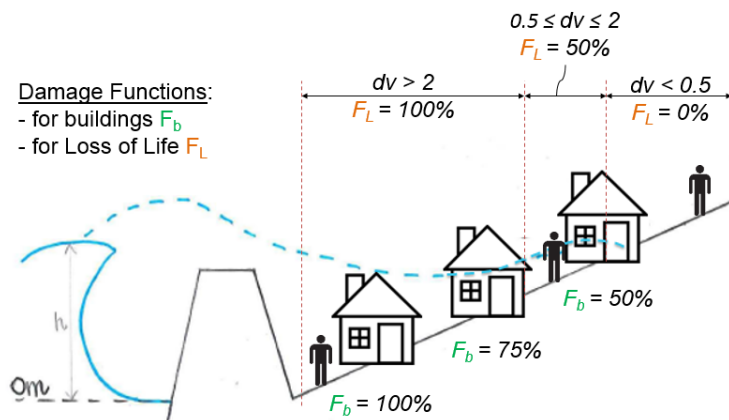


Figure 5.8: 1D Schematization of damage functions for damage to buildings and loss of life

The key inputs for the spatial distribution of economic values and densities of the population and houses are summarized in Table 5.1.

Table 5.1: Key inputs of spatial distributions and economic values

Total population exposed (at risk)	98349	ppl
Population density	4400	ppl/ km^2
Housing density	750	houses/ km^2
Cost of a human life	2.1	M€
Market value of a residential building	0.28	M€

It is important to realize that the results would most probably be very different with non-uniform spatial distribution of people and houses. In reality, as can also be seen in Figure 6.1, the houses are more

densely built in the coast, which also means that there are more people near the coast. Moreover, in this thesis, the tourists are not included in the population at risk. Most of the tourists who visit Kamakura enjoy the beach or the recreational areas near the coast, which would also influence the amount of casualties which would be recorded. This is an improvement for the damage assessment which could have a large influence in the results.

This risk assessment for tsunamis will be used to quantify and evaluate risk for the current situation (baseline) and for different interventions.

6

TSUNAMI RISK QUANTIFICATION FOR KAMAKURA

In this chapter, the risk will be quantified for the baseline situation and for situations with different interventions. In order to do so, a brief overview of existing protection measures and how they are included in the risk assessment is given. Next, of the many possible interventions, two which have been chosen for this thesis, dike heightening and improvement of evacuation, will be presented and their risk will be quantified. Finally, the risk for the combination of the interventions will be quantified.

6.1. BASELINE RISK QUANTIFICATION

The baseline risk can be quantified following the flow chart illustrated in Figure 5.2. Firstly, the baseline condition with the existing protection measures will be introduced. Here, the inclusion of these protection measures in the risk assessment will also be presented. This is followed by an explanation on the procedure of quantifying risk, and finally the results of the baseline risk will be given.

6.1.1. EXISTING PROTECTION MEASURES

The two protection measures which currently exist in Kamakura are the road dike along the coast, and an evacuation system consisting of an early warning system.

ROAD DIKE

The road dike along the coast of Kamakura is 8 km long, and is 3 m high relative to the beach which is 5 to 6 m high relative to mean sea level depending on the location along the coastline. From [Google Earth \[2016\]](#), it is clear that Kamakura is isolated with mountains and high hills separating it from other neighboring cities, as also illustrated in Figure 6.1. Therefore, it can be assumed that there is no flooding resulting from the lack of protection in the neighboring cities.

The road dike is assumed to be structurally strong enough to withstand the tsunami forces without failing, the outer and inner slope of the dike is assumed to be 1V:3H. The road dike is also located approximately 30 m behind the shoreline. The dike height and slope is inputted into SWASH as boundary conditions of the bottom, similar to the way the bathymetry and topography is included.

EVACUATION SYSTEM

An evacuation system for tsunamis exist in all coastal cities in Japan. The influence of the evacuation system is difficult to assess, as the awareness for tsunamis varies according to the history of tsunamis in the area. For example, Kamakura has not experienced any tsunamis in almost one hundred years, while



Figure 6.1: Satellite plan view of Kamakura [Google Earth, 2016]

the Tohoku area have experienced five tsunamis in the last hundred years.

After the 2011 earthquake and tsunami which occurred in Tohoku, the Kamakura city municipality provided a hazard map of the worst case scenario tsunami, showing the location of available evacuation areas and which areas are more prone to high inundation heights. This hazard map can be seen in Appendix D. In Kamakura, however, there is a house construction code which limits the height of houses which can be constructed to 15 m, which is approximately 4 stories high [Kamakura City, 2012]. This height may not be high enough for the protection of large scale tsunamis. For the case of this thesis, the reliability of the designated evacuation centers and different categorizations of evacuation areas will not be covered. Instead simple landward evacuation and vertical evacuation in the center of the 1D cross-section will be considered.

The selection of the evacuation fraction of the baseline condition, and necessary assumptions, have been made based on the recorded evacuation fractions of the Tohoku tsunami event in 2011, and will be discussed elaborately in Section 6.1.2. The two important factors of evacuation, evacuation speed and evacuation behavior, will be explained and discussed in order to introduce the evacuation model.

6.1.2. EVACUATION MODEL

The steps of the evacuation model and their assumptions are shown in Figure 6.2.

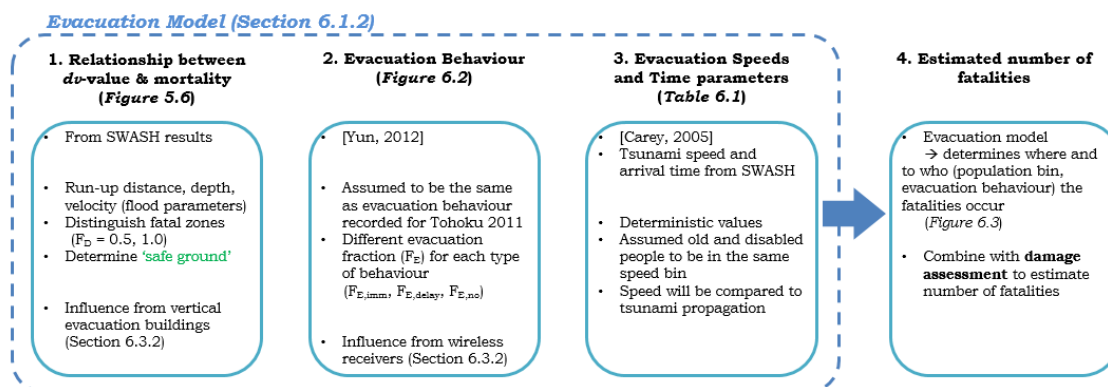


Figure 6.2: Flow chart for evacuation model

The first step which is to determine the relationship between dv -value and mortality was obtained based on the SWASH results in the Chapter 5 (illustrated Figure 5.6). The speed at which people can evacuate and evacuation behavior have a large influence in the rate of survival as included in steps 2 and 3. These steps in the flow chart will be explained in the following sections.

Evacuation speed The age distribution of the population in Kamakura will be given to get an overview of the speed at which people evacuate. This is an important factor which influences evacuation as it can be compared directly to the arrival time and propagation speed of the tsunami wave. This speed of evacuation is different according to age and health. The population bins in percentage relative to the total population is illustrated in Table 6.1.

Table 6.1: Population age distribution and each of the selected evacuation speeds

	Age distribution	Percentage of Population	Evacuation Speed [m/s]
Children	0 - 14	12	1.20
Average Adults	15 - 64	56	1.38
Old/Disabled	> 65	32	1.00

These values will also be illustrated in m/min as the arrival time and propagation speed are more easily comparable in the unit of minutes. Table 6.1 includes the 3% of the total population who carry a disability [Kanagawa Prefecture, 2016], and are assumed to be evenly distributed amongst the entire population. Here, a person with a disability is defined as a person who has a mental and/or a physical disability, and who may not be able to act as an average adult during an evacuation. They are included in the same population bin as old people with the age of 65 years and above because these two population categories are assumed to have similar evacuation speeds, i.e. 1 m/s (60 m/min).

From research results, it can be assumed that an average adult can evacuate at 1.38 m/s (83 m/min), and an elderly person can evacuate at 1 m/s (60 m/min) [Carey, 2005]. Based on these values, it will be assumed that a child can evacuate at a speed in between an old person and an adult. Moreover, the toddlers are also included in the bin for children because they often receive help to evacuate from adults which make the evacuation smoother for this population bin. This is the case which was seen in the Tohoku tsunami in 2011 [Yun and Hamada, 2012]. Under these circumstances, computations will be made

with these assumptions for the 1D cross-section. Since this thesis is looking at a 1D schematization, the most simple mode of evacuation which is to evacuate landward will be used to describe the evacuation movement.

Evacuation behavior Due to human behavior and other possible failure mechanisms, such as the EWS not working, some correction factors must be included to compute the amount of people whom will be at risk. The first correction factor to be included is that not all people evacuate even when there is a warning of a tsunami. The second correction factor, is to take into account the time it takes till people start evacuating, i.e. a delay in evacuation. The third correction factor is to include the failure probability of the early warning system. This failure could occur due to the problems in the system, network failure (as most systems are linked to TVs and mobile phones), and more. All these factors which influence evacuation under a disaster situation was clearly recognized during the Tohoku earthquake in 2011 [Yun and Hamada, 2012].

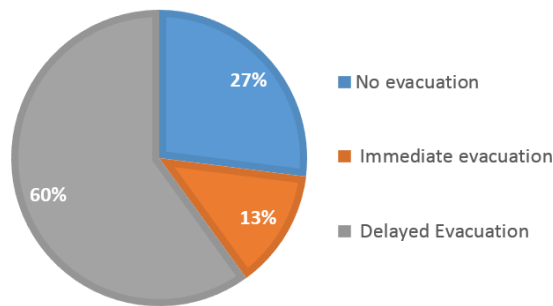


Figure 6.3: Tsunami evacuation behavior based on Great Eastern Japan earthquake and tsunami event in 2011 [Yun and Hamada, 2012]

This evacuation behavior shown in Figure 6.3 illustrates that even for a location where people are more accustomed to tsunami evacuation, a surprisingly high percentage of the population, 27% of the total population, did not evacuate immediately. This may have been the contributing factor to the large amount of casualties recorded for the Tohoku event. According to the report of Yun and Hamada [2012], there were reasons for these human behaviors. For the people which did not evacuate, the reasons were due to no information or wrong information on evacuation, ignoring warnings based on past experiences, or being on duty to help with the evacuation. This also covers the reasoning behind the third correction factor, i.e. the failure of the EWS. For the delayed evacuation, the reasons were due to traffic jams from trying to evacuate with a car, helping others, searching for relatives, and not going to the assigned evacuation areas. Finally, those who evacuated immediately stated that they did this because they followed others or remembered former disasters.

The statistical values illustrated in Figure 6.3 will be used for Kamakura to include human evacuation behavior. These statistics illustrate the overall behavior which was recorded for the entire Tohoku coastline. The amount of delay in evacuation ranged from 5 to 60 minutes from this research, and the tsunami arrival times for this event ranged from 25 to 55 minutes for all areas except the Sendai plain. Although the exact human behavior is difficult to infer, also due to the fact that these evacuation data is not specific to location, an assumption will be made for Kamakura based on this. The tsunami arrival time is on average 21 minutes for Kamakura based on SWASH results, therefore, the delay is taken to be a deterministic value of 5 minutes. This is one fourth of the time before the tsunami arrives, which is assumed to be the maximum delay a person would be willing to take under a stressful disaster situation. Here, it is assumed that the EWS does not reach everybody, and is the reason for the delay or no evacuation.

EVACUATION MODEL

The evacuation is modeled along a 1D cross-section, and equation 6.1 is used to determine whether a fatality occurs or not when evacuation is considered.

$$t_{tsu} > t_{evac} = \frac{x_{max} - x_0}{c_{evac}} + t_{delay} \quad (6.1)$$

Here, t_{tsu} is the time at which the tsunami reaches a cell [min], t_{evac} is the time it takes for the people from a cell to evacuate to a safe ground [min] (past the maximum run-up point with fatal dv values), x_{max} is the maximum run-up distance location in the computational grid with fatal dv values [m] (Figure 5.6), x_0 is the location of the considered cell in the computational grid [m], c_{evac} is the evacuation speed [m/min], and t_{delay} is the amount of time of delay till a person starts evacuating [min]. A fatality is assumed to occur when $t_{tsu} > t_{evac}$ for a cell, and on the contrary, a person survives if $t_{tsu} \leq t_{evac}$. The evacuation speed c_{evac} is dependent on the type of population, and the evacuation distance is dependent on the location of the cell being considered. For example, $(x_{max} - x_0)$ is much larger for cells located near the coast than cells located landward.

The evacuation model can also be explained by the example of the evacuation model computed for the 14 m tsunami in the baseline condition illustrated in Figure 6.4. It can be assumed that at time 0, the earthquake occurs and the early warning is immediately executed.

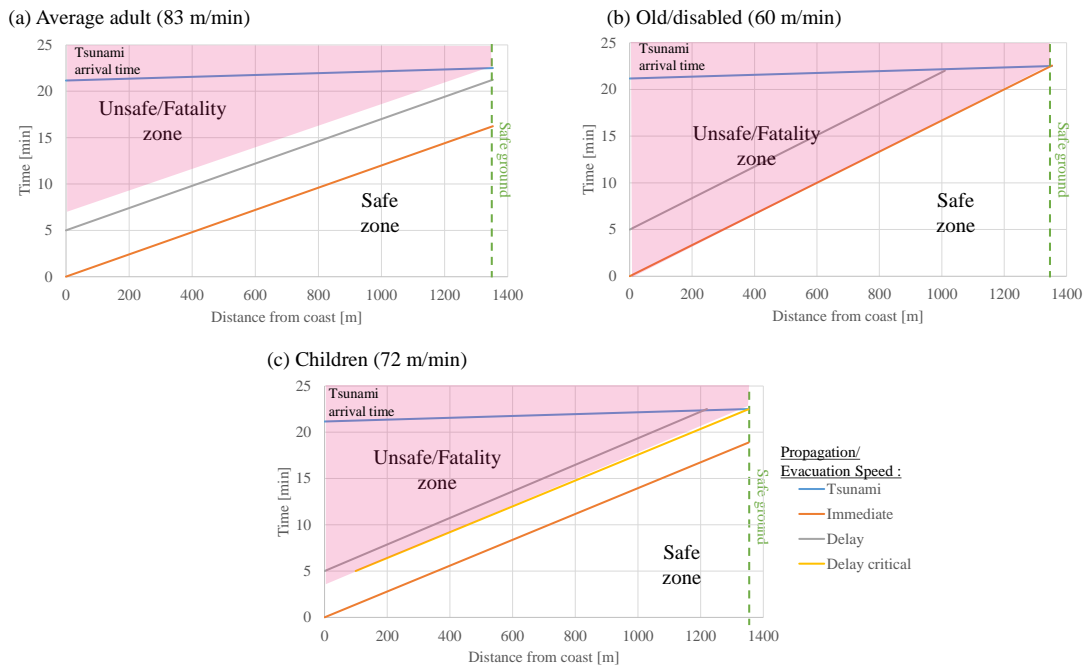


Figure 6.4: Evacuation model for the flood scenarios of a 14 m tsunami

The main underlying concept which Figure 6.4 aims to illustrate is that if the people arrive to the 'safe ground' (illustrated by the green line) before the tsunami, the people will survive, and people who start anywhere in the pink area (unsafe/fatality zone) will not survive. Hence, the key factor is when and from where the people evacuate.

For example, in the scenario which was conducted in this thesis with only a 5 minute delay in evacuation, all adults who evacuate will survive (Figure 6.4(a)). This is not the case, however, for the children

and old/disabled people. Looking at Figure 6.4(b), the old/disabled people who are at the coast in the time of the warning, barely make it to safe grounds with immediate evacuation and do not make it to safe grounds with delayed evacuation. Therefore, based on these results, it is crucial for the old and disabled people who want to survive to evacuate immediately, or to reside further away from the coast. For the children, the result is similar, and the children with delayed evacuation do not survive.

As you can see from the amount of area shaded in pink, the old/disabled people are most vulnerable. For this thesis, the delay time was chosen to be a deterministic value of 5 minutes, and some of population with delayed evacuation, for this case the children and the old people, result in fatalities. For example, the old/disabled people who are delayed in evacuation and are located in the first 300 m of the cross-section is expected to not survive from the model. The remaining number of the fatalities result from not evacuating.

Equation 6.1 is a general equation for a simplified evacuation model in a 1D schematization for a simply landward evacuation. The evacuation behavior F_E is estimated to be the same as those collected for the Tohoku 2011 event, and the evacuation speed is taken from research [Carey, 2005]. The results of the evacuation model combined with the damage assessment will be discussed in results for the baseline risk (Section 6.1.4). Here the number of fatalities and damage to buildings will be presented.

6.1.3. RISK ASSESSMENT

The quantification of the baseline risk can be done by establishing a relationship between return period of the incoming wave height and damage resulting from the wave. The relationship between return period T and incoming wave height h is derived from the methods given in Chapter 3, and is used to get the probability of flooding for different tsunami levels - This is illustrated in Figure 6.5(a). To get a wide range of this Th curve, seven different tsunami levels with return periods from 88 to 1809 years are taken. The smallest return period was taken to be 88 years, corresponding to an incoming wave height of 6 m, as the distribution curve is fitted to plots which start around 75 years. The largest return period of approximately 2000 years was taken, in order to avoid inaccuracy due to extrapolation, and to not shift too far from the more familiar return periods used in Japan; as the general safety level in Japan is similar to the US to be around 1/100 years which is approximately equal to the Level 1 categorization.

With the tsunami frequencies chosen, the flood scenarios are simulated in SWASH for the seven different tsunami levels. To conduct flood scenarios, the existing protection measures introduced in Section 6.1.1 must be included in the boundary conditions/calculations - these inputs are shown in Table 6.2. The evacuation fraction F for immediate and delayed evacuation is presented.

Table 6.2: Baseline risk inputs for existing protection measures

Dike height (m)		3
Evacuation	$F_{E,imm}$	0.13
	$F_{E,delay}$	0.60
	$F_{E,no}$	0.27

The dv_{max} values in each cell are obtained from each of the flood scenario SWASH results to be used for the damage functions. The damage functions are combined with the economic values and spatial distributions to estimate the damage in monetary terms. The estimated damage in relation to the tsunami wave height is illustrated in Figure 6.5(b). Here, the damage computed for both the loss of life and damage to buildings are illustrated along with the total damage (Total Damage (B€) = Loss of Life (B€) + Building damage (B€)).

The TD curve illustrated in Figure 6.5(c) combines the relationships from curves (a) and (b), to get a direct relationship between return period and damage of a given scenario. In this way, a relationship

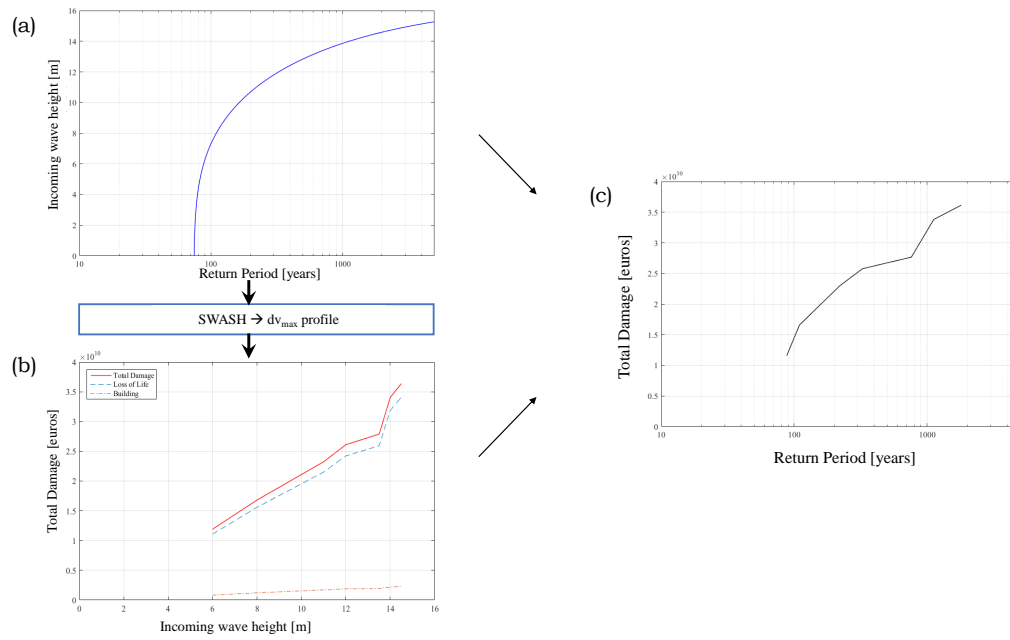


Figure 6.5: Relationship between damage, return period and wave height for a given scenario under the baseline conditions

between probability of flooding and damage can be derived. This is easily done as the probability of flooding and return period have an inversely proportional relationship.

6.1.4. RESULTS FOR BASELINE RISK

Before computing the baseline risk, some important assumptions and concepts will be highlighted. As mentioned before, the probability of flooding is assumed to be equal to the probability of exceedance of the dike, which is also equal to the probability of exceedance of the incoming wave height (Section 5.1.2). And most importantly, risk is the product of probability and consequence, in this case consequence is represented by damage, and this risk can be approximated by the area under the damage-probability curve.

The sum of the areas illustrated with letters from A to M under the curve in Figure 6.6 is the risk for the baseline condition. When computing the risk using equation 5.3, care should be taken not to include multiple overlapping areas since this will lead to an overestimation of risk. As it is done in Figure 6.6, the overlapping areas must be removed from the calculation. This is simply realized by subtracting the overlapping areas when computing the risk.

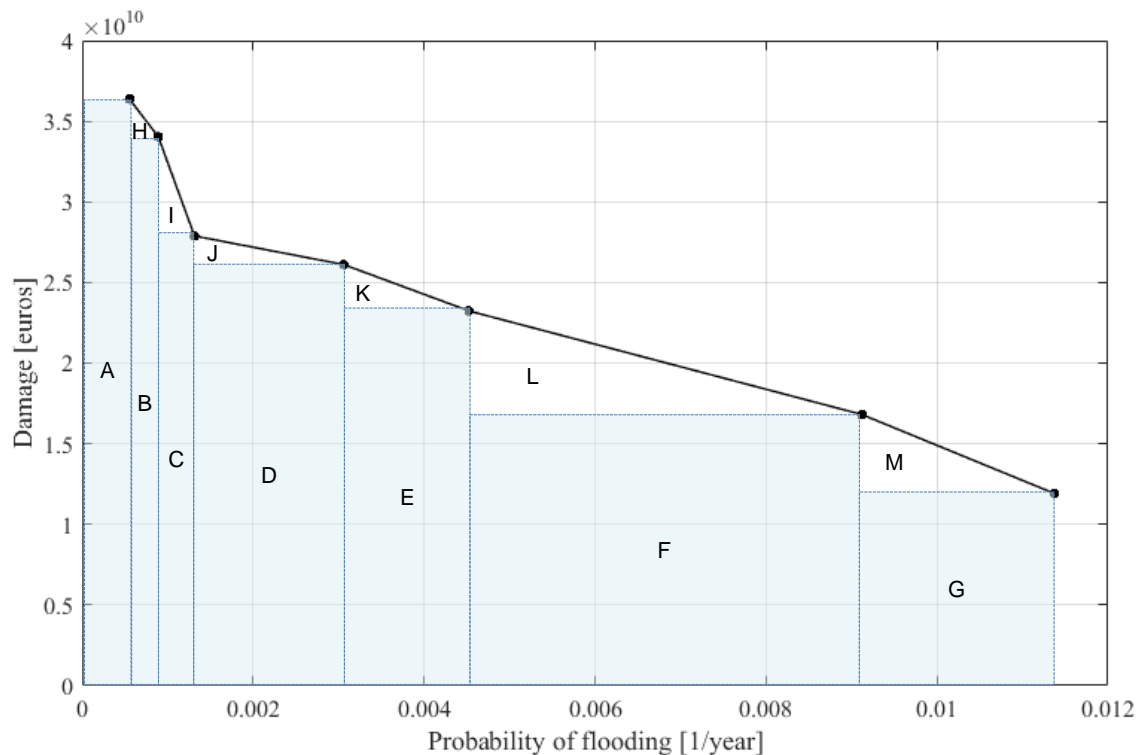


Figure 6.6: Relationship between damage and probability of flooding (probability of exceedance), along with total risk (area under the curve)

The risk value, the sum of the areas below the curve, is the annual total risk which is €257.5 million. This will be adjusted to be expressed in terms of net present value with the adjusted real discount rate which is chosen in Section 5.1.4 according to equation 5.3. This NPV risk value will be illustrated as one point in the total cost curves which will be given and further explained in Chapter 7. For the case of the baseline risk, the NPV risk is calculated to be €10.3 billion.

The curve in Figure 6.6 ends abruptly at a P_f of 0.011 (return period of 88 years) due to the fact that no

flood scenarios are taken for more frequent tsunamis with a return period less than 88 years. The data for more frequent tsunamis were not available for Kamakura, so the distribution was not fitted for more frequent tsunamis of a return period of less than 75 years. This is not very realistic as the damage is expected to reduce gradually with respect to more frequent tsunamis, and reach a damage value of 0 at smaller return periods (less than 75 years). Including this range in the risk quantification without having simulated results from SWASH or a approximated return period and incoming wave height relationship increases the uncertainty by including more assumptions, hence it is preferred to keep the abrupt start. You also expect some 'cut-off' as some tsunamis will not overtop the dike, as it was seen in this thesis for a 6 m tsunami with a 16 m dike. Consequently, the total risk is underestimated, but interpolating a curve would again result in a larger uncertainty in the model which is not wanted. Thus, simplifying the calculation by taking an assumption of no damage below this probability of flooding is more appropriate for the case of this thesis.

Similarly, the curve in Figure 6.6 also starts abruptly at a P_f of approximately 5×10^{-4} as no flood scenarios are taken for less frequent tsunamis with return periods of more than 1809 years. Extrapolating the data more could possibly undermine the reliability of the distribution. Moreover, extreme scenarios of return periods much larger than 1000 years is rarely considered in Japan, and for the scope of this thesis, the return periods considered was aimed to stay within a familiar range for the Japanese categorization. In reality, the curve is expected have and increase in damage with a decrease in the probability of flooding, hence the curve increases exponentially while approaching 0. Again, the total risk is slightly underestimated, but often risk is determined by the more frequent events, so for the scope of this thesis, this abrupt start will be assumed to be appropriate.

Here, it is important to recall that for the quantification of the total risk in baseline situation, the influence of interventions is not included. Only the existing protection measures which are introduced in Section 6.1.1 are included in the quantification of this baseline risk.

Now the damage costs will be looked at in more detail. The contributions for the damage cost from the loss of life and damage to buildings are illustrated in Table 6.3.

Table 6.3: Expected casualties and building damage for each tsunami level, with its corresponding damage costs

Tsunami Level (m)	Return Period (years)	Expected Casualties (# of ppl)	Loss of Life (B€)	Expected building damage (# of buildings)				Building damage (B€)	Total Damage (B€)
				0%	50%	75%	100%		
6	88	5280 (5.4%)	11.09	13867	396	330	2508	0.83	12.1
8	110	7423 (7.5%)	15.59	12481	264	462	3894	1.22	17.0
11	221	10245 (10.4%)	21.52	10765	264	264	5808	1.72	23.2
12	327	11536 (11.7%)	24.23	10171	264	330	6336	1.88	27.6
13.5	761	12348 (12.6%)	25.93	9907	264	330	6600	1.95	28.7
14	1124	15168 (15.4%)	31.85	9049	330	330	7392	2.19	34.7
14.5	1809	16232 (16.5%)	34.09	8785	264	330	7722	2.29	37.6

The damage costs illustrated in Table 6.3 show the significance of loss of life in the damage costs, for all tsunamis levels contributing to over 90% of the total damage costs. This is most probably due to the high population density in Kamakura. To give an idea of the population density at risk behind the dike in Kamakura, it is 3.4 times more densely populated than South Holland Province ($1300/km^2$) without including the 21.93 million tourists who visit Kamakura each year [Provincie Zuid Holland].

The loss of life also increases in number with the increase in the tsunami level. When these number of casualties are looked at relative to the population at risk in Kamakura, a 6 m tsunami results in casualties of 5% of the total population considered in the flood scenarios (= total population at risk), and the

largest tsunami of 14.5 m results in casualties of 16% of the total population at risk. This percentage estimating the casualties is very high, as mentioned in Chapter 2. Having casualties of more than 2% of the total population is considered a 'catastrophic disaster' in Japan. Moreover, this mortality rate is in line with the Tohoku tsunami in 2011, where in some cities (i.e. Namie, Onagawa) the casualties reached up to 11% of the population of the inundated areas [Yamao et al., 2015].

An overview of the mortality with respect to the population bins, which is dependent on the evacuation speed, and the mortality with respect to the evacuation behavior for the baseline condition is given in Appendix D. Most of the deaths result from not evacuating, and when looking at the mortality relative to the population bin, a larger percent of the adult population die. This is most probably because the adults have the largest percentage of the population.

The individual risk (IR) for Kamakura is computed using equation 5.4. As mentioned before, the individual risk is determined from the mortality fraction which is a function of the dv -value, and is determined for the two fatality zones (where $F_D = 0.5$ and 1.0). In reality, this should be spatially dependent, but this concept is simplified by relating the mortality to the dv -value. An example of the two mortality zones is clearly illustrated in Figure 5.6. The individual risk for the baseline in the area where $F_D = 1.0$ is computed to be 2.44×10^{-3} per year, and in the area where $F_D = 0.5$ is computed to be 3.98×10^{-5} per year. As mentioned in Section 5.1.1, the acceptable individual risk level for flooding in the Netherlands is 10^{-5} per year, thus this IR value is high for the $F_D = 1.0$ area, but is seen to be within the acceptable limit for the $F_D = 0.5$ area. This individual risk value will later be compared with scenarios with interventions.

The societal risk (SR) for Kamakura is illustrated in Figure 6.7. As is clearly illustrated, the baseline situation results in a large number of fatalities for each of the tsunami levels with different return periods, and is also far from the TAW limit line for flood protection used in the Netherlands. Again, it is important to realize that Japan does not define an acceptable level of societal risk, and is unsure whether even having a limit line is it applicable for tsunamis.

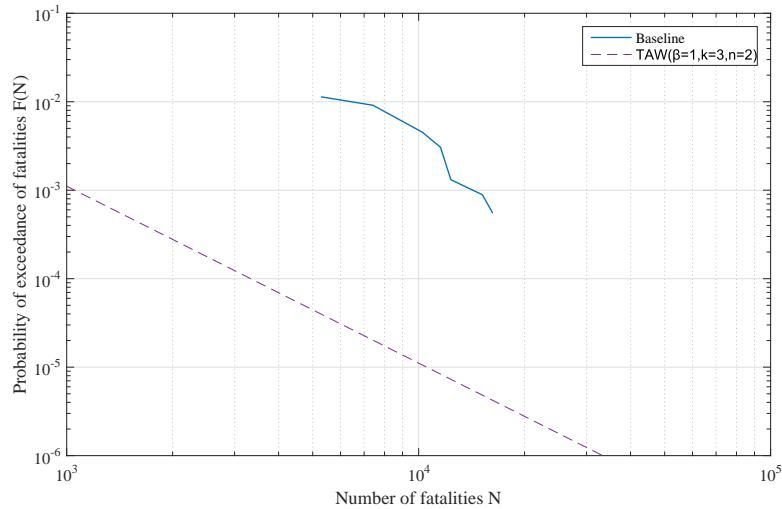


Figure 6.7: Societal risk curve for the baseline risk in Kamakura, with TAW limit line for flood protection in the Netherlands

From the results, it is clear that the damage, annual total risk, and NPV risk area are all calculated to be very high, and shows that Kamakura is vulnerable to tsunamis. Now different interventions will be implemented in order to reduce the risk.

6.2. OVERVIEW OF POSSIBLE INTERVENTIONS

As mentioned in Chapter 2, there are many possible interventions which could be implemented for tsunami protection. An overview of interventions is illustrated in Figure 2.7. In this figure, interventions such as building offshore breakwaters, tsunami walls or sea levees, evacuation buildings with flood proofing, relocating social infrastructure to higher ground, and creating evacuation routes to higher ground are introduced. All of these interventions mentioned here have been implemented in the reconstruction of Tohoku, as well as heightening the ground for an entire community.

The coastal topographic and bathymetric characteristics, along with the societal demands, determine which types of interventions are possible in the different cities. For the case of Kamakura, there are some limitations to which types of interventions are possible. For example, the construction of an offshore breakwater in Kamakura is not ideal due to the steep profile of the near-shore bathymetry, which would result in very high construction costs. On top of that, the community and local economy highly rely on tourism, therefore, offshore breakwaters and other interventions which would disrupt the coastal and ocean aesthetics are not favored. Dike heightening intervention will be considered as a small dike of 3 m already exists, and it is expected to not affect the coastal aesthetics if the dike height is only increased by a few meters. This dike is a road dike, so a few meters of increase could also be seen as an advantage for better view. It can also have the benefit of slowing down the propagation for tsunamis.

Other limitations of interventions especially lie in the spatial solutions. The city is intact and built very densely, so changes to the type of building and relocation of buildings would be very difficult. And since the buildings are very densely built, it is also difficult to build a secondary defense in a more landward location to reduce the run-up distance.

Under these circumstances, the interventions which are chosen for Kamakura are the heightening and widening of the road dike along the coast, and the improvement of evacuation. This interventions were inferred to be more feasible for Kamakura compared to the other interventions.

6.3. RISK QUANTIFICATION WITH 1 INTERVENTION

Now the influence of interventions on the seven different tsunami levels will be looked at. The different tsunami levels modeled in SWASH are combined with different interventions, which are also included in the SWASH and risk assessment model, similar to the boundary conditions included for baseline risk quantifications. For this thesis, the heightening of the road dike and an improved evacuation system is implemented to reduce the risk resulting from a flood.

As mentioned in Section 4.4, parameters such as run-up distance, inundation height, flow velocity and arrival time will determine the damage criteria, which will be coupled with the spatial distribution of economic values, and the densities of the population and houses given in Section 5.2 along a 1D cross-section. Especially the maximum depth velocity product dv_{max} parameter is the determining factor for damage, as was explained in Section 5.1.3. An example of the parameters obtained from the SWASH simulation for the damage criteria is illustrated for the dike heightening in Section 6.3.1.

6.3.1. DIKE HEIGHTENING

The first intervention is the heightening and widening of the road dike located along the coast of Kamakura. Different dike heights will be implemented to quantify the reduction in damage relative to the amount of heightening. The dike heights which were simulated were 4 m, 8 m, 12 m and 16 m. The initial condition is the road dike which is 3 m high, located along approximately 30 m behind the beach on the coast. Since the surroundings of the dike have densely built buildings, minimizing the width of the dike is preferable, therefore the outer and inner slope of all the dikes are assumed to be 1:3, similar to the baseline situation. In other words, if the dike is heightened, the dike width is also increased by a

factor of 3.

The damage functions only look at the cells after the inner toe of the dike, as it is assumed that there are no residential buildings before or on the dike, and if there are people on the beach, these people would at least have enough time to evacuate behind the dikes. The total population at risk which is considered does not change.

The dikes are also assumed to be structurally strong enough to withstand the forces from the tsunami. Based on survey research of past tsunamis, the main cause of dike failure resulting from tsunamis was the failure from scouring at the landward toe of the dike [Kato et al., 2012]. Other failure mechanisms include failure from the top of the landward armor (crown), scour on the seaward toe, although these mechanisms were only a small fraction of the failure cases compared to the scouring in the landward toe. Thus, dikes built to protect against tsunamis must have sufficient scour protection in both the landward and seaward toe.

In most parts of Tohoku, these dikes were protecting rural areas, and urban and rural areas have different dike structures in Japan. In urban areas, there are impermeable hard structures to protect the roads and urban environment behind the dike, and in those cases it showed better protection level (Dr. M. Esteban, personal communication, 6/6/2016). So most of the places where the surveyed failure mechanisms were recorded were in rural areas of Tohoku. Thus, it is difficult to know the necessary level of dike strength protecting an urban area like Kamakura. Protection against tsunamis is the topic of this thesis, but it is worthy to note that the coastline of Kamakura has also faced damages caused by typhoons in the past.

6

RESULTS

The results of each of the different dike height interventions as a function of damage and probability of failure is illustrated in Figure 6.8.

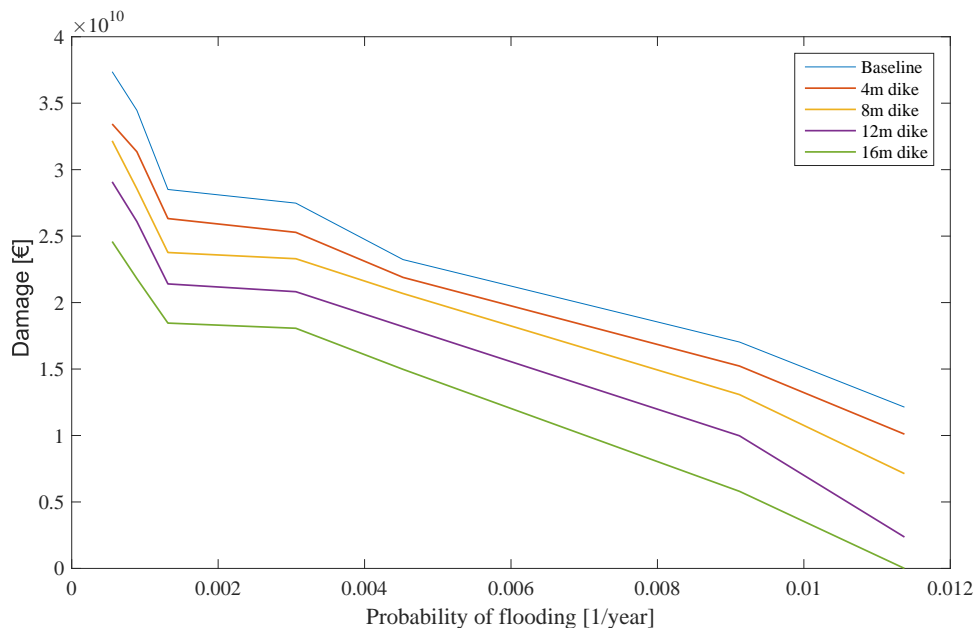


Figure 6.8: Relationship between damage and the probability of exceedance for each dike height intervention

The blue line illustrates the baseline damage curve which was computed Section 6.1, and it is clear that

as the dike height is increased, there is some damage reduction. The amount of damage reduction for each intervention relative to the baseline situation is illustrated in Table D.3 in Appendix D.

Similar to the case of the baseline risk, tsunamis with a more frequent return period than 88 years is assumed to have no damage for the same reasonings mentioned in Section 6.1.4. It is clear that the damage reduces with respect to the increase in dike height. The amount of damage reduction is also larger with larger dike heights. Here it is important to note that since the flooding variable considered is incoming wave height, there is still damage with a wave height smaller than the dike height. This is due to the fact that these tsunami waves have a lot of energy, and for example, even with an 16 m dike, an 8 m incoming wave is overtopping this dike based on the SWASH results.

Again, the area under each of the curves represent the amount of risk for each of the dike interventions, and the risk reduction is the area difference between the baseline and intervention curves. The risk values will be adjusted to be NPV values, and can be plotted together as a curve shown in Figure 6.9. The red plots along the curve are the five different NPV risk values which can be said to be derived from the areas under the five curves in Figure 6.8. For example, the first point on the curve is the plot representing the baseline risk.

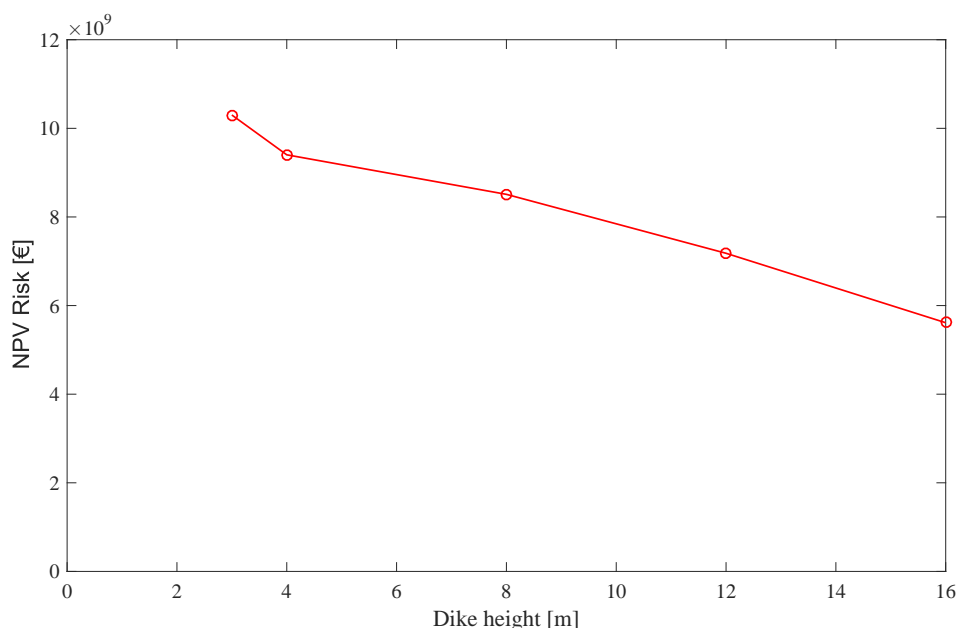


Figure 6.9: NPV risk for dike heightening

As can be seen from Figures 6.8 and 6.9, the risk reduction is limited for the dike heightening intervention for two main reasons. First, there is overtopping of the waves even with large dikes. The only combination of scenarios from the SWASH results which have no damage is a 16 m dike with a 6 m tsunami, illustrating that even the smaller waves require a large dike to fully stop the tsunami. And the second reason is because of the dense population of Kamakura. The baseline risk showed that casualties were the determining factor of total damage, so even if only a small area is inundated, it still results in billions of damage. The combination of these two reasons result in large damage even with high dikes.

6.3.2. IMPROVEMENT OF THE EVACUATION SYSTEM

The second intervention which will be looked at is the evacuation system. Evacuation management is the most reliable protection measure existing in Japan as people are taught from a young age of what to do in case of a tsunami. Moreover, from the baseline and the previous intervention of dikes, it is known that the large amount of the damage results from the loss of life. Thus an improved evacuation system could substantially reduce the total risk.

There are many ways to include the influence of evacuation for a protection system, such as creating the evacuation routes, building evacuation centers and more. In a 1D cross-section which is considered in this thesis, two measures will be implemented to improve the evacuation system. The first measure is to add an evacuation center along this cross-section to reduce the evacuation distance, and the second measure is to distribute wireless receivers to every household to improve the evacuation behavior.

The first measure, which is to add an evacuation center along the cross-section, aims to reduce the amount of casualties by decreasing the time needed to evacuate. Vertical evacuation proved extremely valuable during the disaster in 2011 [Fraser et al., 2012], and there have been vertical evacuation buildings developed by many companies. Of the many developments, one type developed by Daiwa House Group will be used as a reference for this thesis. These evacuation areas are approximately 15 m high, and have a requirement of being built in areas where there is less than 5 m of inundation. Since flood protection measures for vital infrastructure such as evacuation areas follow approximately a 1 in 1000 year safety standard, the location of these vertical evacuation buildings will be taken where the inundation height of a 1 in 1000 year tsunami does not exceed 5 m - this is approximately 960 m inland from the inner toe of the dike. The schematization of this evacuation measure is illustrated in Figure 6.10.

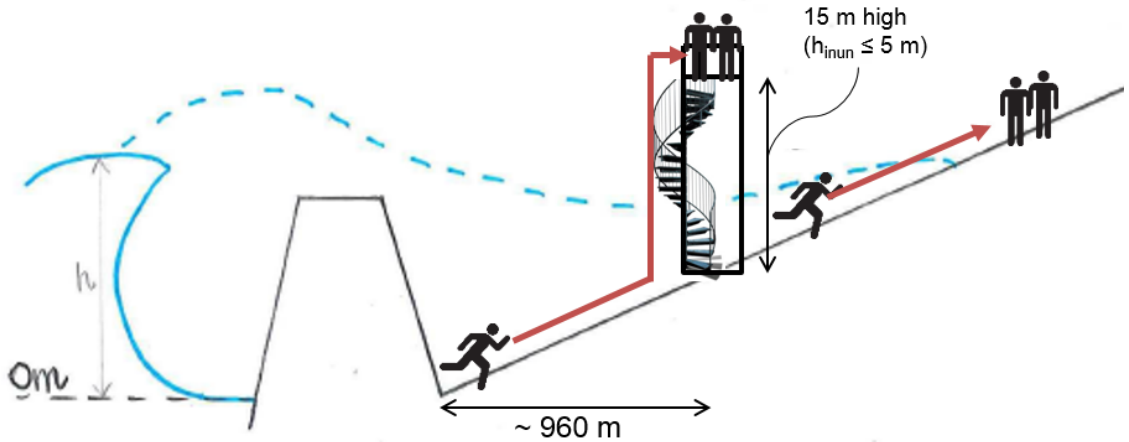


Figure 6.10: Schematization of evacuation with vertical evacuation buildings

Evacuation with the vertical evacuation buildings is modeled in the following way:

$$t_{tsu} > t_{evac} = \begin{cases} \frac{x_{max} - x_{building}}{c_{evac}} + t_{delay}, & \text{if } x_{evac} > x_{building} \\ \frac{x_{building} - x_0}{c_{evac}} + t_{delay}, & \text{if } x_{evac} \leq x_{building} \end{cases}$$

Here, x_{evac} is the distance from a cell to safer ground (which is higher than the maximum run-up point), and $x_{building}$ is the location of the vertical evacuation building measured relative to the coastline. Explained verbally, if x_{evac} is larger than the $x_{building}$, people evacuate to safer ground (landward evacuation), and if x_{evac} is shorter than the $x_{building}$, people evacuate to the evacuation building (vertical evacuation). In any case, the people are modeled to evacuate in the landward direction and not to the

closest evacuation center. This improved evacuation model with the vertical evacuation is illustrated in Figure 6.11.

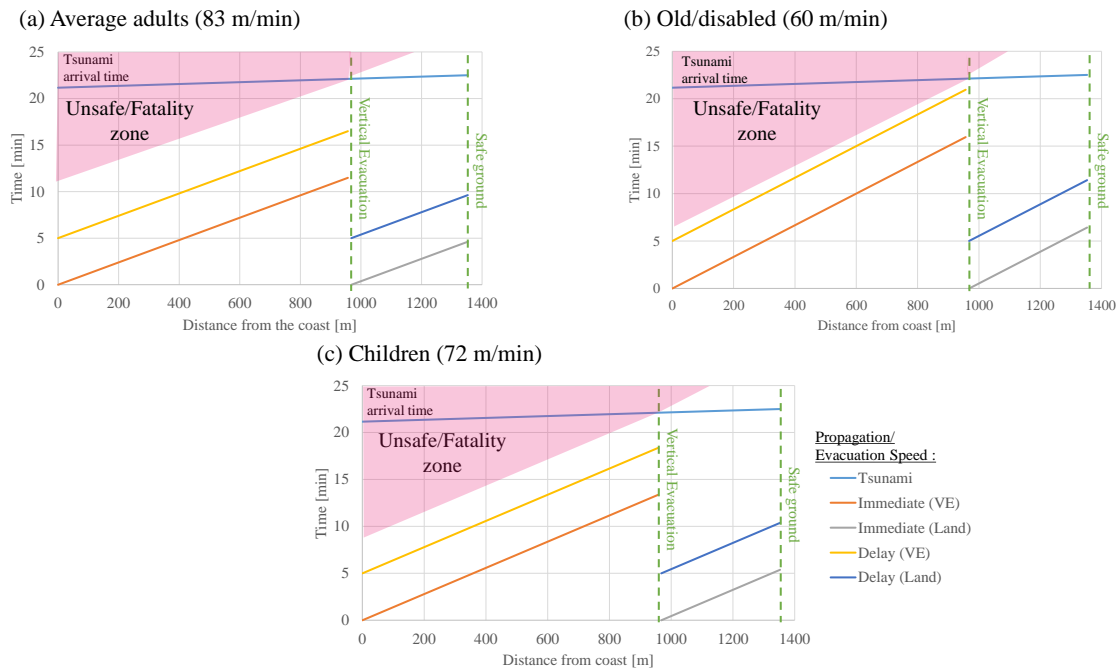


Figure 6.11: Evacuation model improved with shortened evacuation distance due to the implementation of vertical evacuation buildings for the flood scenario of a 14 m tsunami

Compared to the baseline situation evacuation, the 'unsafe/fatality zone' (pink) in Figure 6.11 has substantially reduced with the implementation of vertical evacuation buildings. The concept in this figure is the same as for the baseline, where people must evacuate to either the vertical evacuation building or safe grounds before the tsunami arrives in order to survive. For the case of this thesis where only the deterministic value of 5 minutes of delay time is considered, the results show that all of the people who evacuate will survive. Hence, the fatalities which are computed are due to people not evacuating. It is important to note that if other more long delay times were considered, the results would differ as you could see by shifting the lines vertically in the figures.

The second measure, which is to distribute wireless receivers for evacuation to every household, aims to reduce the distribution of people who do not evacuate or are delayed. An example of this wireless receiver is illustrated in Figure 6.12.

This system disseminated the tsunami warning very effectively during the 2011 tsunami in Minami-Sanriku [Fraser et al., 2012]. By distributing these wireless receivers, the evacuation behavior is assumed to improve as illustrated in Table 6.4. These receivers may seem old fashioned, but in case of the failure in the mobile and tv network it is useful - this wireless receiver network can be assumed to be auxiliary back-up solution. It is important to note that this improvement is an assumption based on an educated guess, as improvements were not measured from previous tsunami events.

The remaining boundary conditions such as the height of the road dike (= 3m) remains the same. Therefore, this intervention aims to quantify the influence of the improvement of the evacuation system which involve these two measures.



Figure 6.12: Photo of wireless receivers distributed in Minami-Sanriku [Fraser et al., 2012]

Table 6.4: Distribution of evacuation behavior with and without the wireless receivers

Evacuation fraction	Initial	With Wireless receivers
$F_{E,imm}$	0.13	0.25
$F_{E,delay}$	0.60	0.65
$F_{E,no}$	0.27	0.1

6

RESULTS

Given this information about the influence of different measures to improve evacuation, the amount of risk reduced from each of these measures and the combination of the measures are computed. Improving the evacuation system only influences the part of damage related to the loss of life, thus, the same values for damage to buildings is used as for the baseline damage calculations. The relationships between the damage and probability of exceedance is illustrated in Figure 6.13, and again the area under the curves show the risk.

The importance of evacuation is very clearly illustrated in Figure 6.13. Firstly, it is interesting to see from the results that vertical evacuation is effective for large tsunamis, as was seen for the case in Tohoku. It was not effective for small tsunamis because the run-up distance for the small tsunamis are shorter than that of the distance from the coast to the building. For the vertical evacuation buildings to have an influence, the run-up distance should be larger than that of the distance to the building from the coast, which is the reason why it is modeled to only be effective for large tsunamis. Secondly, the wireless receivers reduces the damage by almost half for all of the different levels of tsunamis relative to the baseline damage. This is due to the assumption of the large improvement in the evacuation behavior. The amount of casualties significantly decreases with the improvement of evacuation, especially with the influence from the distribution of wireless receivers. This can be seen in graph and in Table 6.5.

The damage reduction illustrated on the right of Table 6.5 is the amount of reduction from the baseline to the improved evacuation which combines the influence of both the vertical evacuation and wireless receivers. When looking at the two evacuation measures implemented independently, the effect of wireless receivers is much larger for the reduction of casualties than the effect of vertical evacuation. However, implementing vertical evacuation buildings have a large influence in the reduction of casualties for large scale tsunamis, which can be a very crucial factor. Since human life is much more valuable than property, any possibility which allows the reduction of casualties is important, even if it is only for large scale tsunamis. Therefore, vertical evacuation building are important to provide protection for larger tsunamis.

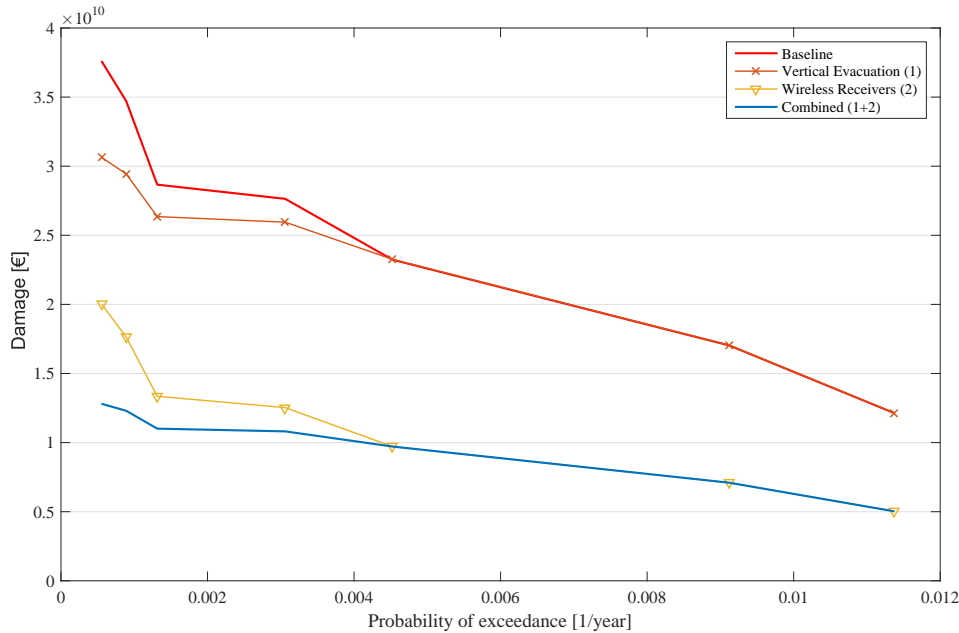


Figure 6.13: Relationship between damage and probability of exceedance with evacuation and with evacuation improvements

Table 6.5: Comparison of the number of casualties between the baseline, each of the improvement measures (vertical evacuation and wireless receivers), and the combined improvement

Tsunami Level (m)	Return Period (years)	Expected Casualties [number of people]				Damage reduction (B€)
		Baseline	Vertical Evacuation (1)	Wireless Receivers (2)	Improved Evacuation (1+2)	
6	88	5384	5384	1994	1994	7.1
8	110	7527	7528	2788	2788	10.0
11	221	10245	10245	3795	3794	13.5
12	327	12265	11448	5126	4240	16.9
13.5	761	12720	11604	5506	4298	17.7
14	1124	15489	12963	7550	4801	22.4
14.5	1809	16824	13486	8705	4995	24.8

It is also important to note that the reduction in casualties has a limit as there are those people who do not evacuate. As can be seen in Figure 6.11, even for a 14 m tsunami, the people have managed to evacuate. Thus, the number of casualties is determined by the number of people who do not evacuate and are in the fatal $d\nu$ -value zones. Hence, the only way to enhance the reduction even more for the case of this thesis is by improving the evacuation behavior.

Similar to the baseline risk, an overview of the mortality with respect to the population bins, which is dependent on the evacuation speed, and the mortality with respect to the evacuation behavior is given in Appendix D. Again, it is clear that most of the deaths come from not evacuating when looking at the mortality relative to the evacuation behavior. As for the mortality relative to the population bins, the casualties are dependent on the size of the population bin, hence, more old people and adults, which hold a larger percentage of the total population, illustrate larger amount of casualties.

6.4. COMBINATION OF INTERVENTIONS

Finally, the influence of the combination of the two interventions, dike heightening and improved evacuation, will be quantified in terms of damage reduction and total risk.

Even when combining the interventions, the damage costs resulting from the damage to buildings remain the same as the situation where only the dike heightening interventions were considered. The resulting relationships between probability of exceedance and damage is illustrated in Figure 6.14. Again, the sum of the area below each of the curves is the risk for each of the combined interventions.

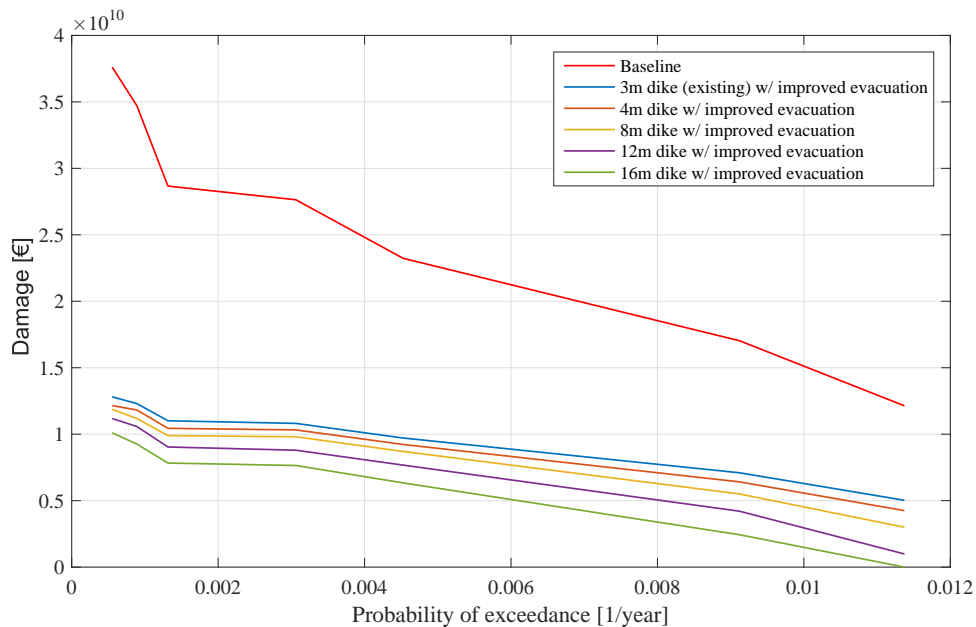


Figure 6.14: Relationship between damage and probability of exceedance with the combination of dike heightening & improved evacuation in comparison with the baseline

In Figure 6.14, the damage curves illustrated are for the combination of dike heightening and both improvements of evacuation. To get an idea of the damage curves for the two evacuation improvement measures independently, the two relationships between probability of exceedance and damage can be found in Appendix D (Figures D.4 and D.5).

The curve representing '3m dike (existing) w/ improved evacuation' corresponds to the risk with only the influence of improved evacuation which was computed in Section 6.3.2. As seen before, the influence of evacuation itself is much larger on the reduction of damage than each of the dike heightening interventions. Nevertheless, the number of casualties reduce more than with only the evacuation intervention itself, as can be seen in Table 6.6.

In the same way the NPV risk for the dike heightening interventions were computed, the area under each of the combination curves are summed and adjusted to net present values - this can be plotted together as curves shown in Figure 6.15.

The 'Combined' curve corresponds to the damage curves illustrated in Figure 6.14, and the vertical evacuation and wireless receivers curve also take into account the influence of dike heightening. The slope of the risk curve with all the combination of interventions is shifted downward compared to the risk

Table 6.6: Comparison of the number of casualties between the baseline situation and the intervention with both dike heightening and improved evacuation

Tsunami Level (m)	Return Period (years)	Expected Casualties (number of people)					
		Baseline	existing dike	4m dike	8m dike	12m dike	16m dike
				<i>improved evacuation</i>			
6	88	5384	1994	1646	1161	387	0
8	110	7527	2788	2478	2129	1626	949
11	221	10245	3794	3562	3369	2962	2439
12	327	12265	4240	3988	3795	3388	2943
13.5	761	12720	4298	4027	3814	3485	3001
14	1124	15489	4801	4569	4317	4066	3543
14.5	1809	16824	4995	4685	4588	4298	3872

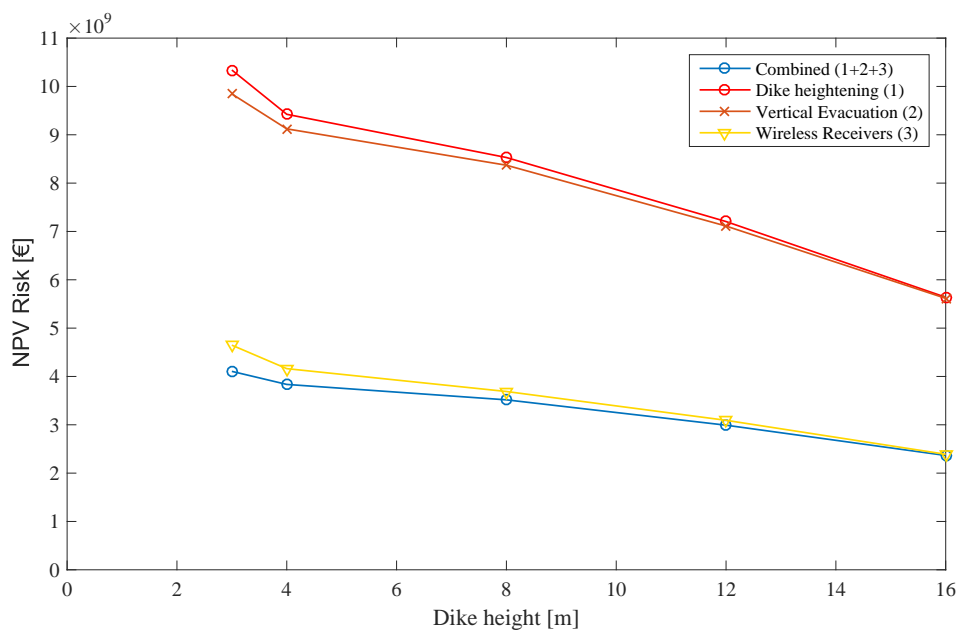


Figure 6.15: NPV risk for the combination of interventions of dike heightening and improved evacuation (vertical evacuation and wireless receivers)

curve with just the dike heightening intervention. The combination of interventions also reduces the total risk for each dike height by more than half compared to the total risk for only implementing each dike heightening measure. The effect of the improvement of evacuation is very large in the NPV risk, as the largest risk reduction is seen for the existing dike with evacuation (first point in blue curve).

6.5. DISCUSSIONS & CONCLUSIONS

The baseline risk was computed to have a representative value of the risk under the current situation for Kamakura, and is a useful value to have to compare scenarios with interventions. The existing protection measures, a 3 m dike and a simple evacuation system, were included in the computation. The evacuation system was modeled as a simple landward evacuation with different behavior types and evacuation speeds, and determined which areas result in fatalities with respect to the fatal dv values, i.e. areas with $dv > 2$ were expected to have 100% mortality. Combining this evacuation model with the damage assessment, the damage with respect to probability of flooding (= probability of exceedance) was derived.

T curve illustrating the relationship between damage and probability of flooding illustrated 'cut-offs'. The abrupt end of the curve was due to the fact that the distribution curve for return period and wave height started at 75 years as a result of the lack of data for more frequent tsunamis. The damage for more frequent tsunamis could have been estimated based on an educated guess, however, this was not conducted to avoid further uncertainty. Next, the abrupt start of the curve was a result of taking the largest tsunami as one with a 1809 year return period. To not have an abrupt start, larger tsunamis require further extrapolation, and this could undermine the reliability of the distribution. For the scope of this thesis, the abrupt start and end of the damage and probability relationship is appropriate. Still it must be realized that this is a first approximation, and there is most probably an underestimation of risk due to the 'cut-offs'. These can be overcome by having more data on smaller and larger tsunamis, and conducting further flood scenarios based on those new data.

6

Considering these inputs and simplifications, the baseline risk for Kamakura was computed. The annual total risk was computed to be €257.5 million, corresponding to a NPV risk of €10.3 billion. The damage costs including both the loss of life and building damage ranged from €12.1 to €37.6 billion, and of these damage costs, over 90% of the total damage costs resulted from fatalities. The number of casualties ranged from 5280 to 16232 people (corresponding to 5.4% to 16.5% of the total population at risk). These results of the percentages of fatalities were in line with the observed fatality proportions in the Tohoku event of 2011 [Yamao et al., 2015]. From the results of the baseline risk quantification, the importance of casualty reduction is realized in order to reduce risk.

In order to reduce the risk, interventions were chosen based on their feasibility and suitability for Kamakura. The first intervention considered was dike heightening, and the existing dike of 3 m was heightened to 4, 8, 12, and 16 m. The results showed that the risk reduction of dike heightening is limited, i.e. the largest risk reduction is approximately €15 billion with a 16 m dike. There is a limit to the risk reduction for dike heightening since there is overtopping observed even with large dikes, as tsunamis have a lot of energy. Also, due to the dense population of Kamakura, there is a large number of casualties recorded even if there is only a small area inundated. For the combination of these two reasons, there are still large damage costs even with the implementation of large dikes.

The second intervention considered was the improvement of the evacuation system. Vertical evacuation buildings were implemented to shorten the evacuation distance, and wireless receivers were distributed to every household in Kamakura to improve evacuation behavior. The vertical evacuation buildings were observed to be effective for large scale tsunamis which can be very valuable to reduce the casualties. The wireless receivers, where the improved evacuation behavior was assumed based on an educated guess, reduced the damage by half and the number of casualties by half or more for all scales of tsunamis. There is a limit to the number of casualties which can be reduced in this model, as there is a percentage of people who do not evacuate; thus further reduction in casualties require improvement in the evacuation behavior.

Finally the combination of dike heightening and improved evacuation was considered. As expected, the combination of all measures resulted in the largest risk reduction. The annual total risk ranged from

€59.1 to €102.6 million, and the corresponding NPV ranged from €2.37 to €4.11 billion. The amount of casualty reduction was recorded to be approximately 13000 people for large tsunamis, and approximately 3000 people for small tsunamis. It is important to note that the largest risk reduction is observed for only implementing the improved evacuation without dike heightening.

These results are assumed to be appropriate for the scope of this thesis, but there are some constraints to the methodology which can be improved. Firstly, the evacuation model is created for a 1D cross-section, and can be greatly improved by conducting a 2-D analysis with locations of evacuation centers, and specifying the closest evacuation area. The evacuation model can also be more accurately represented by giving probabilistic distributions instead of the current deterministic values to the different variables such as evacuation speed and delay time.

Moreover, the population at risk which are considered in this analysis now only take into account the citizens of Kamakura, while in reality there are many tourists (21.93 million recorded in 2014). Thus, the inclusion of these people would create a large difference in the results as the number of casualties is already the main determining factor for risk.

7

RISK EVALUATION

The risk for dike heightening, as well as the combination of dike heightening and an improved evacuation will be evaluated through a Cost-Benefit Analysis (CBA), Individual Risk, and Societal Risk. The different scenarios will be evaluated separately, and compared on their advantages and on the results of the different evaluation methods. The most favorable of the considered options for Kamakura, which here is determined in terms of life loss, economic damage, and or both, will then be chosen. It is important to state that the most favorable, or the optimal, of the considered options is a preliminary solution based on the results of this thesis, and therefore affected by the assumptions and considerations that have been made.

7.1. RISK EVALUATION BASED ON COST BENEFIT ANALYSIS

As mentioned in Chapter 2 and 5, the Cost-Benefit Analysis (CBA) aims to determine which solution is the most economical. In the Netherlands a CBA usually considers the flooding risk and the cost of preventive investments such as dike heightening [Jonkman and Schweckendiek, 2015].

7.1.1. CONCEPTUAL MODEL

This conceptual model illustrates how the Multi-Layered Safety (MLS) System will be evaluated in an economic approach. The general equation for the total cost of a project over the course its lifetime is:

$$\text{Total Cost } TC(h) = \text{Investment } I(h) + \text{Risk } R(h) \quad (7.1)$$

All values in equation 7.1 will be derived relative to the dike height on the coast which is defined in Chapter 6. This general equation 7.1 takes into account the expected damage costs resulting from an undesired flood event. The total cost will be computed for each of the scenarios, and their results will be compared. The total cost is greatly influenced by the lifetime of the solution and will be represented as net present value (NPV). To adjust the cost to NPV, it is divided by the adjusted discount rate of 2.5%. This increases the annual costs by a factor of 40.

For an economically optimized system, the amount of NPV risk should be balanced with the amount of investment to reduce the total cost resulting from a flooding. The lowest total cost would result from the economically optimized strategy that is computed both analytically and through plotting the 'bath-tub' curves. This lowest total cost in the optimal situation must also be a preferable solution over the computed risk in the baseline situation, i.e. the total cost must be smaller than the baseline risk. The quantification of risk was looked at in detail in the previous chapter, so now the investments for the different interventions will be more closely examined.

7.1.2. INVESTMENT

Investments aim to create a safer system, whether it is to meet a safety standard or to economically optimize a project. The optimization process is the main focus for the cost-benefit analysis which will be conducted for the chosen interventions. The investments in a safer system are compared with the reduction of economic risk in the system, and the optimization aims to minimize the sum of the investment costs and risk, which is the expected total cost over the course of its lifetime [Jonkman and Schweckendiek, 2015]. Looking at the variables which influence investment I , there are many possible measures which could be implemented in order to reduce the flood risk from tsunamis for this system. The different variables of Investment I which will be considered for this thesis are illustrated in equation 7.2 and Figure 7.1.

$$I(h) = I_{dike} + I_{evacuation} \quad (7.2)$$

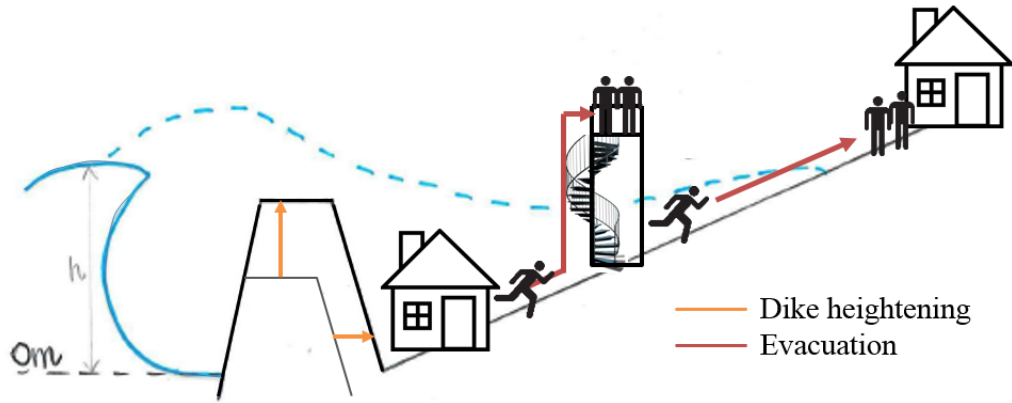


Figure 7.1: Schematization of investment options

INVESTMENTS FOR ROAD DIKE

For the road dike, investment costs such as I_{dike} and $I_{relocation}$ exist. For Kamakura, the primary defense is the road dike existing along the coast, and I_{dike} refers to the heightening and/or widening of this dike. Furthermore, as the city is still intact, $I_{relocation}$ refers to the relocation of houses resulting from the widening of the dike since many houses are densely built behind the road dike.

The investments for dike heightening can be determined with the following equation:

$$I_{dike,tot} = I_0 + I_h \cdot (h - h_0) + I_{relocation} \quad (7.3)$$

Here, $I_{dike,tot}$ is the total investment, I_0 is the initial costs, I_h is the variable costs, h is the new dike height, h_0 is the original dike height, and $I_{relocation}$ is the cost of relocating 1 m^2 of houses due to the widening of the dike.

The initial dike building cost in Japan is based on the rule of thumb for dike construction provided by Ministry of Land, Infrastructure and Tourism [2005], and is chosen to be €48 million per kilometer length. The variable cost is based on the Houston, Galveston bay project where the heightening costs range from €10 to €50 million per meter per kilometer length. This cost is quadratic, and takes into account the cost of heightening and widening the dike. The cost from the Galveston bay project is assumed to be in the similar range as Kamakura, as the economic situations in the US and Japan are similar. A sensitivity analysis is conducted to make the decision for a suitable variable dike heightening cost. The results of the sensitivity analysis of the investment costs from altering the I_h value is illustrated in Figure

7.2. The NPV risk ranges between €2 billion to €10 billion, and the investment cost chosen should lie in a comparable range to illustrate the influence it could have. For this reason, the variable investment cost is chosen to be €10 million per meter per kilometer length.

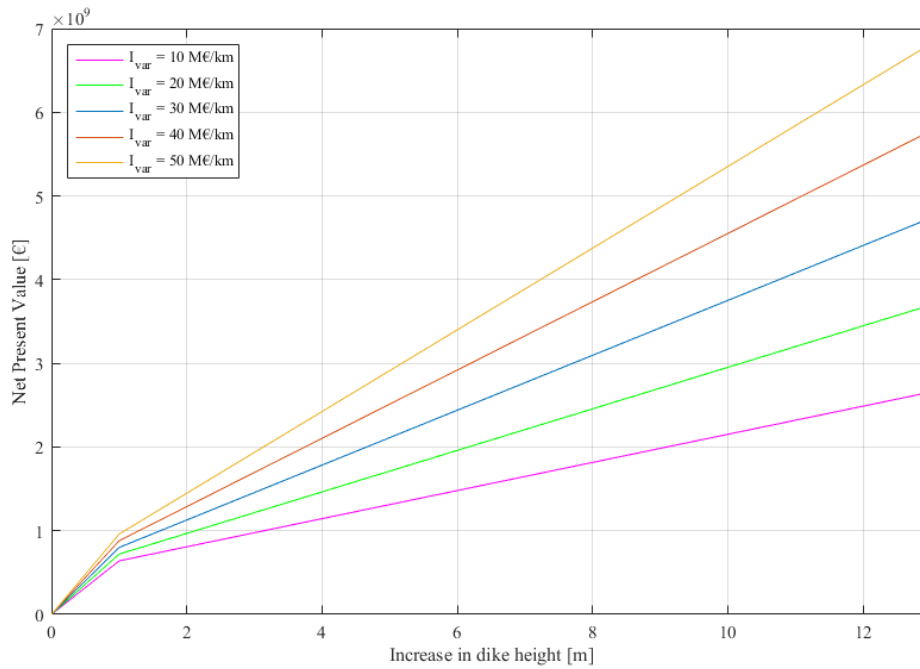


Figure 7.2: Sensitivity analysis of variable investment cost of dike heightening

It is worth noting that the total length of the dike in Kamakura is 8 km, and the amounts of dike heightening conducted in this analysis are 1, 5, 9, and 11 m (dike heights are 4, 8, 12, and 16 m).

The cost of relocation will be computed based on the cost of land in Kamakura. The average cost of land per square meter in Kamakura is ¥240,000, which results to be 1,920 €/m² [Ministry of Land, Infrastructure and Tourism, 2005][Kanagawa Prefecture, 2016]. Although the cost of land is highly dependent on its location, the relocation cost of Kamakura is assumed to be uniform throughout the city. The cost of relocation is dependent on the amount of the dike widened, and the area of relocation ranges from 88,000 to 616,000 m².

INVESTMENTS FOR IMPROVED EVACUATION

The investments for the improvement of evacuation includes several cost, which considers the different measures involved to improve evacuation in this thesis. The investment costs for evacuation improvement are illustrated in equation 7.4.

$$I_{evac} = I_{ews} + I_{VE} + I_{WR} \quad (7.4)$$

Here, I_{ews} is the maintenance and operation costs for having an Early Warning System (EWS), I_{VE} is the cost of implementing vertical evacuation measures, and I_{WR} is the cost of wireless receivers which will be distributed to the households.

In Kamakura, and all other cities in Japan, an EWS exists, thus there is no initial investment necessary for the inclusion of this system. Instead, the annual maintenance and operation costs which are necessary to sustain an effective evacuation system must be included. This value is taken from Given et al.

[2014], which provides costs for an EWS in the West Coast of the United States, which is assumed to be in the same range as costs for a EWS in Japan. The annual maintenance and operation costs presented in this paper is \$16.1 million (€14.4 million) and will be included as a fixed value represented as I_{ews} in the equation.

Secondly, vertical evacuation measures are currently being made to be more flexible, allowing these measures to be added on to existing residential buildings. One of these measures, called the "W-ev Tower", was developed by [Daiwa House Group](#), which aims to add evacuation stairwells on the side of the buildings to allow for smooth vertical evacuation. This allows a possibility of vertical evacuation up to the height of the building, in the case of this thesis it is 15 m, without the construction of new buildings. As mentioned in the previous chapter, this vertical evacuation building is located 960 m in land. The cost of implementing this vertical evacuation measure is ¥6 million (€50,000) per building. In this thesis, it is assumed that this vertical evacuation measure will be built along one cell length of houses (66 houses) to shorten the evacuation distance from the coast, thus, $I_{VE} = 50000 \times 66$.

Finally, wireless receivers, which can be maintained by changing the battery every few years, are ¥50,000 (€400) per receiver [[Fraser et al., 2012](#)]. This cost per receiver will be multiplied by the number of households which exist in Kamakura, which result to be $I_{WR} = 29.3\text{M€}$.

To summarize, the investments for the different measures which will be implemented into this cost-benefit analysis for different situations are illustrated in Table 7.1. The costs of evacuation are illustrated as annual costs, and are converted to NPV for the calculations in the following sections.

Table 7.1: Investment costs for different interventions

Variables		Value	Unit	Source
I_{dike}	I_{h0}	48	M€/km	[Ministry of Land, Infrastructure and Tourism, 2005]
	I_h	10	M€/m/km	Sensitivity analysis results
	I_{reloc}	1920	€/m ²	[Ministry of Land, Infrastructure and Tourism, 2005] [Kanagawa Prefecture, 2016]
I_{evac}	I_{ews}	14.4	M€/yr	[Given et al., 2014]
	I_{VE}	3.3	M€/yr	[Daiwa House Group]
	I_{WR}	29.3	M€/yr	[Fraser et al., 2012]

7.1.3. OPTIMIZATION OF DIKE HEIGHTENING

The risk curve, which was computed in Section 6.3.1, is now combined with the investments for dike heightening, which were computed in the Section 7.1.2. The results illustrating the total costs for the dike heightening intervention, where the damage costs include both the loss of life and damage to buildings, is illustrated in Figure 7.3.

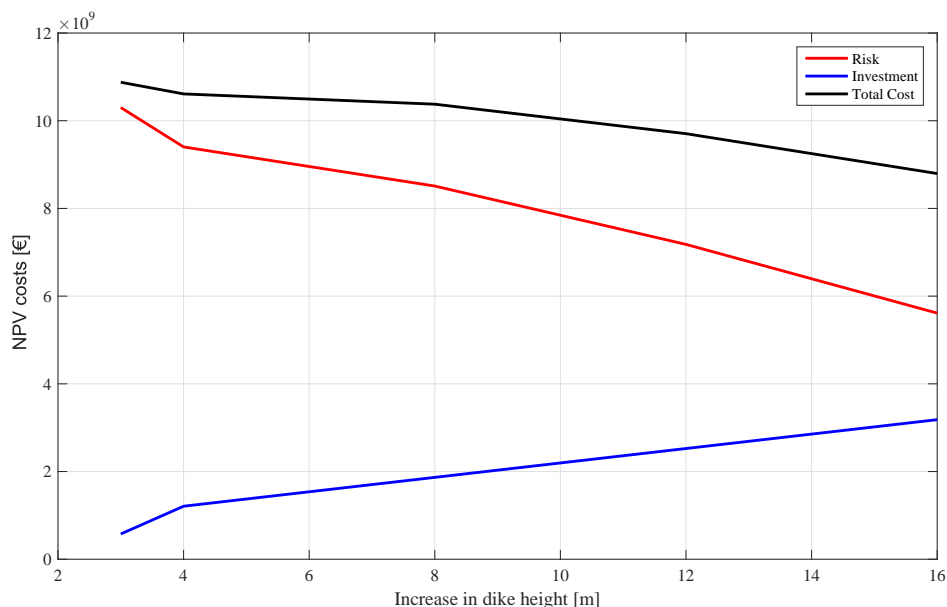


Figure 7.3: Economic Optimization curve of dike heightening considering both the damage to residential buildings and the loss of life

From Figure 7.3, if the most favorable solution is simply defined by the minimum total cost within the range of solutions considered, this dike height would be 16 m. This can be found at the lowest point of the black curve. The total cost of implementing a 16 m dike is €8.80 billion, and the risk in the initial situation is €10.30 billion. Therefore, the optimal solution is €1.5 billion more beneficial than not having any interventions. It may be argued that the most optimal solution may be found for a much higher dike if the curve is extended considering dike heights of 20 m and more, however, simulations with higher dikes were not conducted as it did not seem realistic. Dikes and seawalls being built in Tohoku are approximately 15 m high [BBC, 2016], even after very high tsunamis ranging from 10 to 20 m hit the coastline in the 2011 tsunami event.

It is important to note that the investment is not economically sound if this project were to invest in increasing the dike height to 4 or 8 m. For the dike heights of 4 m and 8 m, the total cost is higher than the baseline risk, requiring approximately €300 million and €70 million more in the total cost respectively.

7.1.4. OPTIMIZATION OF COMBINED INTERVENTIONS

The risk curves for the combination of interventions, which were computed in Section 6.4, is now combined with its corresponding investments. In Figure 7.4, the investments of all the interventions, dike heightening, vertical evacuation and wireless receivers, are included. Similar to the case of optimizing the dike heightening intervention, the damage costs include both the loss of life and damage to residential buildings.

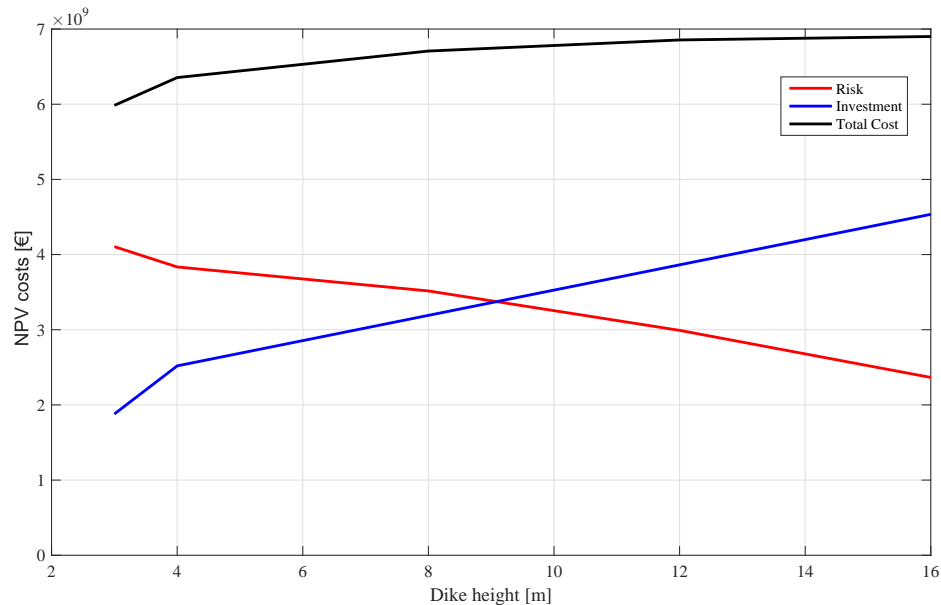
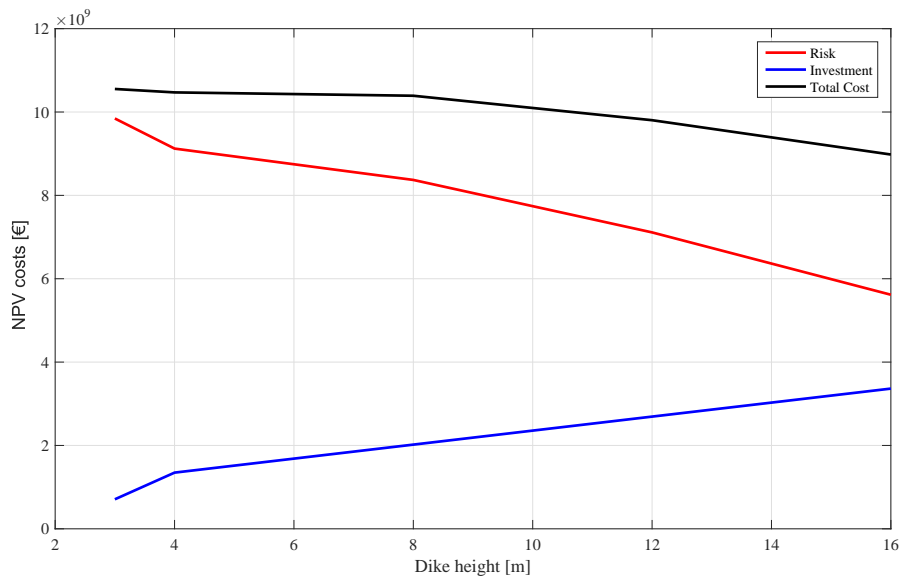


Figure 7.4: Economic Optimization curve of the combination of dike heightening and improved evacuation

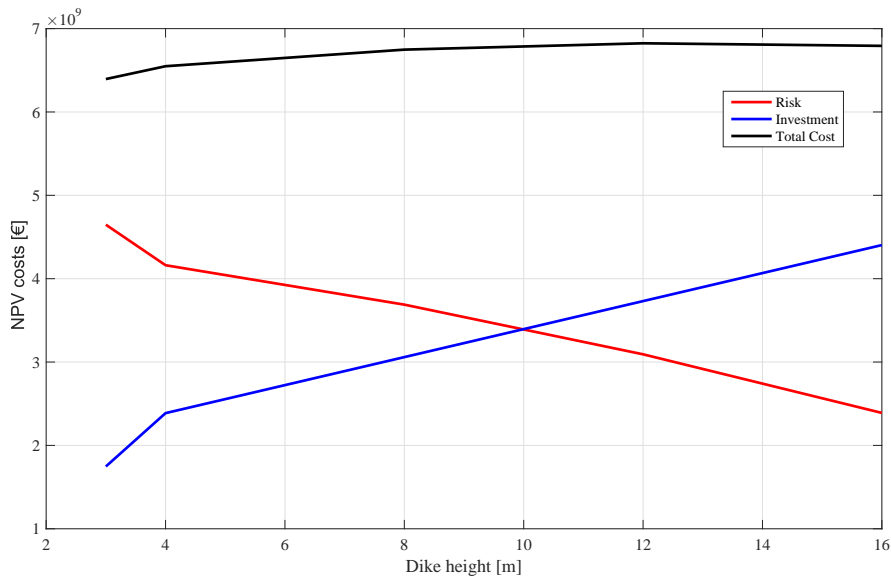
From looking at the total cost curve illustrated in Figure 7.4, it can be seen that the curve starts at €5.98 billion, and continues to increase with the increase in dike height. Therefore, if the most favorable solution is taken to be the intervention with the lowest total cost, the combination of interventions would be to have the existing dike with the improved evacuation system - this means no dike heightening. Here, the improved evacuation system considers both vertical evacuation and the distribution of wireless receivers. The baseline risk, which is the starting point of the risk curve in Figure 7.3, is €10.34 billion. The optimal solution for the combination of interventions yields a total cost of €5.98 billion, resulting in a €4.36 billion decrease in the total cost.

Due to the fact that this intervention of improved evacuation was seen to have a large influence in the risk reduction, the influence of the two evacuation measures will be looked at separately. Figure 7.5 illustrates two graphs, one graph only includes influence of vertical evacuation [Figure 7.5a], and the other only includes the influence of wireless receivers [Figure 7.5b].

The first evacuation improvement measure was to implement vertical evacuation buildings at a central part of the 1D cross section, in order to reduce the evacuation distance from the coast. From looking at this resulting total cost curve in Figure 7.5a, if the most favorable solution is taken to be the lowest total cost, it would be to have a 16 m dike along with the effect from vertical evacuation. This intervention yields a total cost of €8.98 billion, resulting in a €1.32 billion decrease of the total cost.



(a) Dike heightening & Vertical Evacuation buildings



(b) Dike heightening & Wireless Receivers

Figure 7.5: Economic Optimization curve of the combination of dike heightening and implementation of (a) vertical evacuation buildings, and (b) Wireless Receivers

For the other evacuation improvement measure of distributing wireless receivers to make the evacuation behavior more efficient, the total cost curves are different from the vertical evacuation measure. Looking at Figure 7.5b, assuming the most favorable solution to have the lowest total cost, this would be to have just the influence of the wireless receivers without any dike heightening. This intervention yields a total cost of €5.98 billion, resulting in a €4.32 decrease of total cost.

7.1.5. SUMMARY

Since the 'bathtub' total cost curves (curves such as Figure 7.3 and 7.4) did not illustrate the risk reduction as clearly as hoped, another curve with the relationship between investment and risk for each intervention is illustrated in Figure 7.6. In the graph, both the risk and investment are illustrated in terms of net present value.

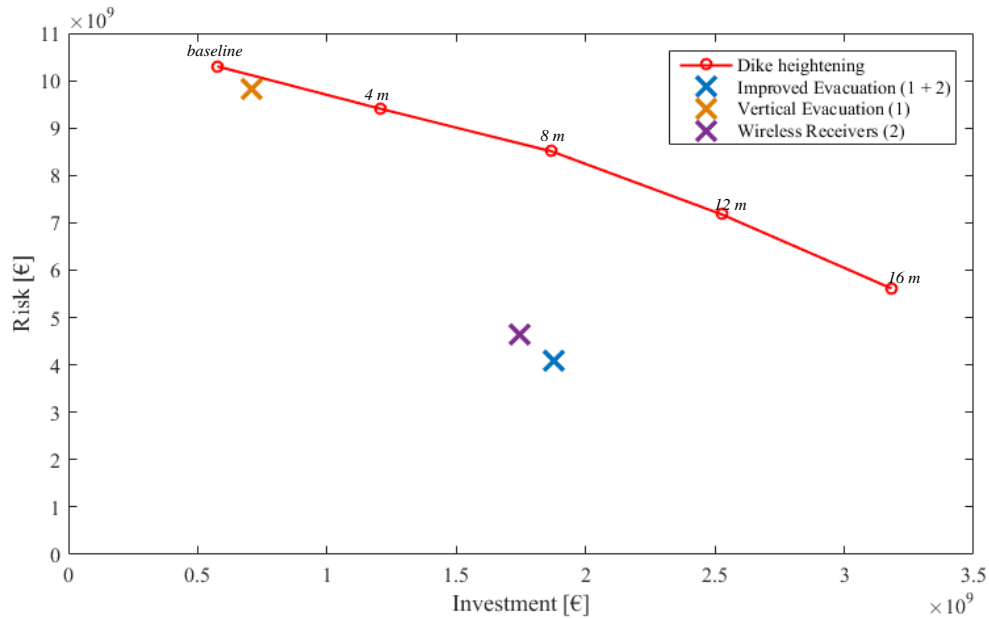


Figure 7.6: The relationship between investment and risk for the different interventions

It is clear that the wireless receivers and the combination of the two evacuation improvement measures reduce the risk the most. Based on the figure, the lowest NPV risk can be obtained by the combination of evacuation improvements. This will be further looked at in Table 7.2 which presents each of the results of investment, NPV risk, expected total cost over the lifetime, and the benefit-cost ratio.

Table 7.2: Baseline risk with most favorable solutions for each intervention

	Dike height (m)	Investment (B€)	Risk (B€)	Total Cost (B€)	Benefit-Cost Ratio
Baseline Risk	3	0.58	10.30	10.88	-
Dike heightening	16	3.18	5.61	8.80	0.47
Vertical Evacuation (1)	3	0.71	9.85	10.56	0.45
Wireless Receivers (2)	3	1.74	4.65	6.40	2.57
Improved Evacuation (1 + 2)	3	1.88	4.11	5.98	2.61

The benefit-cost ratio is determined by dividing the risk reduction by the investment cost, and it can be assumed that interventions with larger benefit-cost ratios are more beneficial. Again, the most favorable solution of the considered interventions based on the CBA supports the findings in Figure 7.6, which was the combination of improving evacuation measures with no dike heightening. The most favorable solution of the considered interventions, also with respect to the results of individual and societal risk evaluation, will be discussed in Section 7.4.

7.2. RISK EVALUATION BASED ON INDIVIDUAL RISK

As mentioned in Section 5.1.1, individual risk illustrates the probability of death of an average, unprotected person that is constantly present at a certain location [Jonkman and Schweckendiek, 2015]. The individual risk for the baseline situation was computed to be 2.44×10^{-3} per year for the areas where the mortality is 100%, and is 3.98×10^{-5} per year for areas where the mortality is 50%. This individual risk for the baseline situation was computed using equation 5.4, dependent on the mortality zones based on the dv_{max} values, and the same will be done to compute the individual risk in the situation with different interventions.

Table 7.3: Individual Risk for different interventions

	Dike height (m)	Individual Risk (where $F_D=1.0$)	Individual Risk (where $F_D=0.5$)
Baseline	3	2.44.E-03	3.98.E-05
Dike heightening (1)	4	2.41.E-03	3.88.E-05
	8	2.16.E-03	3.37.E-05
	12	1.75.E-03	3.68.E-05
	16	1.25.E-03	2.59.E-05
Vertical Evacuation (2)	3	2.42.E-03	3.98.E-05
Combination (1 + 2)	4	2.17.E-03	3.88.E-05
	8	1.88.E-03	3.37.E-05
	12	1.41.E-03	3.68.E-05
	16	9.99.E-04	2.59.E-05
Wireless Receivers (3)	3	9.84.E-04	1.48.E-05
Combination (1 + 3)	4	8.54.E-04	1.44.E-05
	8	7.20.E-04	1.25.E-05
	12	5.35.E-04	1.36.E-05
	16	3.72.E-04	9.61.E-06
Combination (2 + 3)	3	8.96.E-04	1.48.E-05
Combination (1 + 2 + 3)	4	8.02.E-04	1.44.E-05
	8	6.97.E-04	1.25.E-05
	12	5.23.E-04	1.36.E-05
	16	3.70.E-04	9.61.E-06

From the results shown in Table 7.3, it is clear that the individual risk in the 100% mortality zone is lower with more interventions. The dike heightening slightly reduces the individual risk in comparison to the baseline, and the combination of dike heightening and improved evacuation reduces the individual risk much more compared to the baseline. Similar results are seen for the individual risk in the 50% mortality zone. The individual risk is further reduced, and the magnitude of the individual risk is much lower than the individual risk which was computed for the 100% mortality zone.

As mentioned in Chapter 5, the acceptable level of individual risk for areas in the Netherlands protected by flood defenses is proposed to be 10^{-5} per year [Jonkman and Schweckendiek, 2015], thus, none of these interventions meet this limit for the 100% mortality zone, and only some meet the limit in the 50% mortality zone. Therefore, it could be inferred that this flood protection limit is too high, or in other words too conservative, to be used for tsunamis.

7.3. RISK EVALUATION BASED ON SOCIETAL RISK

In Chapter 6, risk under different situations were quantified, and the results showed that 90 % of the damage costs were due to the loss of life. For cases where the fatalities contribute to a large part of the damage, societal risk is very relevant as it is derived from a relationship between the probability of an event and the number of fatalities resulting from that event, which is represented as an FN curve.

The societal risk for tsunamis in Kamakura is represented with an FN-curve illustrated in Figure 7.7, along with the limit line for water related hazards in the Netherlands. Based on the national societal risk criterion proposed by TAW which was also introduced in Section 5.1.1, the variables used for the limit line formula (equation 5.5) are: policy factor $\beta = 1$, risk aversion index $k = 3$, and the steepness of the limit line $n = 2$ [Vrijling et al., 2014]. For the number of polders $N_A = 1$, as only one area is considered for this hazard.

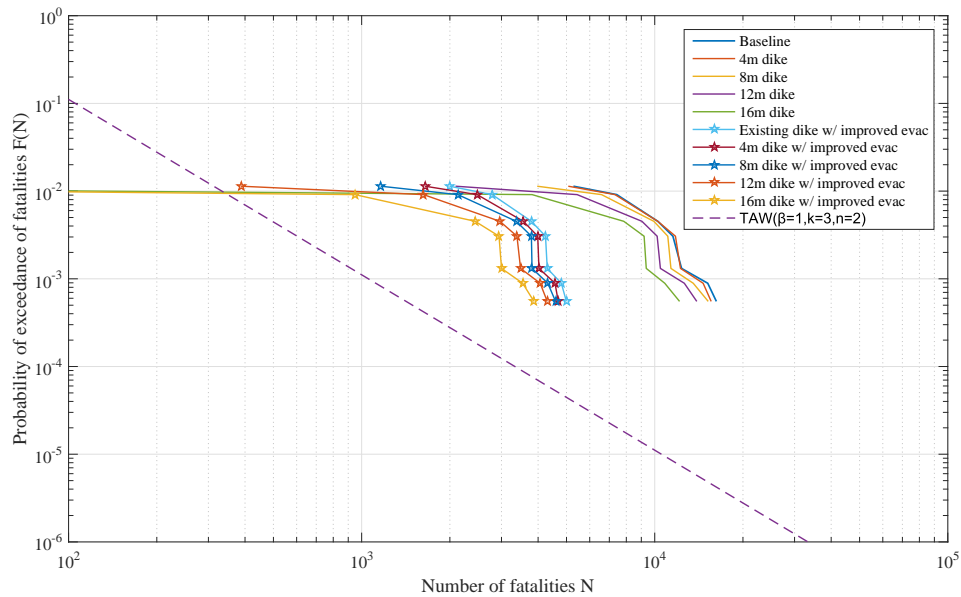


Figure 7.7: FN curve illustrating the societal risk for tsunamis in Kamakura with the baseline, dike heightening and combined interventions, along with the limit line for water related hazards proposed by TAW used in the Netherlands

From Figure 7.7, it is clear that compared to the baseline condition, the curves illustrating the different intervention scenarios shift in the left direction. The improvement in evacuation illustrates a large decrease in the amount of fatalities. For example, in a situation with a 3 m dike, the improvement of evacuation reduces the number of fatalities by more than half relative to the baseline curve. Similar to the results of individual risk, the societal risk curves shift closer to the acceptable limit with more interventions. The influence of the two different evacuation improvement measures shown in separate curves can be seen in Figure 7.8.

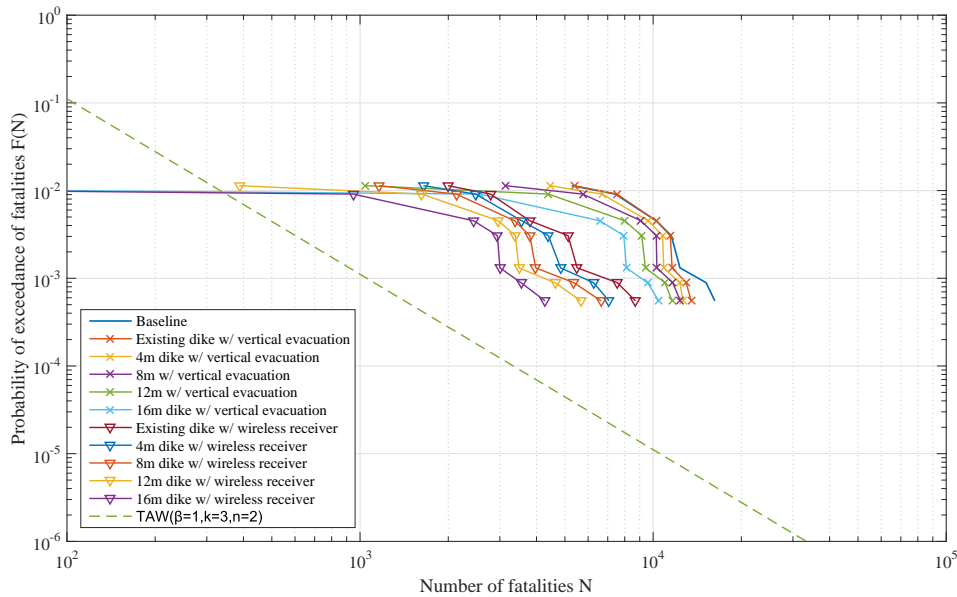


Figure 7.8: FN curve illustrating the societal risk for tsunamis in Kamakura with the different evacuation improvement measures (Vertical evacuation and Wireless receivers), along with the limit line for water related hazards proposed by TAW used in the Netherlands

The situation is considered safe when the curve lies within the limit line. There are two ways to move these curves within the limit line: to reduce the consequences or to reduce the probability. In the case of this thesis, only a part of the range of probability of flooding is looked at, thus, the shift in the downward direction is not recognizable in the graph. However, it is clear that with the interventions, the damage is reducing, in other words the consequences of a hazard is being reduced.

An overview of different societal risk levels used for hazardous installations in other countries is presented in Appendix D. This is meant to give an idea of the differing levels of risk accepted in different countries, however, it is important to realize that hazardous installations most probably have higher safety levels than what may be expected for an acceptable societal risk level for tsunamis.

7.4. DISCUSSION

With all of the different methods of assessing risk computed, the different results will be compared and contrasted in order to choose the most favorable intervention of the considered options. All of the results from the different risk evaluation methods are illustrated in Table 7.4.

Table 7.4: Summary of risk evaluation results of CBA, individual and societal risk

Intervention	Dike height (m)	Total Cost (B€)	B/C Ratio	Individual Risk		Societal Risk
				$F_D=1.0$	$F_D=0.5$	
Baseline	3	10.88	-	2.44.E-03	3.98E-05	Figure 7.7, 7.8
Dike heightening (1)	4	10.61	-0.10	2.41.E-03	3.88E-05	Figure 7.7
	8	10.37	-0.02	2.16.E-03	3.37E-05	
	12	9.71	0.19	1.75.E-03	3.68E-05	
	16	8.80	0.47	1.25.E-03	2.59E-05	
Vertical Evacuation (2)	3	10.55	0.47	2.42.E-03	3.98E-05	Figure 7.8
Combination (1 + 2)	4	10.47	0.30	2.17.E-03	3.88E-05	Figure 7.8
	8	10.39	0.24	1.88.E-03	3.37E-05	
	12	9.80	0.40	1.41.E-03	3.68E-05	
	16	8.98	0.56	9.99.E-04	2.59E-05	
Wireless Receivers (3)	3	6.40	2.57	9.84.E-04	1.48E-05	Figure 7.8
Combination (1 + 3)	4	6.55	1.81	8.54.E-04	1.44E-05	Figure 7.8
	8	6.75	1.35	7.20.E-04	1.25E-05	
	12	6.82	1.09	5.35.E-04	1.36E-05	
	16	6.79	0.93	3.72.E-04	9.61E-06	
Combination (2 + 3)	3	5.98	2.61*	8.96.E-04	1.48E-05	Figure 7.7
Combination (1 + 2 + 3)	4	6.35	1.80	8.02.E-04	1.44E-05	Figure 7.7
	8	6.71	1.31	6.97.E-04	1.25E-05	
	12	6.86	1.04	5.23.E-04	1.36E-05	
	16	6.90	0.88	3.70.E-04**	9.61E-06	

*Optimum solution based on CBA

**Optimum solution based on IR and SR

In Table 7.4, the column illustrating the benefit-cost(B/C) ratio refers to the ratio between risk reduction and investment. The larger this value, it can be inferred that there is more benefit per cost from this intervention, or in other words the intervention is more economical. If this value is negative (also illustrated in red), this means that the total cost (= investment + risk) increased due to this intervention and there was no risk reduction.

As mentioned before, there are no guidelines for the individual risk or societal risk, thus, on one hand it cannot be clearly said whether the computed safety levels are safe enough or not. It is also unclear whether this concept of having an acceptable level of risk is applicable for a place like Japan. This is because Japan has many hazards, and tsunamis are very destructive compared to hazards which exist in the Netherlands. In addition to the differences in hazard, the cities near the coast are much more densely populated than in the Netherlands, which would result in high numbers of individual risk. On the other hand, using the CBA as the main decision-making tool for a city where 90% of the damage costs result from fatalities, brings up the question of the moral judgment of assigning an acceptable total cost to the amount of human lives which could be lost in a tsunami. Therefore, it is important to keep in mind that this choice is a preliminary solution concluded from the results of this thesis, along with assumptions of possible demands relating to the type of intervention which is preferred by different stakeholders.

The results of individual risk and societal risk show that with more interventions implemented, the lower

both the risk levels become. Therefore, the lowest risk level, which is the optimum strategy under these two risk evaluations, is observed for the combination of interventions with improved evacuation, including both vertical evacuation and wireless receivers, with a 16 m dike. This intervention presents an individual risk level of 3.72×10^{-4} in the 100% mortality region ($F_D=1.0$), and 9.61×10^{-6} in the 50% mortality region ($F_D=0.5$), also illustrated with ** in the table.

The most favorable strategy chosen based on the CBA is different from the one chosen based on individual and societal risk as the criteria is different. The most favorable strategy of the considered options for the CBA is the solution with the lowest total cost and the maximum benefit-cost ratio. This is the combination of having wireless receivers and vertical evacuation, without any dike heightening. This intervention presents the cost of €5.98 billion, also illustrated with * in the table.

It is important, however, to choose the most favorable of the considered options with respect to all the risk evaluation methods conducted in this thesis. This type of approach to choose interventions with respect to multiple risk evaluation methods is conducted in the Netherlands [Jonkman and Schweckendiek, 2015], which is presumed to be advantageous as it assesses the safety from different perspectives. Looking at Table 7.4, the first step taken to choose the most favorable of the considered options was to narrow down the interventions to those which have B/C ratios larger than 1. This was seen for interventions with (numbers are corresponding to table): Wireless Receivers (3), Combination (1 + 3), Combination (2 + 3), and Combination (1 + 2 + 3). The total costs for these interventions range from €5.98 to €6.88 billion. These interventions also have low individual risk with respect to the baseline in the magnitude of 10^{-4} in the 100% mortality areas, closer to the acceptable risk limit of 10^{-5} used in the Netherlands. The societal risk curves are also shifted closer to the TAW limit lines.

In reality, once the risk is evaluated, the results of the evaluation are weighed with different stakeholders demands. Now, assumptions will be made for the different demands from stakeholders, as the stakeholders were not interviewed for this thesis. As mentioned before, Kamakura has many tourist (21.93 million in 2014), and one of the most popular locations visited by these tourist is the beach and the coastal areas. For this reason, the society will most likely not favor an intervention where a large dike would be built on the coast, blocking the view of the sea from the city.

On top of the demands of the citizens, the local and national government would most probably want an intervention which is easily and quickly implemented with maximized benefit (largest B/C ratio). The decision making done by the national and local government is most likely aimed to benefit the government by conducting projects with small investments and large return, which also results to furnish a good life for the people in the area of consideration. With this political reasoning in mind, the final choice of the most favorable strategy of the considered options for Kamakura is the improvement of evacuation with both the vertical evacuation and wireless receivers. The individual risk and societal risk are in the lower range with respect to the other results, and the total cost reduction by implementing this measure is €4.36 billion. Furthermore, the feasibility and ease of this measure is also expected to be another selling point of this particular intervention.

This conclusion is a preliminary solution, and there are many simplifications and assumptions made in this step. One of the simplifications was the initial investment costs of dike heightening. In Japan, the ground is often weak, and earthquake resistance must also be considered as a part of the construction. The initial dike building costs in Japan are highly dependent on the strength of the soil layer. The coastline of Kamakura has a very large siltstone layer [Kanagawa Prefecture, 2016], which has soil characteristics that act inelastic when subjected to high differential stress [Miller et al., 2013]. For this reason, it may be possible that the initial investment result to be higher than what will be taken for this thesis, in order to strengthen the soil.

Furthermore, the individual risk was taken as two spatial zones of 100% mortality and 50% mortality. This is very simplified as in reality, individual risk is represented in terms of distance from the hazardous area, for a tsunami, this would be the distance from the coast. Further research must be done in order to define the individual risk more precisely.

Finally, in this chapter, an acceptable risk level for the individual and societal risk was not defined for tsunamis in Japan. This is a very difficult step as it is unclear whether this concept would be accepted in Japan, and whether it is applicable for such a destructive hazard such as a tsunami. Thus, for these levels to be defined for tsunamis in Japan, more research must be done to look at risk levels defined for other hazards in Japan, such as nuclear reactors, to see what a familiar safety level in Japan is to finally find a level which would be acceptable for tsunamis. This could also be linked to the currently existing categorization of level 1 and level 2 tsunami events.

8

CONCLUSIONS AND RECOMMENDATIONS

The main conclusions of this thesis are listed below. Section 8.1 summarizes the main conclusions and the applications and relevance to other tsunami prone areas. Section 8.2 discusses the reflection on the methodology. Finally, Section 8.3 summarizes the recommendations.

8.1. CONCLUSIONS

The flood risk assessment conducted for Kamakura presented that a tsunami risk assessment is possible. A tsunami risk assessment methodology was developed in order to achieve the main objective of this thesis, which was to determine how to evaluate a risk-reducing system against tsunamis for Kamakura. This proved possible but contained some difficulties and uncertainties. There were four main steps in the flood risk assessment for this thesis, which were (1) Determination of tsunami return periods, (2) Flood scenarios, (3) Risk quantification, (4) Risk reduction interventions, and (5) Risk evaluation. The most important of these steps was the determination of the tsunami return periods. Each of these steps has its conclusions and will be highlighted in chronological order. Finally, the relevance to other tsunami prone areas will be explained.

In step (1), the relationship between the tsunami return periods and its corresponding undisturbed, incoming wave height was determined to estimate the tsunami probability. This was very difficult, as tsunamis do not occur frequently, they are dependent on many factors including influence from earthquakes, and it is necessary to have data on incoming wave heights and the time since its occurrence. This step was the most important in the risk assessment as the chosen fitted distribution was a determining factor of the results for the following steps. For this thesis, the chosen distribution, which was the GEV Type 3 distribution, was assumed to be sufficient to conduct the risk assessment as the return period considered was short (88-2000 years), and the more frequent tsunamis determine the risk. This method of determining tsunami return periods has inaccuracies, but allows the inclusion of area specific characteristics by fitting the distribution to incoming wave heights, which incorporates the influence of bathymetry.

In step (2), SWASH was used to develop a 1D run-up model in order to estimate damage. This approach and model was verified for Sendai, as the results captured essential features of the observation data from the 2011 event. It was assumed that the same model can be used for Kamakura, not only due to the verification of Sendai, but also as the boundary conditions of Kamakura are similar to that of Sendai. The run-up distance and other flood parameters were dependent on the incoming wave height, hence outputs from SWASH were obtained to be used as representative values for the flood parameters.

Next in step (3), the flood scenarios were combined with the damage assessment to estimate the loss of life and damage to buildings. The damage was assessed with the maximum depth-velocity product, and integrated with the economic values and spatial distribution of people and houses to obtain damage in monetary terms. The results for the baseline risk which presents the risk under the current condition, showed that the total damage resulting from tsunamis are high. The flood scenarios were interpolated from the 1D cross-section, which assumed 57% of the total population of Kamakura lived in the flood prone area. The total damage ranged from €12.1 to €37.6 billion (annual total risk of €257.5 million), confirming the vulnerability of Kamakura. More precisely, over 90% of the total damage costs were a result of fatalities (casualties were ranging from 5280 to 16232 people).

From the results of the baseline risk, it was clear that interventions which would reduce the casualties would be effective in reducing the total risk. In step (4), two interventions were chosen to reduce the tsunami risk in Kamakura. The first intervention was dike heightening. This intervention had a limit to the risk reduction as the resulting damage was high even with the inclusion of a high dike. This was due to the fact that tsunamis have a large amount of energy, which was why even small waves would overtop the dike, and since Kamakura is densely populated, the resulting damage is very high even if only a small area is inundated.

The second intervention was improving the evacuation system, and two measures which were seen to be effective during the Tohoku event in 2011 were chosen. The first measure was the implementation of vertical evacuation buildings to reduce the evacuation distance. The results showed that this measure was valuable for large tsunamis which have large run-up distance, and reduced up to approximately 3000 casualties. The second measure was the distribution of wireless receivers to improve the evacuation behavior (i.e. to promote more people to evacuate). This measure was observed to be very effective, reducing the casualties by half or more.

Finally, in step (5), the computed risk for all the interventions were evaluated by the cost-benefit analysis (CBA), individual risk and societal risk, to determine the most favorable intervention of the considered options. When only considering the results of the individual and societal risk evaluation, the lowest risk level is seen for the combination of having vertical evacuation, wireless receivers and a 16 m dike relative to MSL. When only considering the results of the CBA, the lowest total cost and the maximized Benefit-Cost (B/C) ratio presents the most favorable solution. This was observed for the combination of interventions of having vertical evacuation and wireless receivers.

It is important to realize that the most favorable solution is preliminary, and derived with respect to the evaluation results of this thesis and assumptions made for the different demands of stakeholders. Determining the most favorable option was very difficult as there presently are no guidelines for the required safety level to make the decision. Moreover, deciding this based on the CBA results, where fatalities were the major source of costs, questioned the moral judgment of assigning an acceptable cost to the amount of fatalities which could occur in case of a tsunami. The political decision makers were assumed to most likely prefer interventions with low cost and high return (maximized B/C ratio), and it was deemed plausible for the society to favor interventions which minimize the disruption of the coastal aesthetics. The preliminary solution for the most favorable intervention of the considered options was to improve evacuation with both vertical evacuation buildings and distribution of wireless receivers, without any dike heightening measures. The feasibility and ease of implementation was another advantage of this intervention.

This risk management process was conducted for Kamakura, but it can be said that it is relevant to other areas which are also prone to tsunamis. Similar methodologies can be used to determine the distribution between the return period and incoming wave height with available data for that particular region. If there is no available data, using simulated data on historical tsunamis as done in this thesis is also

a possibility, as the importance was to gain an insight of tsunami return period and corresponding incoming wave height. Furthermore, the flood scenarios in SWASH, the spatial distribution of economic values and population densities should be adjusted for the area. Finally, different risk reduction interventions, more suitable for the area in question, can be chosen. The main underlying process can be conducted in a similar manner as this thesis.

8.2. REFLECTION ON METHODOLOGY

One of the objectives of this thesis was to develop a method for determining the relationship between the return period of the tsunami and its incoming wave height on the coast. Data was obtained from historical tsunami simulations, as there was one data set for tsunamis in Kamakura available on the national tsunami repository of Japan. The return period approximations were made based on the data, then fitted with extreme value distributions. According to the extrapolation reliability limit of 1/1000 from the method of regression, the corresponding incoming wave height for the fitted distributions for this level should be reliable. This, however, was very dependent on the distribution, and had a very large difference in the corresponding incoming wave height ranging from approximately 14 to 24 m. Even with the possibility of the underestimation of wave height, the choice of the GEV Type 3 distribution was made - this distribution showed a 14 m incoming wave height for a 1000 year return period. Tsunamis with return periods of less than 80 years, and greater than 1800 years were not considered, hence the reliability of low frequency tsunamis were not weighed heavily in this thesis and maybe underestimated.

Another objective was to develop a method to model the damage potential of tsunamis. The damage potential was determined by the flood scenarios, which were modeled in 1D in SWASH. The wave development was dependent on the chosen transect, and the damage for the entire city was interpolated from the damage results of the cross-section. In reality, not only are the different sections along the coastline expected to have different results for incoming wave heights and run-up distances, but also real wave phenomena such as refraction and reflection are observed. This is because the coastal characteristics differ, and the existence of rivers and small streams may influence the tsunami run-up as well as other flood parameters. Nevertheless, it was assumed that the 1D run-up model captured the essential features which were necessary for this thesis, and the damage potential was completely dependent on the SWASH flood scenario results. There are many other ways to model tsunami generation, and suggestions for which model to be used for better tsunami modeling will be given in Section 8.3.

For the tsunami risk assessment, there were also many assumptions and simplifications made. Most of the assumptions made in this step were accepted methods from flood risk management in the Netherlands, thus these were assumed to be relevant for Japan. One factor which has a large influence in the risk quantification was the assumption of uniform distribution of houses and people. In reality, the houses are more densely built near the coast, hence more people are expected to be near the coast. Furthermore, the temporary population, which refer to the many tourists (21.93 million in 2014) which visit Kamakura, are not included in the population at risk. These changes in the damage assessment are expected to have a large influence on the results, especially as casualties were seen to contribute to more than 90% of the total damage costs. In spite of this, the uniform distribution of people were assumed to give a good first approximation.

Of these constraints mentioned above, the step which has the largest uncertainty comes from determining the relationship between the return period of the tsunami and its incoming wave height on the coast. This step is also chosen because the entire risk assessment is highly dependent on the choice of the distribution. The simulated historical tsunami data was assumed to be reliable and close to what would have been measured, thus, there is already some uncertainty in the data. Also, the GEV Type 3 curve reaches an upper bound for the incoming wave height, and if the fitted curve is inaccurate, this could result in a large underestimation of the scale of less frequent tsunamis. The first uncertainty of

data is very difficult to be overcome, but it can be inferred that although the simulations do not perfectly capture the tsunami parameters, it does capture the essential features. The uncertainties contained in this step can be reduced by:

- Analyzing the data available for neighboring cities with similar coastal and bathymetric characteristics in order to have more data
- Bootstrapping to include confidence intervals

Finally, as a reflection on the overall risk assessment methodology, even with the simplifications and the constraints, the results give a good first approximation of the possible risk from tsunamis. The results of the risk assessment have clarified the idea of the Japanese tsunami categorization method, i.e. Level 1 and Level 2 event, and has clearly substantiated that the existing method is a great strategy for flood management. Currently, the levels are still chosen with respect to the previously occurred extreme event with a freeboard, however, this design choice can be determined more easily by having tsunami return period distributions. Therefore, an inclusion of a risk assessment approach can be expected to further improve the framework of the tsunami categorization method.

8.3. RECOMMENDATIONS

The results of this thesis confirmed that the current condition of Kamakura is very vulnerable to tsunamis, and may result in many casualties. Therefore, in order to avoid large amounts of casualties, it is recommended that Kamakura implement risk reduction measures which have an influence to reduce casualties, such as the evacuation improvement interventions, as suggested in the preliminary solution. In addition, more detailed research can be done to support the decision of risk-reduction measures. The following is a set of recommendations drawn from the findings of the study to optimize some of the steps.

Addition of tsunami data The main constraint of this thesis was the distributed relationship between the incoming wave height and return period, especially for less frequent tsunamis which had more uncertainty. This choice of the distribution can be further supported by having more data on tsunamis. Data for neighboring regions with similar bathymetry, and also data for smaller scale, more frequent tsunamis will improve the distribution fitting. The optimization of this step can also help improve the steps which follow in the risk assessment.

Other tsunami parametric dependencies In this thesis, only the probabilistic relationship between return period and incoming wave height were covered. Looking at the combination of probabilistic relationships between parameters of not only incoming wave height and return periods, but also factors like arrival time, earthquake magnitude and plate deflection may provide further insight into the relationships between hydraulics and seismic variables. Such insight could help optimize the step of determining the tsunami return periods, and present interesting results.

Higher accuracy tsunami propagation model By conducting the simulations with a 2- or 3-D model, the wave development would be more accurate, and could also include real sea bed changes (real deflection of bottom due to an earthquake). Moreover, a higher accuracy model could also have multiple vertical layers, which allows the measurement of depth-varying velocities, other than depth-averaged velocities. These improvements can be expected to highly optimize the flood scenarios, providing different run-up distances for each cross-section which is more realistic. Furthermore, the influence of the Manning's (roughness) coefficient on the run-up distance can also be compared, as different research suggested the use of different values of the coefficient for tsunami modeling. If a choice had to be made on which higher accuracy model to use, a 2-D model is recommended. A 2-D model has faster computational time and easier set up, and have comparable results to that of a 3-D model, as it already includes multiple wave phenomena (i.e. refraction, reflection), hence it is enough to conduct a definitive analysis.

Include GIS vulnerability assessment A 2-D analysis of the city can be conducted to have an accurate distribution of population, and also specify evacuation areas instead of simple landward evacuation. This analysis can be done using Geographic Information System (GIS). The locations of hospitals, schools, retirement homes, evacuation centers and other vital infrastructure can be specified, and the non-uniform distribution of the population can now be included for vulnerability assessments. By specifying evacuation areas for a given region in a GIS analysis, the shortest evacuation distance for the people in a given region can be accounted for, allowing a more realistic evacuation model. Moreover, the restriction of the height of buildings, which is included in the construction code in Kamakura, can be included in the analysis to confirm the reliability of specified evacuation areas. If a 1D analysis is simple 1D analysis is still preferred, obtaining the population density distribution from GIS for a 1D cross-section is also expected to improve results.

Probabilistic approach for evacuation The evacuation model uses deterministic values to portray human behavior. This model can be improved with a probabilistic approach, estimating an evacuation with a more realistic behavior of people. Instead of giving deterministic values to the different evacuation speeds, delay times, and many more factors, using parametric distributions can remove some of the uncertainty of the evacuation model, resulting in a more realistic estimation.

Investigation of other costs The damage costs for this thesis only take into account the direct costs which result from damage to buildings and the loss of life. For a city where tourism supports a large share of the economy like Kamakura, indirect costs resulting from a tsunami, which include the loss of business opportunities and tourism, can be expected to be very large. The inclusion of these values may present different results, hence aimed to optimize the damage assessment step. Moreover, including tourists in the population at risk can be expected to also significantly change the results.

Of these many recommendations, the steps which should be optimized first are the addition for tsunami data and looking at other tsunami parametric dependencies. The tsunami return period distribution is the most influential step in this thesis. These two recommendations can improve this step, which could reduce the uncertainty and improve the accuracy of the results for the entire thesis.

BIBLIOGRAPHY

- Arcas, D. and Segur, H. (2012). Seismically generated tsunamis. *Philosophical Transactions of the Royal Society A: Mathematical, Physical and Engineering Sciences*, 370(1964):1505–1542.
- Bank of Japan (2008). The Basic Discount Rate and Basic Loan Rate.
- Battjes, J. (1986). *Energy dissipation in breaking solitary and periodic waves*. Delft University of Technology.
- Battjes, J. and Labeur, R. (2014). *Open Channel Flow: Lecture notes of CTB3350*. TU Delft.
- BBC (2016). Japan tsunami remembered five years on.
- Bosboom, J. and Stive, M. (2015). *Coastal Dynamics I*. VSSD.
- Bricker, J. D., Gibson, S., Takagi, H., and Imamura, F. (2015). On the Need for Larger Manning ' s Roughness Coefficients in Depth-Integrated Tsunami Inundation Models. *Coastal Engineering Journal*, 0(0):0.
- Bryant, E., Synolakis, C., and Fryer, G. J. (2008). *Tsunami: the underrated hazard*, volume 6.
- Cabinet Office Government of Japan (2007). Research report on economic analysis of damage and loss caused by traffic accidents (in Japanese).
- Caires, S. (2014). Probabilistic Design in Hydraulic Engineering Guest lecture by Sofia Caires: Extreme value analyses in research and advice in Hydraulic Engineering at Deltares.
- Camfield, F. (1980). *Tsunami Engineering*. U.S. Army, Corps of Engineers.
- Carey, N. (2005). Establishing Pedestrian Walking Speeds. *Traffic Engineering*, (503).
- city, I. (2016). Population and city economy.
- Daiwa House Group. Tsunami emergency evacuation space for roof tops "W-ev Tower"(translated from Japanese).
- Dallal, G. E. (2012). Introduction to Simple Linear Regression.
- de Neufville, R. (1990). *Applied Systems Analysis: Engineering Planning and Technology Management*. McGraw-Hill Publishing Company.
- Deltares (2011). Maatschappelijke kosten-batenanalyse Waterveiligheid 21.
- Esteban, M., Onuki, M., Ikeda, I., and Akiyama, T. (2015). Reconstruction following the 2011 Tohoku earthquake tsunami: Case study of Otsuchi Town in Iwate prefecture, Japan. *Handbook of Coastal Disaster Mitigation for Engineers and Planners*, (April 2016):615–631.
- Fraser, S., Matsuo, I., Leonard, G., and Murakami, H. (2012). Tsunami evacuation : Lessons from the Great East Japan earthquake and tsunami of March 11th 2011. Technical Report GNS Science Report 2012/17.
- Fujisawa Civil Engineering Office (2015). Road 134 Sea wall reconstruction Plan.

- General Bathymetric Chart of the Ocean (2016). Bathymetry data of Sagami Bay, and Tohoku coast.
- Given, D. D., Cochran, E. S., Heaton, T. H., Hauksson, E., Allen, R. M., Hellweg, M., Vidale, J., and Bodin, P. (2014). Technical implementation plan for the ShakeAlert production system: an Earthquake Early Warning system for the West Coast of the United States: US Geological Survey Open-File Report 2014-1097. page 25.
- Google Earth (2016). Maps, Satellite Imagery.
- Grilli, S., Svendsen, I., and Subramanya, R. (1997). Breaking Criterion and Characteristics of Solitary Waves on Slopes. *Journal of Waterway, Port, Coastal and ocean engineering*, pages 102–112.
- Holthuijsen, L. (2007). *Waves in Oceanic and Coastal Waters*. Cambridge University Press.
- Jager, T., Smoor, A., Tiehatten, B., and Wester, F. (2013). *Assessment & Mitigation Proposal in case of major tsunami impact: How to reduce the impact of a tsunami in Iquique, Chile*. PhD thesis.
- Jongejan, R. B., Jonkman, S. N., and Vrijling, J. K. (2012). The safety chain: A delusive concept. *Safety Science*, 50(5):1299–1303.
- Jonkman, S. and Schweckendiek, T. (2015). Flood Defences Lecture Notes CIE5314.
- Jonkman, S. N. and Penning-Rowsell, E. (2008). Human instability in flood flows. *Journal of the American Water Resources Association*, 44(5):1208–1218.
- Jonkman, S. N., Van Gelder, P. H. A. J. M., and Vrijling, J. K. (2003). An overview of quantitative risk measures for loss of life and economic damage.
- Kamakura City (2012). Expected Tsunami Inundation map for Kamakura city.
- Kamakura City (2014). The number of tourist and beach visitors.
- Kanagawa Prefecture (2012). Expected Inundation map from Tsunamis.
- Kanagawa Prefecture (2016). Statistics on cities in Kanagawa.
- Kato, F., Suwa, Y., Watanabe, K., and Hatogai, S. (2012). Mechanisms of coastal dike failure induced by the Great East Japan Earthquake Tsunami. *Coastal Engineering Proceedings*, 1(33):1–9.
- Kawai, H., Satoh, M., Kawaguchi, K., Seki, K., and Begoña Pérez-Gómez, B. (2013). Characteristics of the 2011 Tohoku Tsunami Waveform Acquired Around Japan By Nowphas Equipment. *Coastal Engineering Journal*, 55(3):1–27.
- Kumagaya, K. (2011). Historical tsunamis and its damages in Kanagawa Prefecture [PPT in Japanese].
- Madsen, P. A., Fuhrman, D. R., and Schaffer, H. A. (2008). On the solitary wave paradigm for tsunamis. *Journal of Geophysical Research: Oceans*, 113(12).
- Matsuyama, M., Ikeno, M., Sakakiyama, T., and Takeda, T. (2007). A study of tsunami wave fission in an undistorted experiment. *Pure and Applied Geophysics*, 164(2-3):617–631.
- Miller, D., Plumb, R., and Boitnott, G. (2013). Compressive strength and elastic properties of a transversely isotropic calcareous mudstone. *Geophysical Prospecting*, 61(2):315–328.
- Ministry of Land, Infrastructure, T. and Tourism (2005). Construction Cost Distributions.
- Mori, N., Takahashi, T., Yasuda, T., and Yanagisawa, H. (2011). Survey of 2011 Tohoku earthquake tsunami inundation and run-up. *Geophysical Research Letters*, 38(18):6–11.

- Natrella, M., Croarkin, C., Tobias, P., and Filliben, J. J. Exploratory Data Analysis: Kolmogorov-Smirnov Goodness-of-Fit Test. In *NIST/SEMATECH e-Handbook of Statistical Methods: Engineering Statistics Handbook*.
- Pistrika, A. K. and Jonkman, S. N. (2010). Damage to residential buildings due to flooding of New Orleans after hurricane Katrina. *Natural Hazards*, 54(2):413–434.
- Provincie Zuid Holland. Population.
- Real Estate Shonan (2016). Real estate market values in Kamakura, Shonan area [in Japanese].
- Rijnsdorp, D. P., Smit, P. B., and Zijlema, M. (2014). Non-hydrostatic modelling of infragravity waves under laboratory conditions. *Coastal Engineering*, 85:30–42.
- Saito, T., Ito, Y., Inazu, D., and Hino, R. (2011). Tsunami source of the 2011 Tohoku-Oki earthquake, Japan: Inversion analysis based on dispersive tsunami simulations. *Geophysical Research Letters*, 38(21):4–8.
- Savenije, H. (2007). *Hydrology of catchments, rivers and delta's: Lecture notes of CT5450*. TU Delft.
- Sendai City Post disaster reconstruction division (2011). Interplay between Sendai City's Plans Basic Philosophy for Reconstruction. *Sendai City Earthquake Disaster Reconstruction Plan*.
- Shibayama, T., Esteban, M., Nistor, I., Takagi, H., Thao, N. D., Matsumaru, R., Mikami, T., Aranguiz, R., Jayaratne, R., and Ohira, K. (2013). Classification of Tsunami and Evacuation Areas. *Natural Hazards*, 67(2):365–386.
- Shuto, N. (1993). Tsunami Intensity and Disasters. In *Tsunamis in the World*, pages 197–216. Kluwer Academic Publisher.
- Silva, W., Dijkman, J. P., and Loucks, D. P. (2004). Flood management options for The Netherlands. *International Journal of River Basin Management*, 2(2):101–112.
- Smith, R. C., Hill, J., Collins, G. S., Piggott, M. D., Kramer, S. C., Parkinson, S. D., and Wilson, C. (2016). Comparing approaches for numerical modelling of tsunami generation by deformable submarine slides. *Ocean Modelling*, 100:125–140.
- Southern California Earthquake Center (2007). "10.5" - a miniseries with major errors.
- Street, R. and Camfield, F. (1966). *Observations and experiments on solitary wave deformation*. Ft. Belvoir Defense Technical Information Center DEC.
- Synolakis, C. E. (1987). The runup of solitary waves. *Journal of Fluid Mechanics*, 185(-1):523.
- Tadepalli, S. and Synolakis, C. E. (1994). The run-up of N-waves on sloping beaches. *Proceeding of Royal Society London A*, (445):99–112.
- The SWASH team. SWASH version 3.14 User Manual.
- Tsimopoulou, V. (2015). *Economic optimisation of flood risk management projects*. PhD thesis.
- Tsimopoulou, V., Jonkman, S. N., Kolen, B., Maaskant, B., Mori, N., and Yasuda, T. (2012). A multi-layered safety perspective on the tsunami disaster in Tohoku, Japan. *Flood Risk 2012 Conference*, (Fujita 2011):1–10.
- USGS (2016). Topography data (Landsat, GMTED2010).
- van Dantzig, D. (1956). Economic decision problems for flood protection.

- van Gelder, P. (2015). Extreme value modelling in hydraulic engineering [PPT slides].
- Vrijling, J. K., Roos, A., Ale, B. J. M., Van der Brand, D., De Bruyn, L., Bueno de Mesquita, K. G., Van Gelder, P. H. A. J. M., Van Hengel, W., Janssen, J. P. F. M., and Vrouwenvelder, A. C. W. M. (2014). Probability in Civil Engineering. (September).
- Yamao, S., Esteban, M., Yun, N.-Y., Mikami, T., and Shibayama, T. (2015). Estimation of the Current Risk to Human Damage Life Posed by Future Tsunamis in Japan. In *Handbook of Coastal Disaster Mitigation*, pages 253–273.
- Youtube (2016). Video footage of Tohoku tsunami event in 2011.
- Yun, N.-Y. and Hamada, M. (2012). Evacuation Behaviors in the 2011 Great East Japan Earthquake. *Journal of Disaster Research*, 7(7):458–467.
- Zijlema, M., Stelling, G., and Smit, P. (2011). SWASH: An operational public domain code for simulating wave fields and rapidly varied flows in coastal waters. *Coastal Engineering*, 58(10):992–1012.

GLOSSARY

incoming wave height	maximum undisturbed, incoming wave height on the coast, where there is no influence from the primary defenses
inundation height	water levels which have influence from protection measures; everything from the primary defense and beyond
HWL	High Water Level, which is the water level with high tide
MSL	Mean Sea Level
SWASH	Simulating WAVes till Shore
PARI	Port and Airport Research Institute
Baseline Risk	The risk under the current situation, taking into consideration influence of the existing protection measures
EWS	Early Warning System
CBA	Cost Benefit Analysis
TAW	Dutch Technical Advisory Committee on Water Defences
IR	Individual Risk
SR	Societal Risk

LIST OF FIGURES

1	Schematization of risk assessment methodology with general steps	i
2	Schematization of the steps of the risk assessment method	iii
1.1	Flow chart for tsunami flood risk management	5
2.1	Schematic overview of Sagami Bay	9
2.2	Bathymetry of Sagami Bay	11
2.3	Tsunami hazard maps for earthquake simulations under current bathymetric and topographic conditions [Kanagawa Prefecture, 2012]	13
2.5	Tsunami Mechanism [Arcas and Segur, 2012]	15
2.6	Schematic overview of a Multi Layer Safety (MLS) system	18
2.7	Flood risk countermeasures for tsunami areas [Tsimopoulou, 2015]	19
2.8	Cross-sectional view of an MLS system in Sendai, Tohoku [Sendai City Post disaster reconstruction division, 2011]	22
2.9	Construction of MLS system in Tohoku: Embankments along the coast and ground heightening in the disaster risk zones [BBC, 2016]	23
3.1	Coast of Kamakura separated into sections [Google Earth, 2016]	27
3.2	Measurement locations of initial tsunami wave heights, maximum incoming tsunami wave height, and inundation heights [Kanagawa Prefecture, 2012]	28
3.3	Return period with its corresponding incoming wave height derived from the method of regression, and fitted with different GEV distributions for section B	29
3.4	Return period with its corresponding incoming wave height derived from the method of regression, and fitted GEV Type III distribution for section B	31
4.1	The different types of wave theories [Tadepalli and Synolakis, 1994]	36
4.2	Decay of solitary waves near the shoreline [Battjes, 1986]	39
4.3	Cross-sectional information for Sendai case study	41
4.4	Initial tsunami wave height distribution [Saito et al., 2011]	42
4.5	The observed time series for the tsunami wave heights for the 2011 event at buoys GB801 and WG205 Kawai et al. [2013]	44
4.6	Run-up and inundation depths of the solitary and N wave SWASH results with the observed run-up distribution line	44
4.7	Results of the SWASH model for the solitary wave illustrating (a) Shoaling, (b) Dissipation/breaking, and (c) Incoming wave near coast (different scale)	45
4.8	Results of the SWASH model for the N-wave	45
4.9	The time series of similar depth contours (in the transect) as the buoy stations of GB801 (top) and WG205 (bottom) retrieved from the SWASH results	46
4.10	Maximum wave height during the simulation for the non-broken wave, compared with Green's Law and the measured wave height at buoy station GB801	47
4.11	Video and photo material of the Tohoku tsunami at Sendai [Youtube, 2016]	48
4.12	Comparison of the SWASH results with the analytical model of Battjes [1986] and the measured wave data	49
4.13	Bathymetry and chosen design slope for Kamakura case study	51
4.14	Results from the SWASH model for the Kamakura case study	51

4.15	Different tsunami levels obtained from SWASH simulations along the return period distribution line	52
4.16	Arrival time, wave propagation speed and run-up distance for all tsunami levels	53
4.17	The inundation depth, flow velocity and dv -product along the 1D cross-section at the time of maximum run-up for a 8 m tsunami flood scenario with the existing dike	54
5.1	1D Schematization to illustrate steps in the risk analysis	55
5.2	Flow chart of risk analysis for tsunamis	56
5.3	Schematization of dikes and land behind dikes in the Netherlands and Japan	59
5.4	Sketch of the relationship between run-up distance and incoming wave height	59
5.5	Schematization of spatial distribution economic values and densities along the cross-sectional slope	60
5.6	Relationship between dv_{max} and mortality	61
5.7	Sensitivity analysis for discount rate r	64
5.8	1D Schematization of damage functions for damage to buildings and loss of life	65
6.1	Satellite plan view of Kamakura [Google Earth, 2016]	68
6.2	Flow chart for evacuation model	69
6.3	Tsunami evacuation behavior based on Great Eastern Japan earthquake and tsunami event in 2011 [Yun and Hamada, 2012]	70
6.4	Evacuation model for the flood scenarios of a 14 m tsunami	71
6.5	Relationship between damage, return period and wave height for a given scenario under the baseline conditions	73
6.6	Relationship between damage and probability of flooding (probability of exceedance), along with total risk (area under the curve)	74
6.7	Societal risk curve for the baseline risk in Kamakura, with TAW limit line for flood protection in the Netherlands	76
6.8	Relationship between damage and the probability of exceedance for each dike height intervention	78
6.9	NPV risk for dike heightening	79
6.10	Schematization of evacuation with vertical evacuation buildings	80
6.11	Evacuation model improved with shortened evacuation distance due to the implementation of vertical evacuation buildings for the flood scenario of a 14 m tsunami	81
6.12	Photo of wireless receivers distributed in Minami-Sanriku [Fraser et al., 2012]	82
6.13	Relationship between damage and probability of exceedance with evacuation and with evacuation improvements	83
6.14	Relationship between damage and probability of exceedance with the combination of dike heightening & improved evacuation in comparison with the baseline	84
6.15	NPV risk for the combination of interventions of dike heightening and improved evacuation (vertical evacuation and wireless receivers)	85
7.1	Schematization of investment options	90
7.2	Sensitivity analysis of variable investment cost of dike heightening	91
7.3	Economic Optimization curve of dike heightening considering both the damage to residential buildings and the loss of life	93
7.4	Economic Optimization curve of the combination of dike heightening and improved evacuation	94
7.5	Economic Optimization curve of the combination of dike heightening and implementation of (a) vertical evacuation buildings, and (b) Wireless Receivers	95
7.6	The relationship between investment and risk for the different interventions	96

7.7	FN curve illustrating the societal risk for tsunamis in Kamakura with the baseline, dike heightening and combined interventions, along with the limit line for water related hazards proposed by TAW used in the Netherlands	98
7.8	FN curve illustrating the societal risk for tsunamis in Kamakura with the different evacuation improvement measures (Vertical evacuation and Wireless receivers), along with the limit line for water related hazards proposed by TAW used in the Netherlands	99
A.1	Method of Regression - Ranking	121
A.2	Computed probability of exceedance and return period for each event in different sections	122
A.3	Best-fit distributions for each section along the coast with the relationship between approximated return period and inundation height	123
B.1	Time-series of the simulated initial wave front of the solitary wave at the most offshore location in transect	126
B.2	Time-serie of the simulated initial wave front of the N-wave at the most offshore location in transect	127
B.3	Observed x-velocity data at buoy WG205	127
B.4	x-velocity obtained from SWASH results at approximately buoy WG205	127
B.5	The near-shore bore development profile retrieved from SWASH for an 8 m incoming wave height scenario	128
B.6	The bore xvelocity profile right before it reaches the coast, retrieved from SWASH for an 6 m incoming wave height scenario	128
C.1	Run-up distance [km] and inundation height [m] observed along the coastline of Sendai plain, Tohoku for the 2011 tsunami event [Mori et al., 2011]	129
C.2	Time histories of water surface elevation for a case ($T = 20s$, $s = 1 : 200$) [Matsuyama et al., 2007]	130
C.3	Snap shots of the different stages of the breaking wave for both the solitary wave and the N-wave. For the non-broken wave a), the first wave split b) and when multiple solitons are formed c)	131
C.4	Time series of inundation depth d (relative to bottom), flow velocity v and $d v$ -value along locations A to D in cross-section for an 8 m incoming tsunami wave height and 8 m dike scenario	132
C.5	Water level on top of the dike and immediately after the dike for a Level 1 tsunami event for Kamakura	134
D.1	Mortality with respect to evacuation behavior distribution and population distribution for different tsunami levels	136
D.2	Tsunami hazard map for Kamakura	137
D.3	Mortality with respect to evacuation behavior distribution and population distribution with improved evacuation for different tsunami levels	140
D.4	Relationship between damage and probability of exceedance with the combination of dike heightening & vertical evacuation in comparison with the baseline	141
D.5	Relationship between damage and probability of exceedance with the combination of dike heightening & wireless receivers in comparison with the baseline	142

LIST OF TABLES

2.1	Information about major cities along the Sagami Bay coastline (Data from 01/09/2015 [Kanagawa Prefecture, 2016] and 31/12/2015 [city, 2016])	10
2.2	History of earthquakes which resulted in tsunamis in Sagami bay [Kumagaya, 2011]	11
2.3	Guideline of tsunami scale relative to earthquake magnitude <i>Procedures of the Pacific Tsunami Warning Center</i> [USGS, 2016]	15
2.4	Tsunami categorization in Japan for different levels of risk to human life r [Yamao et al., 2015]	17
2.5	Criteria for structural damage to buildings based on analysis of New Orleans [Pistrika and Jonkman, 2010]	21
2.6	Criteria for Loss of Life [Jonkman and Penning-Rowse, 2008]	21
3.1	Troughs/Faults and Approximated Return Periods for historical earthquakes which resulted in tsunamis [Kumagaya, 2011] [Kanagawa Prefecture, 2012]	25
3.2	Expected Maximum Incoming Tsunami Wave height [m] at each section on the coast [Kanagawa Prefecture, 2012]	27
3.3	Goodness of fit for different GEV distributions for coastline Section B	31
3.4	Level 1 and Level 2 event return periods and incoming wave heights for Kamakura	33
4.1	Comparison of the SWASH model results with the measured data	50
5.1	Key inputs of spatial distributions and economic values	65
6.1	Population age distribution and each of the selected evacuation speeds	69
6.2	Baseline risk inputs for existing protection measures	72
6.3	Expected casualties and building damage for each tsunami level, with its corresponding damage costs	75
6.4	Distribution of evacuation behavior with and without the wireless receivers	82
6.5	Comparison of the number of casualties between the baseline, each of the improvement measures (vertical evacuation and wireless receivers), and the combined improvement	83
6.6	Comparison of the number of casualties between the baseline situation and the intervention with both dike heightening and improved evacuation	85
7.1	Investment costs for different interventions	92
7.2	Baseline risk with most favorable solutions for each intervention	96
7.3	Individual Risk for different interventions	97
7.4	Summary of risk evaluation results of CBA, individual and societal risk	100
A.1	Method of Regression - Approximating Return Period T	122
A.2	Goodness of fit results	123
C.1	Run-up distance, inundation height, flow velocity and arrival time results for different tsunami scenarios conducted in SWASH	133
D.1	Mortality with respect to Evacuation Behavior for existing evacuation distribution	135
D.2	Mortality with respect to Population distribution for existing evacuation distribution	136

D.3	Expected casualties and building damage for each tsunami level with the dike heightening intervention, and its corresponding damage reduction	138
D.4	Mortality with respect to Evacuation Behavior for improved evacuation distribution	139
D.5	Mortality with respect to Population distribution for improved evacuation distribution . .	139
D.6	Comparison of the number of casualties between the baseline situation and the intervention with dike heightening and vertical evacuation	141
D.7	Comparison of the number of casualties between the baseline situation and the intervention with dike heightening and wireless receivers	142
D.8	International standards for FN limit line [Jonkman et al., 2003]	143

A

METHOD OF REGRESSION

Here, the steps for calculating the regression to determine the return period and corresponding inundation height are given. The details for each location along the coastline such as the best fit line and its rankings, are also shown.

A.1. PROCEDURE FOR METHOD OF REGRESSION

The regression analysis consists of analyzing the correlation and directionality of the data, fitting the line and evaluating the validity and usefulness of the fitted line. Different distribution models each with its own characteristics are available for this method, and the regression analysis is different according to the model chosen. Examples of models include Hazen/Foster, Gumbel, Bernard, Blom, and more [van Gelder, 2015]. For this thesis, the Gumbel method of regression is used. As the procedure is the same in each location, the method is only illustrated once for Location A.

Firstly, the tsunami wave heights on the coast, which is illustrated in Figure 3.2, are ranked in the order from the highest value to the lowest value A.1.

A		A'	Rank
9.1		10.2	1
8.8		9.7	2
6.2		9.1	3
5.5		8.8	4
9.7		6.2	5
2.9		5.5	6
10.2		2.9	7

Figure A.1: Method of Regression - Ranking

In the figure, A' illustrates the column which is reordered in the order from the highest to the lowest, and in the case of this study, the highest rank is given to the highest inundation height. This does not have to be the case as long as this ranking system is correlated throughout the analysis.

Secondly, the ranks are used to compute the exceedance probability using Equation 3.1. Determining the exceedance probability is very important for this thesis as the failure mechanisms which is considered for this thesis is only overtopping and overflowing, thus the exceedance probability can be assumed to be the flooding probability. The number of years in the record n is 518 years and when this is computed for Location A, the return period for each of the events results to be the following:

Table A.1: Method of Regression - Approximating Return Period T

A'	Ranks	Exceedance Probability p	Return Period T
10.2	1	0.001927	519
10.0	2	0.003854	260
9.0	3	0.005780	173
9.0	4	0.007707	130
4.0	5	0.009634	104
4.0	6	0.011561	87
2.9	7	0.013487	74

As shown in Table A.1, the maximum approximated return period is the recorded number of years. This is repeated for every chosen location along the coast in Figure 3.1. All the points are then plotted with a best fit line for each of the locations, and the result is illustrated in Figure A.3.

A.2. RESULTS

The ranking, exceedance probability, and return period are all shown in Figure A.2. The best fit distributions for each of the locations are shown in Figure A.3. Here, the best fit distributions for each of the locations are separately shown as to clearly see why the section B best fit distribution was chosen to illustrate the entire coast.

A	A'	Rank	p	T
9.1	10.2	1	0.00192678	519
8.8	9.7	2	0.00385356	260
6.2	9.1	3	0.00578035	173
5.5	8.8	4	0.00770713	130
9.7	6.2	5	0.00963391	104
2.9	5.5	6	0.01156069	87
10.2	2.9	7	0.01348748	74

C	C'	Rank	p	T
8.3	11.2	1	0.00192678	519
7.9	10.7	2	0.00385356	260
7.1	8.3	3	0.00578035	173
6	7.9	4	0.00770713	130
10.7	7.1	5	0.00963391	104
3.9	6	6	0.01156069	87
11.2	3.9	7	0.01348748	74

B	B'	Rank	p	T
9.9	14.5	1	0.00192678	519
9.2	12.9	2	0.00385356	260
8	9.9	3	0.00578035	173
7.3	9.2	4	0.00770713	130
12.9	8	5	0.00963391	104
3.8	7.3	6	0.01156069	87
14.5	3.8	7	0.01348748	74

D	D'	Rank	p	T
7.9	13.6	1	0.00192678	519
7.4	11.4	2	0.00385356	260
5.7	7.9	3	0.00578035	173
5.4	7.4	4	0.00770713	130
11.4	5.7	5	0.00963391	104
3.5	5.4	6	0.01156069	87
13.6	3.5	7	0.01348748	74

Figure A.2: Computed probability of exceedance and return period for each event in different sections

As can be seen in Table A.2 which illustrates the goodness of fit of the GEV distributions for each section,

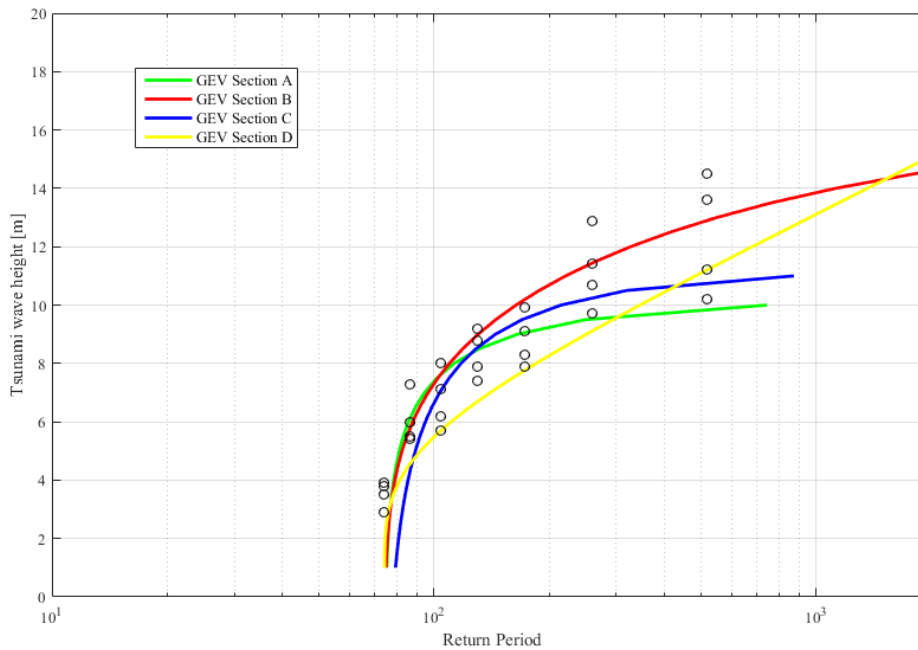


Figure A.3: Best-fit distributions for each section along the coast with the relationship between approximated return period and inundation height

Table A.2: Goodness of fit results

Distribution	Hypothesis test result (KS-test)	p-value (KS-test)	Least Square test outcome
Section A GEV fit	0	0.5473	2.8598
Section B GEV fit	0	0.9506	2.3681
Section C GEV fit	0	0.4135	2.6005
Section D GEV fit	0	0.9881	2.3236

all of the sections and its corresponding distributions are not rejected by the hypothesis test. This means that it has a 5% of larger probability of being observed under the null hypothesis. Moreover, by looking at the p-values, it is clear that either the GEV fit for Section B or Section D are the better fit, and this is also illustrated by the outcomes of the least square test, as the smaller the outcome values, the closer the distribution is to the plots. Therefore, the choice of which distribution will be used as a representative for the whole cross-section has now been narrowed down till Section B or Section D. However, there are limits to the GEV distribution curves depending on approximated wave heights and return periods. Best fit distribution for section B not only does not underestimate the empirical plots, but also runs through the mean of the plots very nicely. Moreover, the curve reaches a bound which can be inferred to illustrate the physical phenomena a shallow water wave goes through when dissipating energy on the coast. Therefore, the different distribution curves for the coastline section B were looked at in more detail for an even better fitting.

B

SWASH COMPUTATIONS

This appendix is created in collaboration with Bas Horsten.

B.1. GOVERNING EQUATIONS

The governing equations of SWASH are the non-linear shallow water equations which are derived from the incompressible Navier-Stokes equations which describe the conservation of mass and momentum [Rijnsdorp et al., 2014]. SWASH considers the depth-averaged form of the equations in Cartesian notation. The governing equations are [Zijlema et al., 2011]:

$$\frac{\delta \zeta}{\delta t} \frac{\delta h u}{\delta x} + \frac{\delta h v}{\delta y} = 0 \quad (\text{B.1})$$

$$\frac{\delta u}{\delta t} + u \frac{\delta u}{\delta x} + v \frac{\delta u}{\delta y} + g \frac{\delta \zeta}{\delta x} + \frac{1}{h} \int_{-d}^{\zeta} \frac{\delta q}{\delta x} dz + c_f \frac{u \sqrt{u^2 + v^2}}{h} = \frac{1}{h} \left(\frac{\delta h \tau_{xx}}{\delta x} + \frac{\delta h \tau_{xy}}{\delta y} \right) \quad (\text{B.2})$$

$$\frac{\delta v}{\delta t} + u \frac{\delta v}{\delta x} + v \frac{\delta v}{\delta y} + g \frac{\delta \zeta}{\delta y} + \frac{1}{h} \int_{-d}^{\zeta} \frac{\delta q}{\delta y} dz + c_f \frac{v \sqrt{u^2 + v^2}}{h} = \frac{1}{h} \left(\frac{\delta h \tau_{yx}}{\delta x} + \frac{\delta h \tau_{yy}}{\delta y} \right) \quad (\text{B.3})$$

Here, t is time, x and y are located at the still water level and the z -axis is pointing upwards. $\zeta(x, y, t)$ is the surface elevation measured from the still water level, $d(x, y)$ is the still water depth, or the bottom level measured downwards from the still water level, and $h = d + \zeta$ is the total depth. $u(x, z, t)$ and $v(x, z, t)$ are the depth-averaged flow velocities in the x - and y - directions respectively, $q(x, y, z, t)$ is the non-hydrostatic pressure normalised by the density. g is the gravitational acceleration, c_f is the dimensionless bottom friction coefficient, and $\tau_{xx}, \tau_{xy}, \tau_{yx}, \tau_{yy}$ are the horizontal turbulent stress terms.

When waves are travelling for a very long distance, in the order of several kilometers, the influence of bottom friction increases. Moreover, the long waves close to the shoreline, such as infragravity waves and nearshore circulations, are affected. Friction can be expressed in many ways, but for the case of this research, friction will be expressed based on Manning's roughness coefficient n , as this provides a better representation of wave dynamics in the surf zone. The expression is:

$$c_f = \frac{n^2 g}{h^{1/3}} \quad (\text{B.4})$$

Along with the governing equations of SWASH, appropriate boundary conditions must be imposed in order to have a complete system. At the offshore boundary, different waves can be specified by local velocity distributions.

B.2. BOUNDARY CONDITIONS

For the validation case study in Sendai, a bore was observed near the shore. Initially, this large wave breaking caused many wiggles to develop, and the motive was to remove them. To be able to do this, the u-momentum and the its advection term were looked at. The u-momentum term will be conserved throughout the simulation as that is what physically happens. Secondly the advection term changes its order of accuracy from higher harmonics in the deep water, to second or even first order accuracies as it is breaking. This allows the reduction of wiggles when simulating a breaking wave such as a bore. These boundary conditions specifically for SWASH will be kept the same throughout the thesis, simulations for both Sendai and Kamakura.

B.3. TIME SERIES OF TSUNAMI WAVES

B.3.1. SOLITARY WAVE

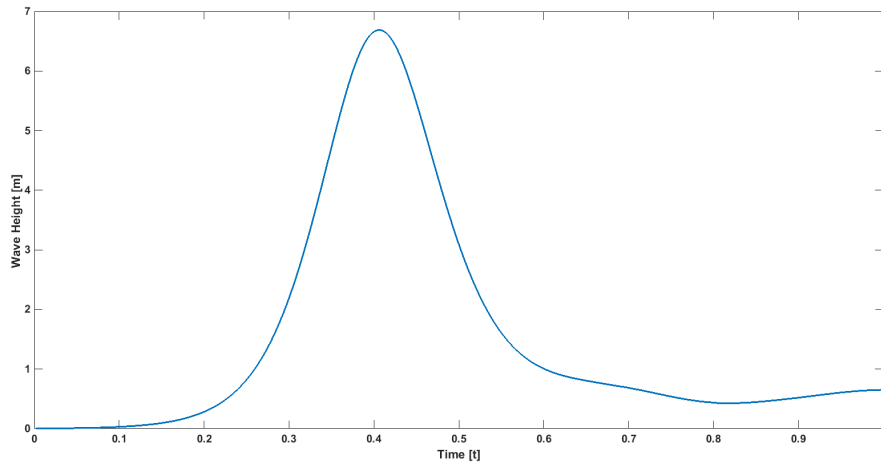


Figure B.1: Time-series of the simulated initial wave front of the solitary wave at the most offshore location in transect

This time series of this wave is first created in MATLAB from wave equations which were introduced before in Section 4.1. It is worthy to note that the initial wave front illustrated in Figure B.1 slightly differs from the time series which was made in MATLAB and put into SWASH, as the wave is already getting influence from the bottom. Here, it can be concluded that the solitary wave theory does not fully agree with the measured wave data. However, the modeled solitary wave does undergo the different wave transformations: the wave shoals, breaks and eventually runs-up.

B.3.2. N-WAVE

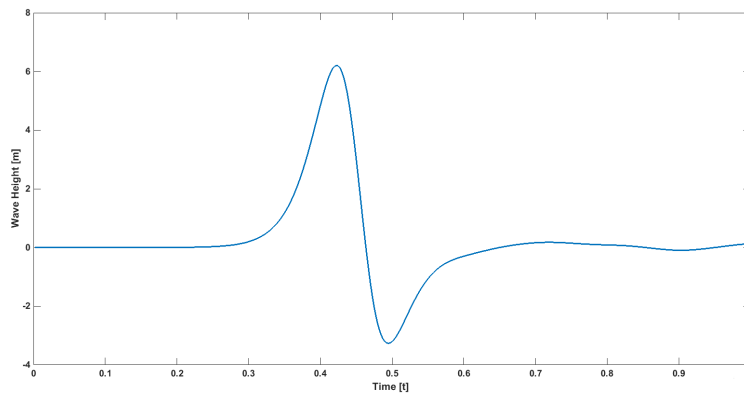


Figure B.2: Time-series of the simulated initial wave front of the N-wave at the most offshore location in transect

From the time-series [Figure B.2] it can be concluded that the modeled initial wave form matches the measured wave form at buoy GB801 [Figure 4.5].

The velocity in the x-direction can be compared and contrasted between the SWASH results with an N-wave [Figure B.4] and observed data at buoy WG205 [Figure B.3].

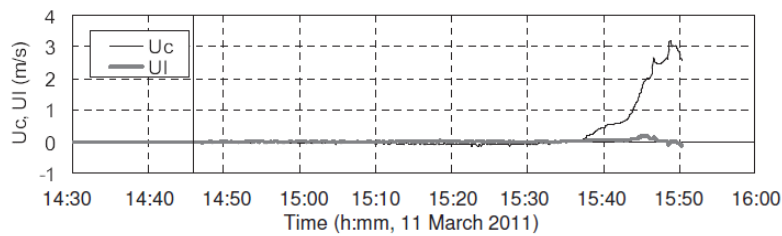


Figure B.3: Observed x-velocity data at buoy WG205

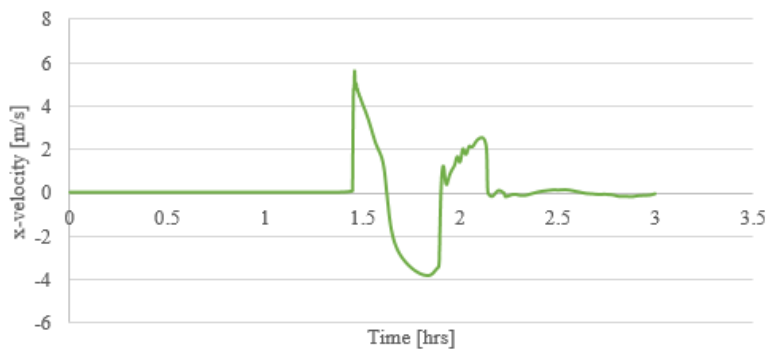


Figure B.4: x-velocity obtained from SWASH results at approximately buoy WG205

Similar to the case for Sendai, a bore develops for tsunamis waves in Kamakura. The bore development profile near the coast is illustrated in Figure B.5. It can be seen that due to the bore development, the wave height decreases as it approaches the coast.

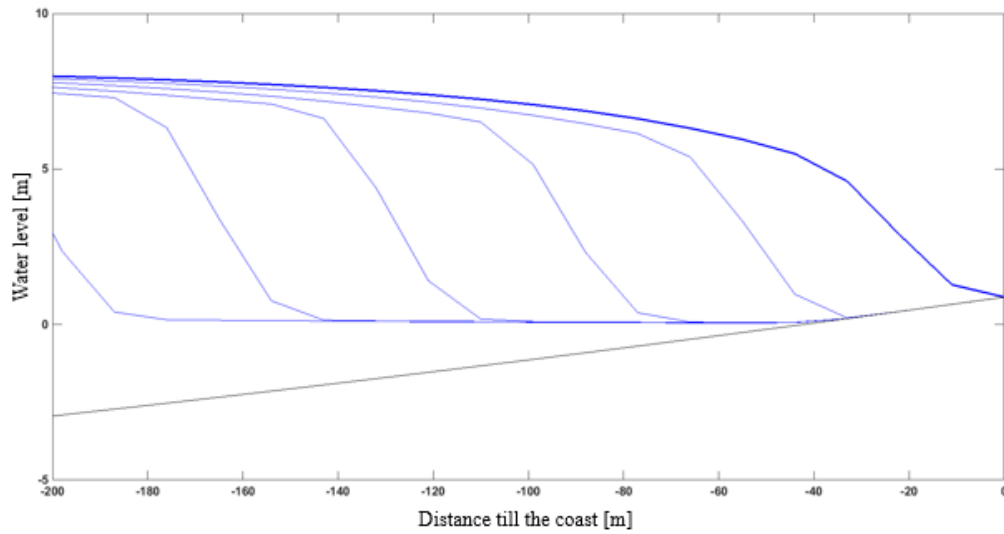


Figure B.5: The near-shore bore development profile retrieved from SWASH for an 8 m incoming wave height scenario

The x-velocity profile for a bore at a point in time right before it reaches the coast is illustrated in Figure B.6. For the reason that the x-velocity is very high on top of the bore, the x-velocity measure on top of the dike in chapter 6 is also high.

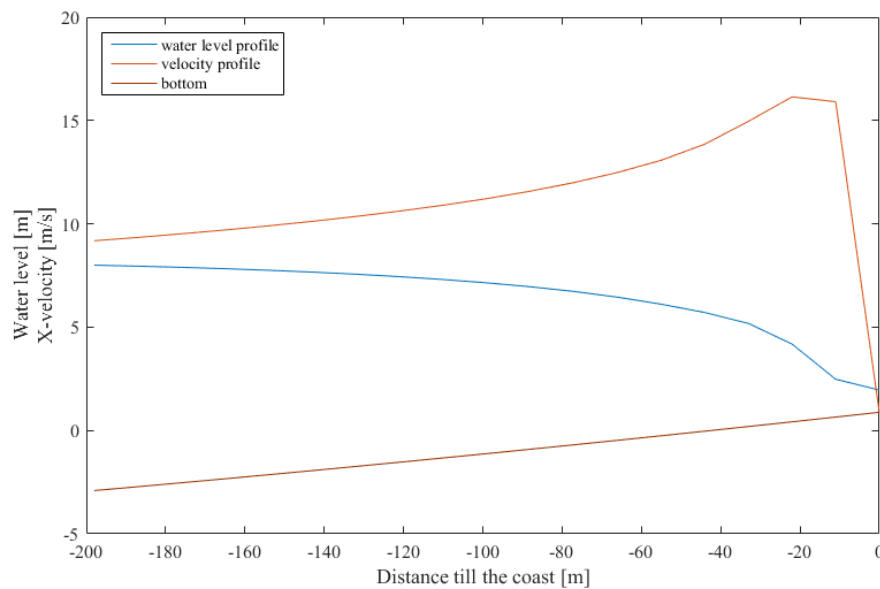


Figure B.6: The bore x-velocity profile right before it reaches the coast, retrieved from SWASH for an 6 m incoming wave height scenario

C

WAVE FORMULATION AND RESULTS

This appendix is created in collaboration with Bas Horsten.

C.1. OBSERVATION DATA

The observation data for the run-up distance relative to the inundation height for the Sendai plain is illustrated in Figure C.1. The observed data was surveyed by different institutions in Japan after the 2011 tsunami event. This relationship between inundation height and run-up distance is represented as an envelop in the graph with the SWASH results to compare the simulated results with the observed data.

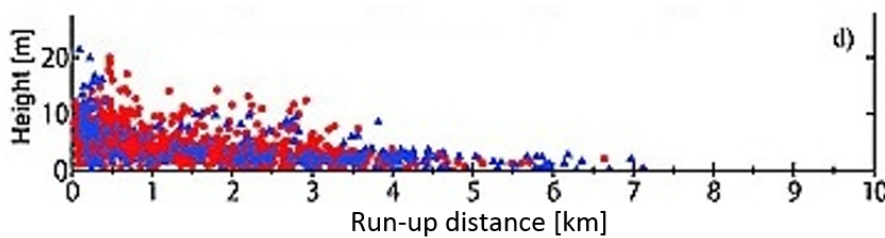


Figure C.1: Run-up distance [km] and inundation height [m] observed along the coastline of Sendai plain, Tohoku for the 2011 tsunami event [Mori et al., 2011]

The red circles is the surveyed inundation height, and the blue triangles are the run-up height both measured relative to MSL.

C.2. TSUNAMI WAVE BREAKING

In Figure 4.11 it is shown that the tsunami wave transforms into several solitons. This phenomenon, known as 'tsunami soliton fission' is also observed during the Nihonkai-Chubu earthquake tsunami in 1983. Short waves split from the tsunami crest due to nonlinearity and dispersion. The new leading wave height increases and breaks [Matsuyama et al., 2007].

The 'tsunami soliton fission' also occurs in both SWASH models [Figure C.3]. The breaking location is defined when the first wave splits from the incoming wave. These results can be compared with the results of the report of Matsuyama et al. [2007] [Figure C.2]. Here, the tsunami soliton fission was studied by means of several large scale experiments. Each model was 100 meter long with slopes of either 1/100, 1/150 or 1/200. There, the incident wave was a sinusoidal wave shape.

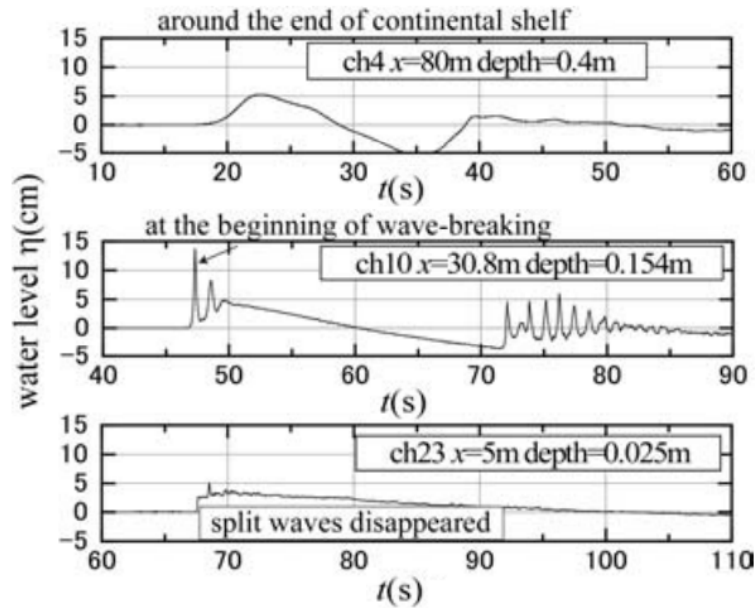


Figure C.2: Time histories of water surface elevation for a case ($T = 20s$, $s = 1 : 200$) [Matsuyama et al., 2007]

C.3. FLOOD PARAMETERS FROM SWASH

The SWASH results derive flood parameters which determine the amount of damage occurring from the tsunami is illustrated in Table C.1 and Figure C.4.

Table C.1 gives a brief overview of all of the results. The tsunami arrival time till the shore reduces as the wave height increases. The run-up distance increases with the wave height, but reduces with the increase in the road dike height. The same is seen for the inundation depth. Finally, the flow velocity at the inner toe of the dike increases with the wave height, but slightly reduces with the increase in dike height. There is no overtopping of a 6 m incoming wave height with a 16 m dike, thus, all the parameters are 0 for that scenario.

To look at the changes in inundation depth, flow velocity and dv -values in time, an example is given with the flood scenario for an 8 m incoming wave with an 8 m dike. Multiple time series of the parameters at different sections along the cross-section (Figure C.4 top) are illustrated. It is important to note that the inundation depth is taken relative to the bottom, thus for the inundation depths for section A, the actual

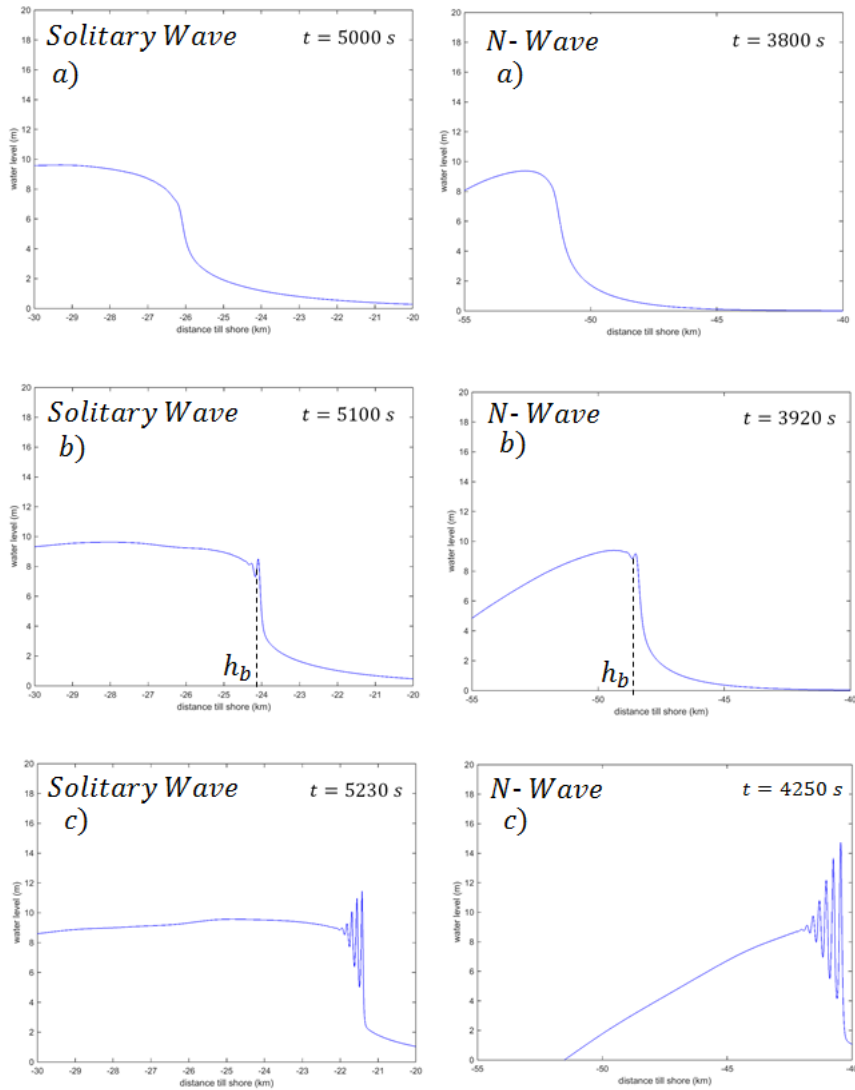


Figure C.3: Snap shots of the different stages of the breaking wave for both the solitary wave and the N-wave. For the non-broken wave a), the first wave split b) and when multiple solitons are formed c)

water level is above the dike. The negative values in the flow velocity graph represent the flow velocity in the seaward direction, in other words it is the retreat of the first wave. Finally, the graph illustrating the time series of the dv -value shows that the dv_{max} occur at a different point in time for the different sections.

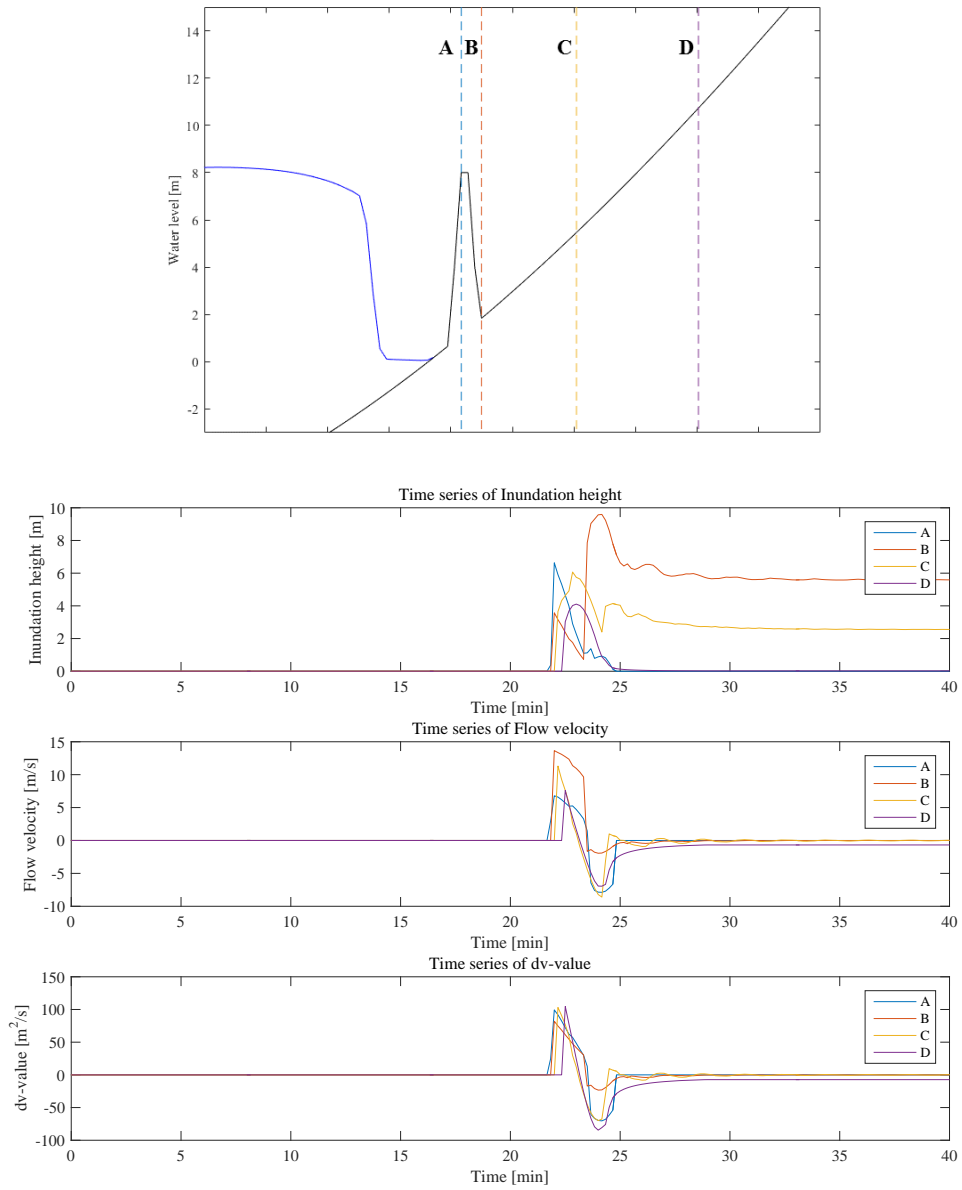


Figure C.4: Time series of inundation depth d (relative to bottom), flow velocity v and dv -value along locations A to D in cross-section for an 8 m incoming tsunami wave height and 8 m dike scenario

Table C.1: Run-up distance, inundation height, flow velocity and arrival time results for different tsunami scenarios conducted in SWASH

		Dike height (m)	6	8	Tsunami heights (m)				
					11	12	13.5	14	14.5
Arrival time (min)			22	22	21.5	21.5	21	21	20.5
Run-up distance (m)	Baseline	550	781	1067	1188	1210	1353	1408	
	4	517	748	1056	1177	1188	1342	1386	
	8	407	671	1012	1133	1155	1287	1364	
	12	209	550	913	1045	1056	1243	1309	
	16	0	374	803	946	957	1144	1221	
Depth (m) @ inner toe of dike	Baseline	3.77	6.13	9.02	9.82	11.35	13.79	14.05	
	4	3.04	5.23	8.21	9.27	9.95	12.46	13.11	
	8	1.74	3.54	5.74	6.74	6.70	8.42	9.32	
	12	0.35	2.57	4.25	4.97	5.72	5.99	6.59	
	16	0.00	1.13	3.02	3.53	3.58	4.08	5.16	
Velocity (m/s) @ inner toe of dike	Baseline	9.97	12.03	14.06	15.32	15.15	15.17	15.43	
	4	11.21	12.75	14.54	15.63	16.06	15.74	16.04	
	8	11.80	14.19	16.85	17.73	18.58	17.94	14.80	
	12	7.46	14.52	17.47	17.71	18.78	16.08	19.39	
	16	0.00	13.61	18.59	18.40	17.81	16.82	17.71	

C.4. RELATIONSHIP BETWEEN DIKE HEIGHT & WATER LEVEL IN FRONT OF DIKE

Finally, more SWASH computations were conducted to reach a dike height which would meet the Level 1 and Level 2 event categorization requirements. As mentioned before, these categorizations are very broad, thus, it is difficult to assess what is an acceptable amount of overtopping. According to Dr. Miguel Esteban, the dike does not have to fully protect the city from a Level 1 event and some "splash" is acceptable, however, this amount of "splash" that is acceptable is not defined (Personal communication, June 6 2016).

To get some insight on the relationship between the dike height and the resulting water level in front of the dike due to reflection, different scenarios will be looked at. The scenarios which are simulated in SWASH is a tsunami with an 8 m incoming wave height, in a situation with no dike, a 3 m dike (existing situation), and an 8 m dike. First, the water levels on top of the dike and the water level immediately behind the dike are compared. The water levels on top of the dike are looked at to visualize the amount of wave reflection that exists.

The different sections where the water level time series are measured is illustrated in Figure C.5. The water levels are relative to the bottom level of that given section, so for example, the water level on top of the dike in reality would be seen as this water level added to the dike height.

From these results it is clear that a 8 m wave with an 8 m dike results in a large amount of reflection, almost doubled in height, although the water level behind the dike is reduced.

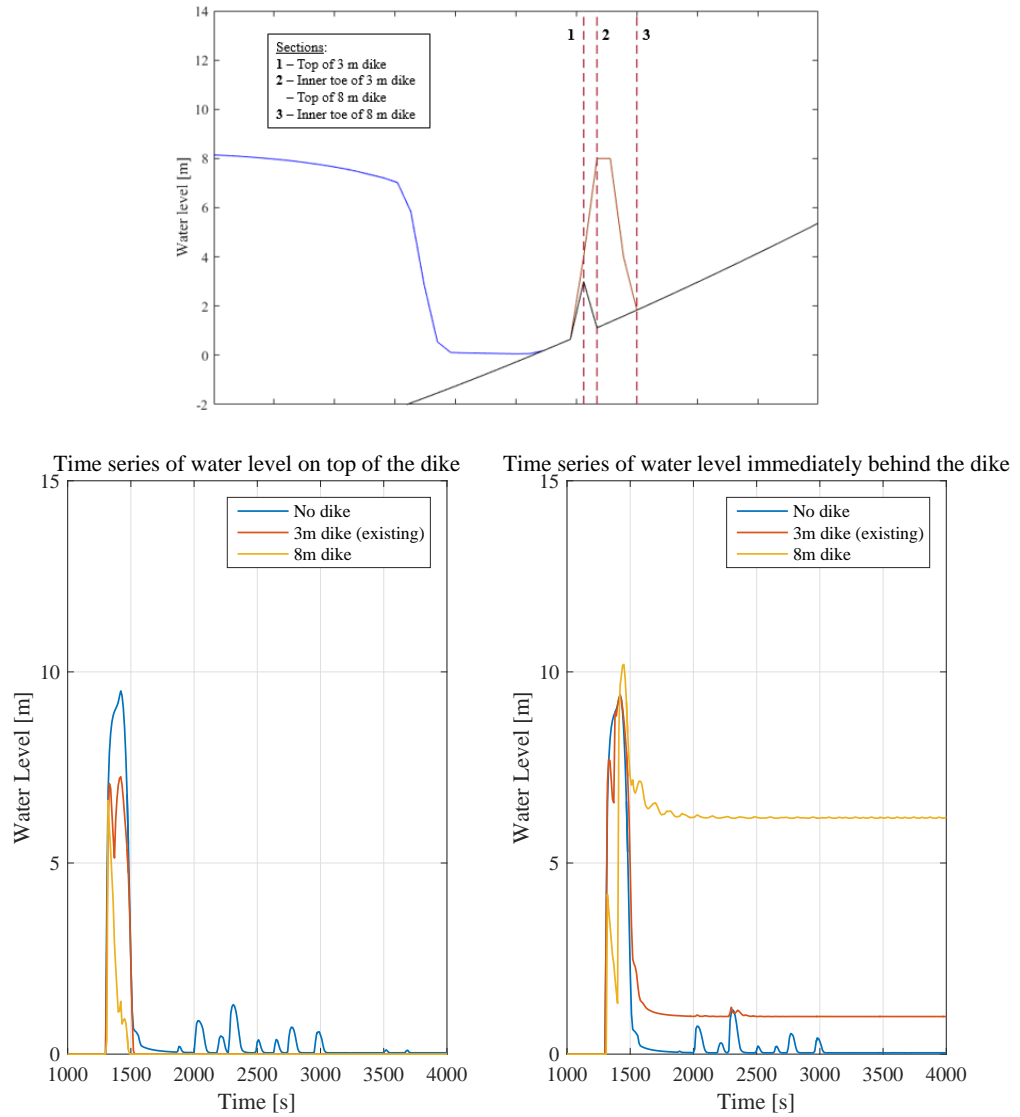


Figure C.5: Water level on top of the dike and immediately after the dike for a Level 1 tsunami event for Kamakura

D

DISCUSSION ON RISK QUANTIFICATION

This appendix aims to support the findings of the risk assessment, which were conducted in Chapters 6 and 7. It also presents more detailed analysis conducted in parallel to the risk assessment, and confirms my conclusions from the risk assessment.

D.1. BASELINE RISK RESULTS

The mortality with respect to evacuation behavior and population distribution is given. This evacuation behavior is the existing evacuation distribution.

Table D.1: Mortality with respect to Evacuation Behavior for existing evacuation distribution

	Tsunami level (m)						
	6	8	11	12	13.5	14	14.5
Immediate (live)	0.130	0.130	0.130	0.130	0.130	0.130	0.130
Immediate (die)	0.000	0.000	0.000	0.000	0.000	0.000	0.000
Delay (live)	0.600	0.600	0.600	0.597	0.593	0.579	0.573
Delay (die)	0.000	0.000	0.000	0.003	0.007	0.021	0.027
No (live)	0.219	0.197	0.168	0.159	0.155	0.140	0.136
No (die)	0.051	0.073	0.102	0.111	0.115	0.130	0.134

Table D.2: Mortality with respect to Population distribution for existing evacuation distribution

	Tsunami level (m)						
	6	8	11	12	13.5	14	14.5
adult(live)	0.531	0.519	0.503	0.498	0.496	0.487	0.485
adult(die)	0.029	0.041	0.057	0.062	0.064	0.073	0.075
old (live)	0.304	0.297	0.288	0.282	0.276	0.259	0.253
old (die)	0.016	0.023	0.032	0.038	0.044	0.061	0.067
child (live)	0.114	0.111	0.108	0.107	0.106	0.103	0.101
child (die)	0.006	0.009	0.012	0.013	0.014	0.017	0.019

The mortality illustrated in the Tables are clarified with Figure D.1, illustrating the mortality for an 8 m tsunami and 14 m tsunami, which are representatively level 1 and level 2 events in this thesis accordingly.

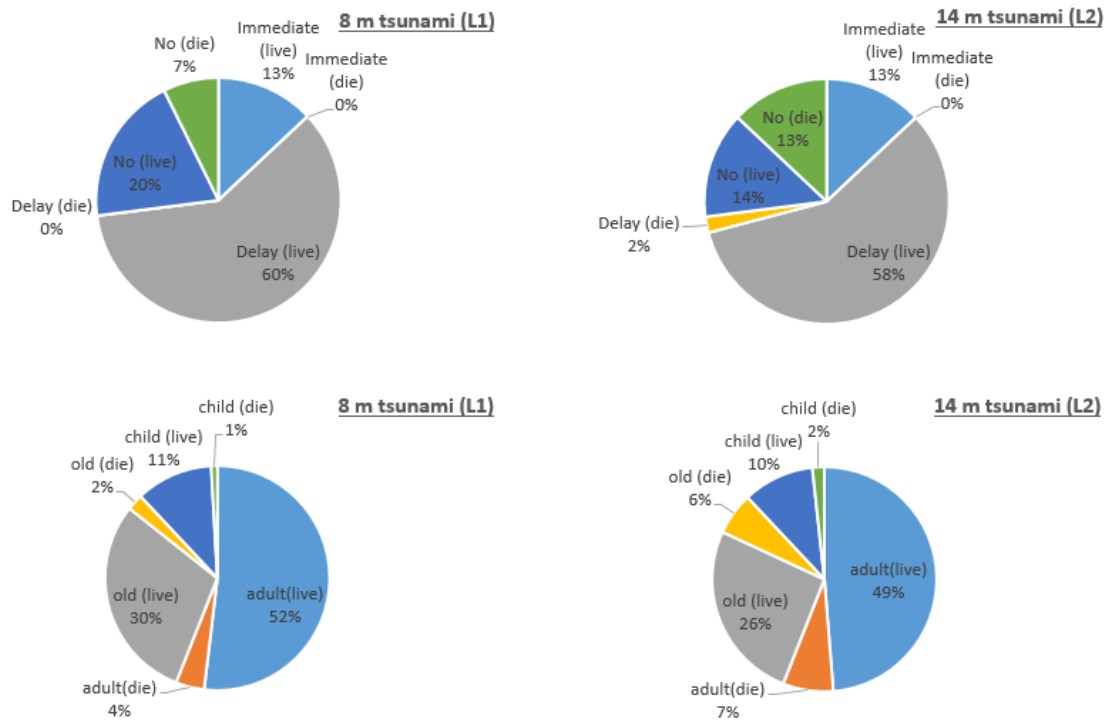


Figure D.1: Mortality with respect to evacuation behavior distribution and population distribution for different tsunami levels

The tsunami hazard map for the 'worst-case' scenario was created for Kamakura by the municipality, after the 2011 tsunami event in Tohoku, and aims to clarify the location of the evacuation centers and highlight the areas which would have higher inundation heights.

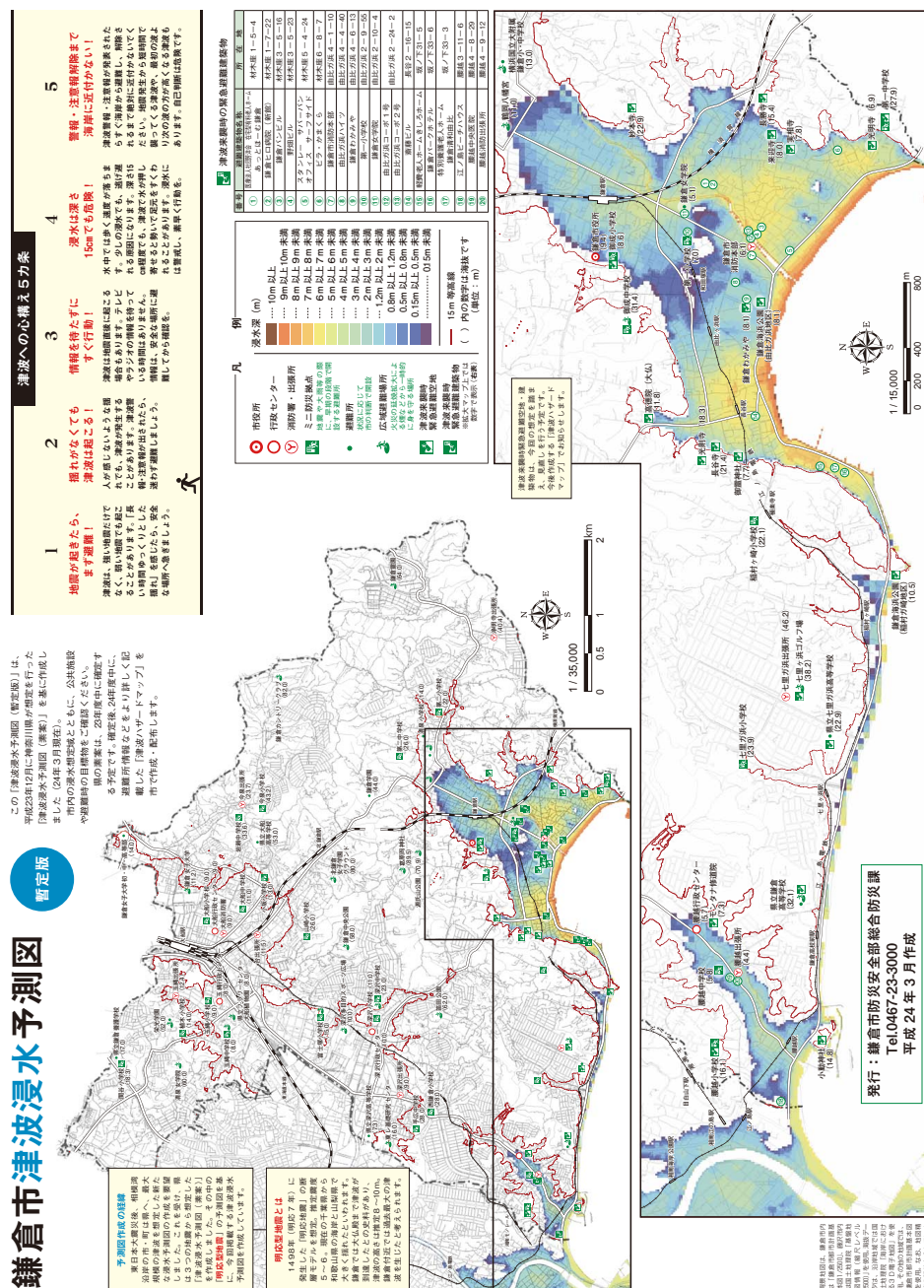


Figure D.2: Tsunami hazard map for Kamakura

D.2. DIKE HEIGHTENING RESULTS

Table D.3: Expected casualties and building damage for each tsunami level with the dike heightening intervention, and its corresponding damage reduction

Dike height [m]	Tsunami Level [m]	Return Period (years)	Expected Casualties (number of ppl)	Expected damaged buildings (# of buildings)	Damage reduction (B€)
3	6	88	5123	3234	-
	8	110	7318	4620	-
	11	221	10141	6336	-
	12	327	11379	6930	-
	13.5	761	12243	7194	-
	14	1124	15064	8052	-
	14.5	1809	16127	8382	-
4	6	88	4914	3036	0.49
	8	110	7214	4422	0.27
	11	221	10141	6270	0.02
	12	327	11662	6996	-0.60
	13.5	761	12139	7062	0.24
	14	1124	14522	7986	1.16
	14.5	1809	15373	8250	1.63
8	6	88	3868	2244	2.92
	8	110	6482	3828	1.98
	11	221	9827	5808	0.80
	12	327	10977	6600	0.94
	13.5	761	11200	6732	2.32
	14	1124	13377	7524	3.68
	14.5	1809	15066	7986	2.34
12	6	88	1986	924	7.25
	8	110	5332	2970	4.64
	11	221	8886	5214	2.96
	12	327	10036	5940	3.09
	13.5	761	10350	6138	4.29
	14	1124	12513	7128	5.59
	14.5	1809	13705	7590	5.31
16	6	88	0	0	11.59
	8	110	3659	1782	8.49
	11	221	7736	4356	5.62
	12	327	9095	5214	5.30
	13.5	761	9200	5346	6.90
	14	1124	10768	6336	9.49
	14.5	1809	11946	6864	9.21

D.3. IMPROVED EVACUATION RESULTS

The mortality with respect to improved evacuation behavior, from the influence of vertical evacuation and wireless receivers, and the mortality with respect to population distribution is given.

Table D.4: Mortality with respect to Evacuation Behavior for improved evacuation distribution

	Tsunami level (m)						
	6	8	11	12	13.5	14	14.5
Immediate (live)	0.130	0.130	0.130	0.130	0.130	0.130	0.130
Immediate (die)	0.000	0.000	0.000	0.000	0.000	0.000	0.000
Delay (live)	0.600	0.600	0.600	0.600	0.600	0.600	0.600
Delay (die)	0.000	0.000	0.000	0.000	0.000	0.000	0.000
No (live)	0.251	0.242	0.232	0.228	0.227	0.222	0.220
No (die)	0.019	0.028	0.038	0.042	0.043	0.048	0.050

Table D.5: Mortality with respect to Population distribution for improved evacuation distribution

	Tsunami level (m)						
	6	8	11	12	13.5	14	14.5
adult(live)	0.549	0.545	0.539	0.537	0.536	0.533	0.532
adult(die)	0.011	0.015	0.021	0.023	0.024	0.027	0.028
old (live)	0.314	0.311	0.308	0.307	0.306	0.305	0.304
old (die)	0.006	0.009	0.012	0.013	0.014	0.015	0.016
child (live)	0.118	0.117	0.115	0.115	0.115	0.114	0.114
child (die)	0.002	0.003	0.005	0.005	0.005	0.006	0.006

The mortality illustrated in the Tables are clarified with Figure D.3, illustrating the mortality for an 8 m tsunami and 14 m tsunami with improved evacuation, which are representatively level 1 and level 2 events in this thesis accordingly.

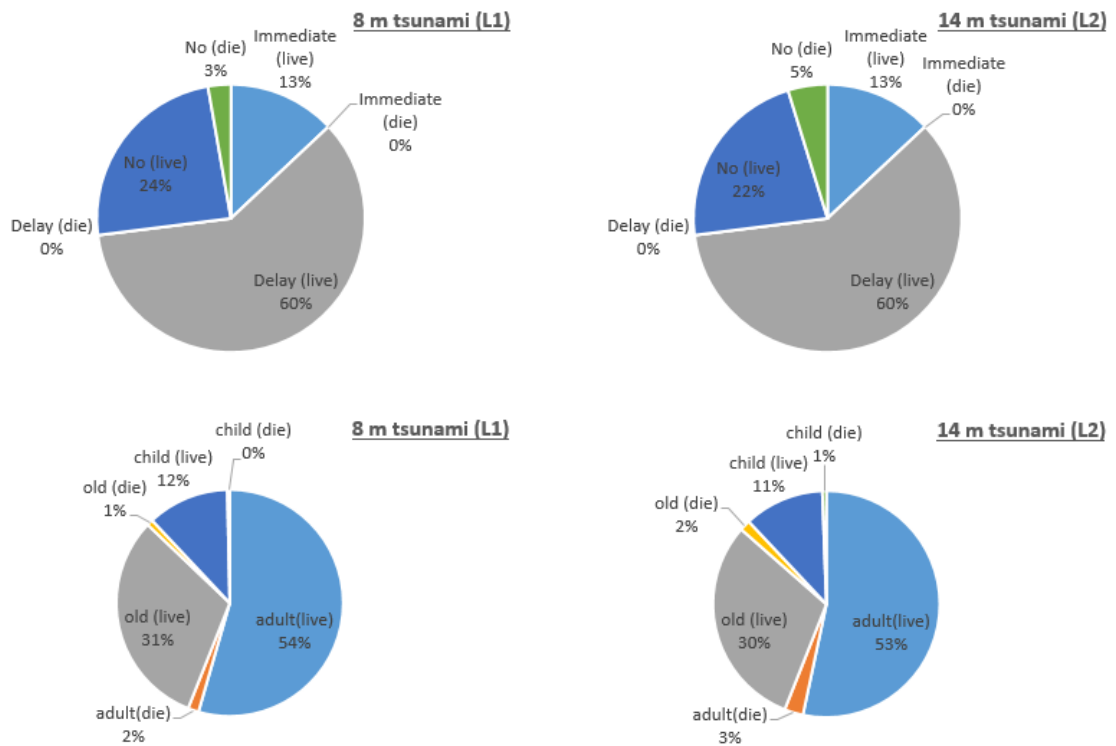


Figure D.3: Mortality with respect to evacuation behavior distribution and population distribution with improved evacuation for different tsunami levels

D.4. COMBINED INTERVENTION RESULTS

Here, the results for the combined intervention results which were not illustrated in Chapter 6 are shown. The influence of the two evacuation improvement measures are shown separately in the figures and tables.

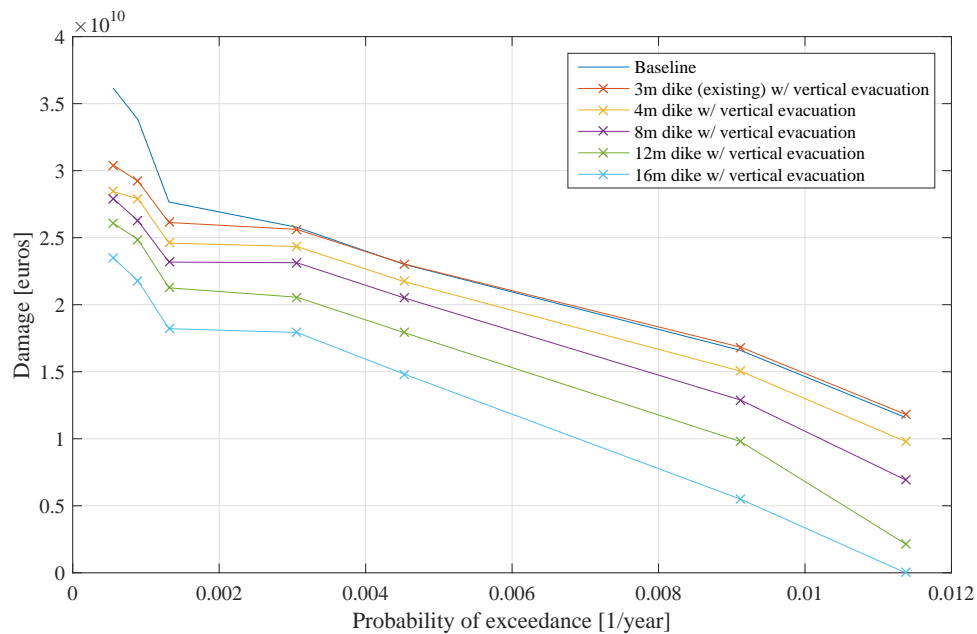


Figure D.4: Relationship between damage and probability of exceedance with the combination of dike heightening & vertical evacuation in comparison with the baseline

Table D.6: Comparison of the number of casualties between the baseline situation and the intervention with dike heightening and vertical evacuation

Tsunami Level (m)	Return Period (years)	Baseline evacuation	Expected Casualties (number of people)				
			3m dike	4m dike	8m dike	12m dike	16m dike
			<i>only vertical evacuation</i>				
6	88	5123	5227	4286	3032	941	0
8	110	7318	7423	6586	5645	4286	2405
11	221	10141	10141	9514	8991	7841	6482
12	327	11379	11291	10663	10141	8991	7841
13.5	761	12243	11500	10768	10141	9304	7945
14	1124	15064	12859	12232	11500	10873	9514
14.5	1809	16127	13382	12441	12232	11395	10245

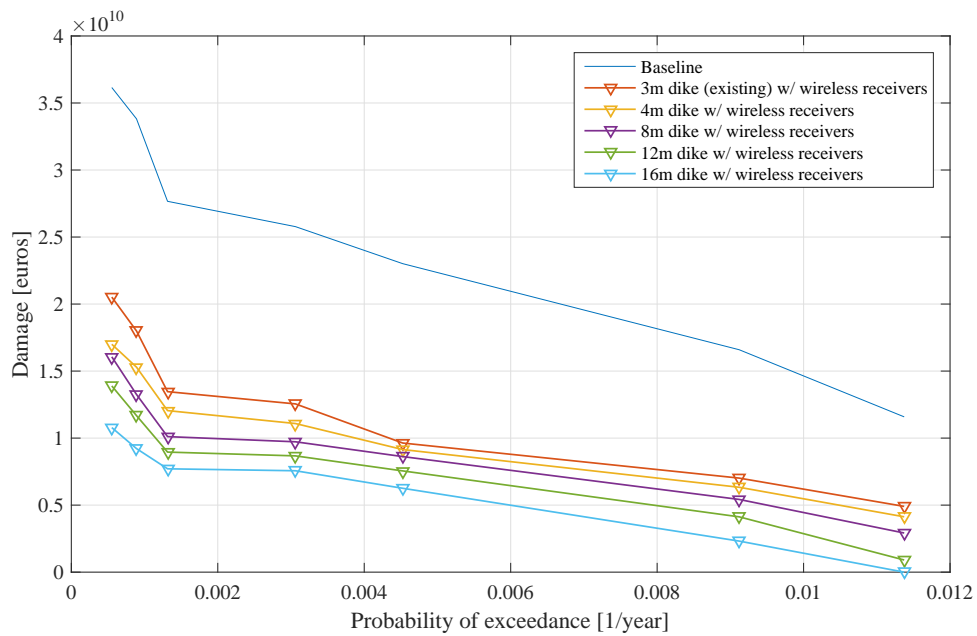


Figure D.5: Relationship between damage and probability of exceedance with the combination of dike heightening & wireless receivers in comparison with the baseline

Table D.7: Comparison of the number of casualties between the baseline situation and the intervention with dike heightening and wireless receivers

Tsunami Level (m)	Return Period (years)	Expected Casualties (number of people)					
		Baseline	3m dike	4m dike	8m dike	12m dike	16m dike
		<i>evacuation</i>			<i>only wireless receivers</i>		
6	88	5123	1936	1588	1123	348	0
8	110	7318	2749	2439	2091	1588	891
11	221	10141	3756	3524	3330	2904	2401
12	327	11379	4182	4352	3756	3330	2904
13.5	761	12243	4259	4794	3917	3446	2943
14	1124	15064	4763	6222	5306	4591	3524
14.5	1809	16127	4956	6994	6584	5590	4197

D.5. SOCIETAL RISK CRITERIA IN OTHER COUNTRIES

In [Jonkman et al. \[2003\]](#), the limit lines for the FN criterion in several countries were compared, so the C values for Japan could be assumed from countries which have similar standards and economic level. The different C and n values for some countries are illustrated in [Table D.8](#). These protection levels are

Table D.8: International standards for FN limit line [[Jonkman et al., 2003](#)]

Country	n	C	Application
UK (HSE)	1	10^{-2}	Hazardous installations
Hong Kong (truncated)	1	10^{-3}	Hazardous installations
The Netherlands (VROM)	2	10^{-3}	Hazardous installations
Denmark	2	10^{-2}	Hazardous installations

illustrated here to show the different protection levels available for each country, and for possible introduction to tsunami protection levels in the future. It is important to realize that hazardous installations require very high safety standards, which may not correlate with what is required for tsunamis in Japan.